CHARACTERIZATION AND PHOTOCATALYTIC ACTIVITY OF SEPIOLITE-TiO_2 AND Na-MONTMORILLONITE-TiO_2 CATALYSTS

by

Elçin Sayınsöz

B.S., Chemistry, Uludağ University, 2002

Submitted to the Institute for Graduate Studies in
Science and Engineering in partial fulfillment of
the requirements for the degree of
Master of Science

Graduate Program in Chemistry
Boğaziçi University

2006

ACKNOWLEDGEMENTS

I would like to give my gratitude to Asst. Prof. A. Neren Ökte for her supervision, guidence and particularly valuble help to complete this project. Beyond these, I am really grateful for her support which raised me when I had difficulties both with my courses and this project. I sincerely thank for her patience.

I also express my thanks to the members of my committee: Prof. Dilek Çalgan and Prof. Işıl Balcıoğlu for reviewing the manuscript and making guiding comments.

My deepest thanks go to all my teachers especially to Prof. Ulviye Özer, from Uludağ University, who envied and encoureged me with her strong personality. She is a very important person that I will never forget throught my life.

Another person that I really want to give my special gratitude for her help on writing is Müge Ensari Özay. More than this and exactly the most important one for me is having both her sincerity and friendship. I am very happy to be having a friend like her. I give my special thanks for you dear Müge.

Ali Kara, my another friend, did not leave me alone while I was working in laboratuory until late hours at night. He worked with me even on weekends. Beyond these, he occupied an important place in my life with his personality. I give my special thanks for his sincerity.

I also thank to Dr. Bilge Gedik Uluocak for SEM analysis, Aslı Çakır for XRD analysis and Gökhan Çaylı for TGA analysis.

It is a good oppurtunity for me to express my great indebptness to my elder sister, Melike, my lovely nephew Dora for their love and also to my mother and to my father, for their endless love and support that encouraged me in every phase of my life.

This project has been supported by Boğaziçi University Reseach Fund (BAP 05B504). This financial help is highly appreciated.

TABLE OF CONTENTS

LIST OF FIGURES

LIST OF TABLES

LIST OF SYMBOLS/ABBREVIATIONS

A	0.9
b	0.001745 radian
B	Full width half-maximum
C_{eq}	Equilibrium concentration
d	Interplaner distance of the crystal
$D_{anatase}$	Average primary particle diameter
e^-	Electron
ε	Molar extinction coefficient
φ_λ	Quantum yield
h^+	Hole
l	Path length of the spectrophotometer
λ	Wavelength of X-ray radiation
n	Integer number
n_{abs}	Number of photons
t	Irradiation time of the actinometer
θ	Angle between X-ray radiation and crystal surface
V_1	Volume of the actinometer
V_2	Volume of aliquot taken for analysis
V_3	Final volume

CB	Conduction band
CEC	Concentration of exchangeable cations
EDX	Energy Dispersive X-ray
ev	Electron volt
FWHM	Full width half-maximum
HPLC	High Performance Liquid Chromatography
O	Octahedral
OD	Optical density
PILCs	Pillared interlayer clays

SC	Semiconductor catalyst
SEM	Scanning Electron Microscopy
STEM	Scanning Transmission Electron Microscopy
TGA	Thermogravimetric Analysis
T	Tetrahedral
VB	Valance band
XRD	X–ray Diffraction
XPS	X-ray Photoelectron Spectroscopy

1. INTRODUCTION

It is well known that various toxic and hazardous organic compounds present in waste water and surface water are difficult to be decomposed by conventional chemicals (ozone, chlorine, hydrogen peroxide, etc.) or biological methods, especially if they are present at low concentrations. Advanced oxidation processes (AOP) are very reactive and oxidizing free radicals are able to decompose numerous organic pollutants to CO_2, H_2O_2 and inorganic salts. They involve mainly UV light in the presence of ozone and/or hydrogen peroxide, UV and near-visible light in the presence of titanium dioxide (TiO_2).

Among many semiconductor photocatalysts investigated, TiO_2 is the most commonly used one, with TiO_2 Degussa P-25 having become a research standard. Considering the surface mediated character of photocatalytic processes, one of the main drawbacks of TiO_2 Degussa P-25 is its relatively low specific surface area, limiting the number of available adsorption sites for pollutants to be degraded. Therefore, preparation of photocatalysts with higher specific surface area is a new research challenge. Nowadays, there is a growing interest in TiO_2 incorporated and pillared clays. It is expected that the sorption behavior of the photocatalysts can be changed by including nanometer-sized TiO_2 particles in the silicate layer of the clays.

In this study, we present the photocatalytic degradation of β-Naphthol, in the presence of TiO_2 incorporated Sepiolite (Sepiolite-TiO_2) and TiO_2 pillared Na-Montmorillonite (Na-Montmorillonite-TiO_2) under UV illumination. Chapter 2 gives a summary of TiO_2 photocatalyst, its composition, crystal structure, synthesis, morphology and structural aspects. Then, clays as supports are summarized together with a general description of clay minerals, their structure, classification, morphology and general properties. Sepiolite and Na-Montmorillonite are introduced and followed with a brief description of pillared clays. Chapter ends up with the literature survey of photocatalytic studies in the presence of different clay structures. Experimental set-up, reagents used in the experiments, procedures and instruments used in the analysis are given in Chapter 3. Chapter 4 includes two sections. In the first section, characterization of Sepiolite-TiO_2 and Na-Montmorillonite-TiO_2 catalysts is presented by using the methods; Thermal

Gravimetric Analysis (TGA), X-ray Diffraction Analysis (XRD) and Scanning Electron Microscopy (Energy Dispersive X-ray Analysis) (SEM-EDX). In the second section, photocatalytic degradation results of β-Naphthol are examined. Preliminary experiments precede the control experiments, at which effect of β-Naphthol concentration, effect of titania-sol amount, effect of dilution in clay solutions are investigated. At the end of the chapter, photocatalytic studies are followed in the presence of Anatase, Sepiolite-TiO_2, Na-Montmorillonite-TiO_2, Sepiolite-TiO_2, Fe-Sepiolite-TiO_2, and Fe-Na-Montmorillonite-TiO_2 catalysts.

2. THEORY

2.1. TITANIUM DIOXIDE: A PHOTOSENSITIVE SEMICONDUCTOR

A semiconductor is usually defined rather loosely as a material with electrical resistivity lying in the range of 10^{-2}-10^{-9} Ω cm. Alternatively, it can be defined as a material whose energy gap for electronic excitations lies between zero and about 3 electron volts (ev) [1]. When a semiconductor catalyst (SC) of the chalcogenide type (oxides (TiO_2, ZnO, ZrO_2, CeO_2,...), or sulfides (CdS, ZnS,...)) is illuminated with photons whose energy is equal to or greater than their band-gap energy, there is absorption of these photons and creation of electron-hole pairs within the bulk or on the surface of the semiconductor, which dissociate into free photoelectrons in the conduction band and photoholes in the valence band [2].

Ideally, a semiconductor photocatalyst should be chemically and biologically inert, photocatalytically stable, easy to produce and to use, efficiently activated by sunlight, able to efficiently catalyze reactions, cheap, and without risks for the environment or humans. Titanium dioxide (with sizes ranging from clusters to colloids to powders and large single crystals) is close to being an ideal photocatalyst, displaying almost all the above properties. The single exception is that it does not absorb visible light [3].

According to the present ideas, main pathway of photomineralization (i.e., the breakdown of organic compounds) carried out in aerated solution can be summarized by the following reaction:

$$\text{Organic compound} \xrightarrow[h\nu>Eg]{TiO_2} CO_2 + H_2O + \text{mineral acid} \qquad (2.1)$$

A schematic representation of this process is displayed in Figure 2.1 [3]. The radical ions formed after the interfacial charge transfer reactions can participate in several pathways in the degradation process: they may react chemically with themselves or surface-adsorbed compounds, they may recombine by back electron transfer reactions, especially when they are trapped near the surface or they may diffuse from semiconductor surface and participate in chemical reactions in the bulk solution.

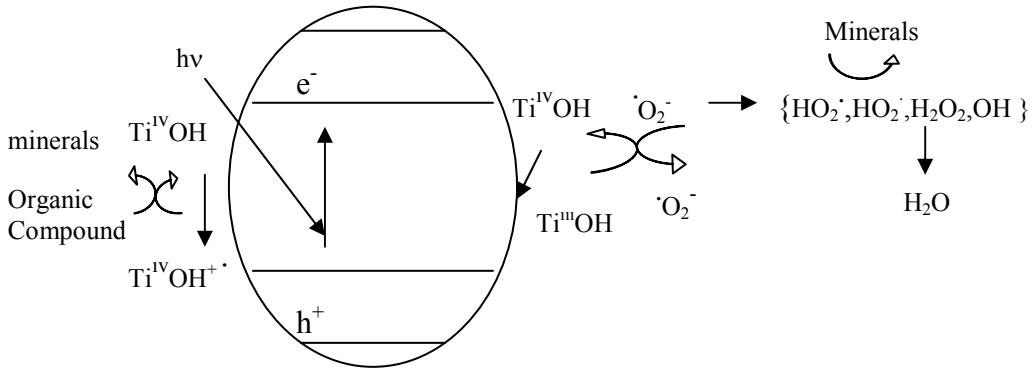

Figure 2.1. TiO_2-sensitized photooxidative mineralization of organic compounds

The detailed mechanism of the photocatalytic process on the TiO_2 surface is still not completely clear, particularly that concerning the initial steps involved in the reaction of reactive oxygen species and organic molecules [4, 5, 6]. A reasonable assumption is that both photocatalytic oxidative and reductive reactions occur simultaneously on the TiO_2 (Table 2.1).

In most experiments, the electron transfer to oxygen, which acts as primary electron acceptor, is rate determining in photocatalysis. Hydroxyl radicals are formed on the surface of TiO_2 by reaction of holes in the valance band (h^+_{VB}) with adsorbed H_2O, hydroxide, or surface titanol groups (>TiOH). The photogenerated electrons are reduced enough to produce superoxide (O_2^-). This superoxide is an effective oxygenation agent that attacks neutral substrates as well as surface-adsorbed radicals and / or radical ions. Theoretically, the redox potential of the electron-hole pair permits H_2O_2 formation either by water oxidation (by holes) or by two conduction band electron reduction of the adsorbed oxygen. The latter represents the main pathway of H_2O_2 formation. H_2O_2 contributes to the degradation pathway by acting as an electron acceptor or as a direct source of hydroxyl radicals due to homolytic scission. Depending upon the reaction conditions, the holes, $OH^{\cdot}$ radicals, O_2^-, H_2O_2, and O_2 can play important roles in the photocatalytical reaction mechanism [7, 8].

If non-oxygenated products, derived from ion radicals, are desired, oxygen has to be replaced with other electron acceptors [6].

Table 2.1. Photocatalytic oxidative and reductive reactions on TiO_2

Primary Processes

1. Charge-carrier generation:
$$TiO_2 + h\nu \rightarrow e_{CB}^- + h_{VB}^+$$

2. Charge-carrier trapping:
a. $h_{VB}^+ + >Ti^{IV}OH \rightarrow \{Ti^{IV}OH^{\cdot}\}^+$
b. $e_{CB}^- + >Ti^{IV}OH \leftrightarrow \{>Ti^{III}OH\}$
(shallow traps, dynamic equilibrium)
c. $e_{CB}^- + >Ti^{IV} \rightarrow Ti^{III}$
(deep traps, irreversible)

3. Surface charge-carrier recombination:
a. $e_{CB}^- + \{>Ti^{IV}OH^{\cdot}\}^+ \rightarrow Ti^{IV}OH$
b. $h_{VB}^+ + \{>Ti^{III}OH\} \rightarrow >Ti^{IV}OH$

4. Interfacial charge transfer
a. $\{>Ti^{IV}OH^{\cdot}\}^+ + Red \rightarrow >Ti^{IV}OH + Red^+$

b. $e_{CB}^- + Ox \rightarrow \{>Ti^{IV}OH + Ox^-$

According to the above-mentioned mechanism and time characteristics, two critical processes determine the overall quantum efficiency of interfacial charge transfer: the competition between charge-carrier recombination and trapping (picoseconds to nanoseconds), the competition between trapped carrier recombination and interfacial charge transfer (microseconds to milliseconds).

An increase in either charge-carrier lifetime or the interfacial electron-transfer rate is expected to lead to higher quantum efficiencies.

A first source of debate is whether VB holes can react directly with organic compounds before they are trapped, or whether oxidation occurs indirectly via surface-bound hydroxyl radicals (i.e., a trapped hole at the surface). It was suggested that the first pathway might play an important role at a high coverage of organic compounds. The hydroxyl radical mediated oxidation mechanism was used to explain the degradation of substituted aromatic compounds and chlorinated ethanes [7]. For the first class of compounds, hydroxylated structures were detected similar to those found when these aromatics are reacted with a known source of hydroxyl radicals. For the second class of

compounds, the rate of oxidation was correlated with C-H bond strengths, which indicates that the abstraction of H atoms by $OH^{\cdot}$ radicals is an important factor in the rate detrmining step for oxidation. In conclusion, this hydroxyl radical mediated oxidation mechanism involves two pathways: hydroxyl radical addition and hydrogen abstraction. Both reaction pathways are expected to give oxygenated products in a solution saturated with oxygen. In the absence of water or in competition with water in an aqueous solution, the substrate can undergo a direct electron transfer to the photogenerated holes to yield a radical carbon [8]. Then the radical can react with water or oxygen to form oxygenated compounds. Although hole-catalyzed and hydroxyl radical mediated pathways are vastly different processes, the two give similar product distributions in oxygenated aqueous solutions, thus making the distinction between the two difficult.

Another source of debate is the localization of the degradation process. Adsorption of organic compounds on the semiconductor surface is often reported as a prerequisite for organic photodegradation. Other studies suggest that in the case of radical formation, adsroption of organic contaminants would increase the reaction rate but is not required, since the reactive $OH^{\cdot}$ radicals can diffuse into the solution to react with the organic pollutants [9,10]. Due to their high reactivity, they can not diffuse far and the reaction has to take place close to the surface. Whether a prerequisite or not, the possibility of adsorption is critical. The summation of chemical and electrostatic forces between substrate molecules and the semiconductor surface includes: van der Waals force, (induced) dipole-dipole interactions, hydrogen bonding, ion exchange, surface-matter partitions (i.e., the distribution of the adsorbed molecules on the surface).

Due to the complex reaction mechanism, it is difficult to develop a model for the dependence of the photocatalytic degradation rate on the experimental parameters for the whole treatment time. Models focused on the initial disappearance rate of organics or the initial formation rate of CO_2. Some additional complexity may arise from the possibility of different adsorption sites and the presence of pores [3].

2.1.1. Composition and Crystal Structure of TiO_2

Titanium, the world's fourth most abundant metal (exceed only by aluminum, iron, and magnesium) and the ninth most abundant element (constituting about 0.63 per cent of the Earth's crust), was discovered in 1791 in England by Reverend William Gregor, who recognized the presence of a new element in ilmenite. The element was rediscovered several years later by the German chemist Heinrich Klaporth in rutile ore who named it after Titans, mythological first sons of the goddess Ge (Earth in Greek mythology).

TiO_2 contains not less than 99 per cent and not more than 100 per cent O_2 calculated on the dry basis. The theoretical composition of the oxide is: Titanium 60 per cent, Oxygen 40 per cent. It contains iron, columbion and tantalum in important amounts; tin, chromium and vanadium have also been reported [11].

Titanium metal is not found unbound to other elements that are present in various igneous rocks and sediments. It occurs primarily in minerals like rutile, ilmenite, leucoexene, anatase, brookite, perovskite, and it is found in titanates and many iron ores. Titanium is also found in coal, ash, plants, and even in the human body [3].

From the thermodynamic point of view, rutile is the stablest phase at all temperatures and pressures up to 60 kbar, where TiO_2 (II) becomes the thermodynamic favorable phase. Particle size experiments affirm that the relative phase stability may reverse when particle sizes decrease to sufficiently low values due to surface energy effects (surface free energy and surface stress, which depend on particle size). If the particle sizes of the three crystalline phases are equal, anatase is the most thermodynamically stable at sizes less than 11 nm, brookite is most stable between 11 and 35 nm, and rutile is most stable at sizes greater than 35 nm.

The enthalpy of the anatase-rutile phase transformation is low (ranging from–1.3 to–6.0 kj/mol) [12]. Kinetically, anatase is stable, i.e., its transformation into rutile at room temperature is so slow that the transformation practically does not occur. At macroscopic scale, the transformation reaches a measurable speed for bulk TiO_2 at $T > 600ºC$ [13].

Pure anatase phase is the most active crystalline phase in comparison with pure rutile. In 1991, Brickley et al. suggested a model to describe the composition of Degussa P25 TiO_2 in order to explain its photocatalytic activity. Degussa P25 is supposed to be made of three kinds of particles, some are pure anatase, some are pure rutile, and some are made of anatase nuclei inside a rutile layer. This third type of particle would be responsible for the high efficiency, since it offers a junction between two crystallographic phases. Electrons produced under UV irradiation are attracted in the anatase phase, whereas holes are driven in rutile phase. This phase contact could enhance the charge separation and reduce the recombination rate. Consequently, electrons and holes are more available for reduction and oxidation reactions [14].

2.1.2. Synthesis

TiO_2 can be prepared in the form of powder, crystals, or thin films. The sol-gel method has many advantages over other fabrication techniques such as purity, homogeneity, felicity, and flexibility in introducing dopants in large concentrations, stoichiometry control, ease of processing control over the composition, and the ability to coat large and complex areas. Very recently, sol-gel method was applied to prepare very large surface area titania phases, which exhibit a mesaporous structure. Two types are known: the non-alkoxide and the alkoxide route. The non-alkoxide route uses inorganic salts [15] (such as nitrates, chlorides, acetates, carbonates, etc.), which requires additional removal of the inorganic anion, while alkoxide route (the most employed) uses metal oxides as starting material. As titanium sources, Ti (*O*-E)$_4$, Ti(*i*-OP)$_4$ [16] and Ti (O-*n*Bu)$_4$ [17]. This method involves the formation of a TiO_2 sol or gel, and then precipitation occurs by hydrolysis and condensation (with polymer formation) of titanium alkoxides [18].

Acid catalysis increases hydrolysis rates and ultimately crystalline powders are formed from fully hydrolyzed precursors. Acetic acid may be used in order to initiate hydrolysis via an esterification reaction, and alcoholic sols prepared from titanium alkoxid using amino alcohols have been shown to stabilize the sol, reducing or preventing the condensation and the precipitation of titania. These reactions are followed by a thermal treatment (450-600ºC) to remove the organic part and to crystallize anatase [19]. The

calcination process will inevitably cause a decline in surface area (due to sintering and crystal growth), loss of surface hydroxyl groups, and even induce phase transformation. Cleaning of particles is usually achieved by washing the surface with water, which could be an effective method of removing soluble impurities without introducing new species to catalyst surface [3].

2.1.3. Structural and Morphological Aspects

The photocatalytic activity is not necessarily dependent on catalyst surface area, but rather on the availability of active sites. Therefore, properties like crystalline structure, pore size, density of OH groups, number and nature of trap sites (both in lattice and at surface), and adsorption-desorption characteristics play an important role in photocatalytic efficiencies.

A large surface area can be the rate determining factor in certain photodegradation reactions, as a large amount of adsorbed organic molecules promotes the reaction rate. However powders with a large surface area are usually associated with large amounts of crystalline defects, which favour the recombination of the electrons and holes leading to a poor photoactivity. According to the recent studies, the photocatalytic activity of amorphous TiO_2 is negligible indicating that crystallinity is an important requirement. Then balance between surface area and crystallinity must be found in order to obtain the highest photoactivity.

Particle size is an important parameter for the photocatalytic efficincy, since the predominant way of electron-hole recombination may be different depending on the particle size. The average particle sizes are determined from the Scherrer's equation (Equation 2.2) using the broadening of the (101) anatase peak reflection with the usual assumption of spherical crystallites [20]

$$D = \frac{A\lambda}{(B\text{-}b)(Cos\theta)} \qquad (2.2)$$

where D = average primary particle diameter, A=0.9, λ=0.1542 nm, B=FWHM, b=0.001745 radian, θ=radian.

It is well known that the nanometer-size range, physical and chemical properties of semiconductors are modified (compared with bulk). Small variations in the particle diameters lead to great modifications in the surface/bulk ratio, thus modifying the significance of volume and surface electron-hole recombinations [21]. According to the literature, optimum particle size of TiO_2, where photocatalytic oxidation rates of organic substrates are maximized, lies around 10 nm.

Surface hydroxyl groups also play an important role in the photodegradation process due to direct participation in the reaction mechanism by trapping of photogenerated holes that reach the catalyst surface producing very reactive surface $OH^{\cdot}$ radicals and/or a change in the adsorption of reactant molecules both by acting itself as active sites for pollutant adsorption and by covering the sites (exposed titanium cations with unsaturated coordination) where electron trapping by adsorbed oxygen takes place. This process is not only important for producing oxygen radicals but also for hindering electron-hole recombination.

2.1.4. Supports

As support materials, glass beads, fiber glass, silica, organo clays [22], activated carbon etc. are used. Often the fixation of TiO_2 on solid supports reduces its photocatalytic efficiency. This decline in activity has been correlated with reduction of active sites, mass-transfer limitations, presence of foreign cationic impurities (Si^{4+}, Na^{+}, Cr^{3+}, Fe^{3+}) in a deposit layer (as a consequence of the thermal treatments necessary to improve TiO_2-support adhesion), which increase the e^{-}/h^{+} recombination rate.

The strategies focussed on supported TiO_2 are developed in order to (a) immobilize the TiO_2 photocatalyst, (b) increase the illuminated specific catalyst area, (c) increase the adsorption capacity and surface area of the photocatalyst, (d) influence the selectivity of the photocatalytical reaction [3].

The first demand originates from the requirement to use photocatalysts in continous processes where the utilization of TiO_2 powder is technologically impracticable. Unfortunately, a small particle size leads to high filtration costs of catalyst removal, hindering its industrial application. For this reason, the synthesis of photocatalysts with high activity and effective separation properties simultaneously is a priority topic.

A photocatalyst surface is active only if it is illuminated. It is difficult to illuminate all the catalyst particles in suspended systems, because the particles further away from the light sources are shielded from radiation by those near the light source. Hence the penetration depth of light into suspenions is limited. In immobilized systems, it is possible to obtain a configuration in which all catalyst particles are illuminated [23].

There are several attempts in order to obtain hybrid photocatalysts, which are expected to induce synergism because of the adsorption properties of organic molecules. Adsorbents such as silica, clays (TiO_2 incorporated into the interlayer space of the clays), and active carbon are used [3]. Adsorption of contaminants in the vicinty of the photocatalytic sites promotes the photodegradation of contaminants that normally do not or in low quantities adsorb on the photocatalyst surface. The basic concept is based on the pyhsisorption of reactants on inert substrates followed by their surface diffusion to the interface between the adsorptive sites and photocatalytic sites. The first step is achieved by using supports with large specific surface areas for adsorption and high adsorption capacity for the target substances, while the second is achieved only if the adsorption strength is moderate enough to allow diffusion of adsorbed substrates to the loaded TiO_2 [24,25,26]. The net effects can be summarized as follows an enhanced concentration of substrate compounds is progressively built up around the TiO_2 sites, leading to a high significant increase of the reaction rate, advanced degradation of the pollutant, succeeding their mineralization even in the case where this was not achieved with bare TiO_2, was due to the fact the reaction intermediates are also adsorbed and then further oxidized. So toxic intermediates, if formed, are not released in air or in solution, thereby preventing secondary pollution by intermediates if any, possibility of photodestruction of low levels of pollutants either in water decontamination or for indoor applications, the continued use of the photocatalyst without deactivation, since the adsorbed substances are oxidized finally to CO_2.

The presence of SiO_2 is beneficial in the degradation of phenol in water. The improved photocatalytical efficiency of mixed silica-titania composites arises through the generation of new active sites, due to the interactions between titanis and silica and improved mechanical strength, thermal stability, and of surface area of the titania [3].

2.2 Clay Minerals

Clay minerals are hydrous layer silicates of colloidal dimensions. The term 'phyllosilicate' (phyllo=leaf-like) is applied to the broad group of hydrous silicates with layer structures. The essential components of the phyllosilicate structure are two-dimensional tetrahedra and octahedra of oxygen atoms (or ions). The coordinating atoms (or cations) in the centre of the tetrahedra are for the most part Si, but Al^{3+} or Fe^{3+} may also present [27].

Clay minerals occur abundantly in nature and their high surface area, sorptive and ion-exchange properties have been exploited for catalytic applications through decades [28]. Among all naturally occurring minerals, clays occupy unique position in chemistry and physical chemistry. This position is partly due to the importance of clays in soil fertility, and partly to their exceptionally broad spectrum of applications [29]. They have been and continue to be one of the more important industrial minerals. They are important in geology, agriculture, construction, engineering, process industries, and environmental applications [30].

As far as photocatalysis is concerned, a first point in which should be realized is that clays are not (and will probably never be) photocatalysts by themselves. Indeed, clays are insulating materials, which do not absorb light in the visible and near UV region of the spectrum. In fact, the interest in clays in the field of photocatalysis stems from the possibility of using them as an organized medium for running complex photochemical reactions involving molecular species. Clays are very versatile ensemble of colloidal solid particles, with different morphologies, surface-electrical and surface-chemical properties which make them suitable as catalyst support and (or) as adsorbent for controlling the position or the movements of molecular species [29].

Traditional applications are many. Some of the more important include ceramics, paper, paint, plastics, drilling fluids, chemical carriers, liquid barriers, decoloriazation, and catalysis. The industrial applications of the three most important clay mineral types are varied and in most instances quite different. This is primarily because of differences in their physical and chemical properties, which are depend on structure and composition [30].

2.2.1. Structure of Clay Minerals

Clay minerals are made of layered silicates. They are crystalline materials of very fine particle size ranging from 150 to less than 1 micron (colloidal form). There are two basic building blocks tetrahedral and octahedral layers, which are common to clay minerals.

Different classes of clay minerals, namely the 1:1, 2:1, etc. have different arrangement of tetrahedral and octahedral layers. Structural units of clays therefore consist of either alternating tetrahedral or octahedral sheets (OT or 1:1 structure), e.g. kaolinite group, a sandwich of one octahedral sheet between two tetrahedral sheets (TOT or 2:1 structure), e.g. smectite clay minerals of which the most common member is montmorillonite or an arrangement in which the three layer TOT units alternate with a brucite layer (2:1:1 structure), e.g. chlorite [28].

2.2.2. Classification and morphology

The layer type, the charge on the layer and the nature of the interlayer material provide the basis for the classification of clay minerals [29]. The clay minerals kaolinite, smectite and polygorskite-sepiolite are among the world's most important and useful industrial minerals [30].

The most common mineral by far in the kaolin group of minerals is kaolinite. Kaolin is usually white or near white in color. Other important properties are; relatively low surface area in comparison to smectite and polygorskite-sepiolite, and the low absorption capacity, which relates to the minimal layer charge and the low surface area.

Smectite group of clay minerals consists of several clay minerals, but the two most important industrially are sodium montmorillonite and calcium montmorillonite. Smectites have very different properties than kaolins. Both the octahedral and tetrahedral sheets can have substitutions, which creates a charge imbalance in the 2:1 layer. Alumina substitutes for silica in the the tetrahedral sheet and iron and magnesium substitute for aluminum in the octahedral sheet. It has been reported that many analysis have shown that the charge imbalance in smectite is about 0.66 per unit cell. This net positive charge deficiency is balanced by exchangeable cations absorbed between the unit layers and on the edges. The high layer charge, the very fine particle size, the thin flakes the high cation exchange capacity, and the high surface area result in the physical and chemical properties that determine the many industrial applications.

Polygorskite and attapulgite are synonymous for the same hydrated magnesium aluminum silicate mineral. Sepiolite is almost structurally and chemically identical to polygorskite except it has a slightly larger unit cell. There is considerable substitution of aluminum by magnesium and iron in the octahedral layer, which gives the particles a moderately high layer charge. This layer charge and the high surface area give polygorskite an intermediate cation exchange capacity normally about 30 to 450 meq/100g. The high surface area, the charge on the lattice, and the inverted structure, which leaves parallel channels through the lattice, give the polygorskite and sepiolite a high absorption capacity [30].

2.2.3. Properties of Clay Minerals

Ion exchange, swelling, intercalation and cation exchange are the most important properties of clay minerals.

Ion Exchange: Isomorphous substitution of cations in the lattice by lower valent ions, e.g. the substitution of aluminum for silicon, magnesium and/or ferrous ion for aluminum or sometimes lithium for magnesium, leaves a residual negative charge in the lattice that is balanced by other cations when brought into contact with these ions in aqueous solution [28].

Swelling: Many clay minerals absorb water between their layers, which move apart and the clay swells. For efficient swelling, the energy released by cations and/or layer solvation must be sufficient to overcome the attractive forces (such as hydrogen bonding) between the adjacent layers. In 1:1 (OT) clay minerals (kaolinite), water forms strong hydrogen bonds with hydroxyl groups on hydrophilic octahedral layers, allowing swelling to occur.

With 2:1 (TOT) clay minerals, the ability to swell depends on the solvation of interlayer cations and layer charge. Clays with 2:1 structures and low layer charge (e.g. talc and pyrophyllite) have very low concentration of interlayer cations and therefore do not swell readily. At the other extreme, those with verify high layer charges (e.g. mica) have strong electrostatic forces holding alternate anionic layers and the interlayer cations together, thus preventing swelling. Those with univalent interlayer cations swell most readily and with divalent, trivalent and polyvalent cations, swelling decreases accordingly. The extent of swelling can be observed by measuring interlayer separations using powder X-ray diffraction [29].

Intercalation and Cation exchange: In swelling clay minerals, the interlayer cations can undergo exchange with cations from external solutions. The concentration of exchangeable cations is called CEC, usually measured in mill equivalents per 100 g of dried clay [28]. The degree of separation is dependent on the size of the cation and its state of hydration [27].

2.2.4. Sepiolite

The clay mineral Sepiolite is a hydrated magnesium silicate with the therotical half unit cell formula ($Mg_4Si_6O_{15}(OH)_26H_2O$) structurally formed by blocks similar to talc (i.e.,

an anhydrous magnesium 2:1 layer silicate). Each block is formed of an octahedral sheet of magnesium oxide / hydroxide packed between two tetrahedral silica layers. Each one of the Mg^{2+} cations is located at the edges of the octahedral sheets, i.e., those with access to the tunnels, complete their octahedral coordination by bonding to two molecules of water (coordinated water). The periodic inversion of the SiO_4 tetrahedra is the origin of the structural cavities (i.e., tunnels) extending along the *c*-axis, i.e., the axis of the microfibers, with openings of 1.08 nm x 0.4 nm. These tunnels are accessible to water molecules (zeolitic water) and also to a large variety of species, the only restriction being related to the dimensions of the guest species, the Sepiolite acting as a molecular sieve. The external surface of Sepiolite microfibers are formed by channels (external tunnels) and structural steps, as determined by the external blocks' distribution (Figure 2.2) [31]. Sepiolites have typically a surface area of 200 m^2/g and this structure makes them suitable materials as supports in heterogeneous catalysis [32].

The thermal behavior of Sepiolite has been the subject of several publications, the morphological changes taking place being rather well known. The first structural change takes place at 300-350ºC, when two of the four water molecules coordinated to magnesium are lost. If the heat treatment continues, the loss of the other two water molecules takes place around 500ºC, and the structure folds. The folding of the structure is associated with a decrease in the adsorption properties since the channels become narrower and the superficial slots sinter. A further increase in temperature to 800ºC produces the dehydroxylation of the structure and leads to the formation of clinoenstatite.

The change in the structure occurring up to 500ºC is useful to analyze the adsorption process on the material, because (i) the micro porosity becomes inaccessible to simple molecules such as N_2, CO_2, NH_3 and H_2O; and (ii) there are no important changes in chemical nature of the material. In this way, the changes observed in the adsorption isotherms on both a natural sepiolite dried at 110ºC and the Sepiolite subjected to a heat treatment at 500ºC can be interpreted on the basis of only the reduction of porosity upon the heat treatment [33].

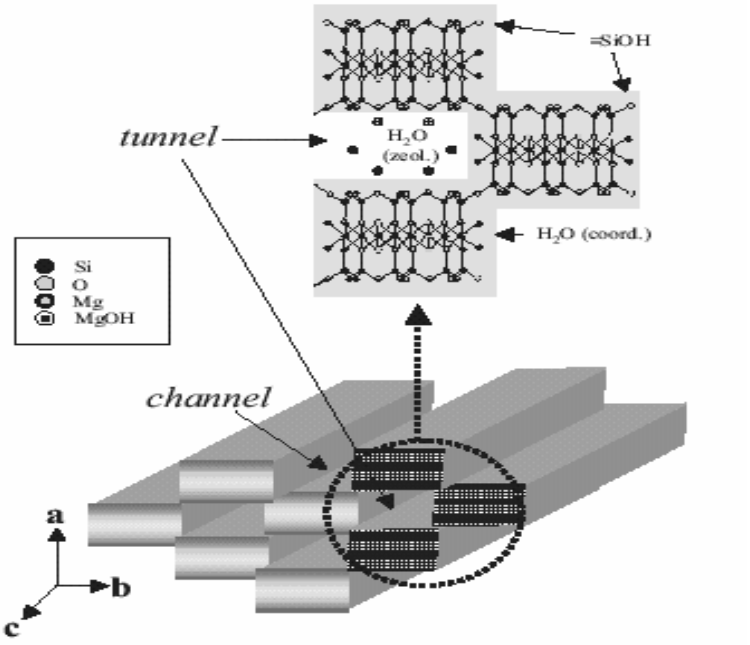

Figure 2.2. Structural model of Sepiolite showing the arrangement of tunnels and channels.

2.2.5. Montmorillonite

Montmorillonite is an expanding layer silicate mineral, composed of aluminosilicate layers stacked one above the other. Each layer has a small net negative charge because of isomorphous substitution of ions in the framework. The charge is compensated by interlayer hydrated cations, which are known as exchangeable cations. It is well known that Montmorillonite can accommodate various types of compounds in its interlayer spaces to give an intercalation type of inclusion compound [34]. The structure of Montmorillonite is shown in Figure 2.3 [35]. Their crystal lattice consists of two-dimensional layers where a central octahedral sheet of alumina or magnesia is fused to two external silica tetrahedron by the tip so that the oxygen ions of the octahedral sheet also belong to the tetrahedral sheets. The layer thickness is around 1nm. These layers organize themselves to form stacks with a regular van der Waals gap in between them called the interlayer or the gallery. As the forces that hold the stacks together are relatively weak, the intercalation of small molecules between the layers is easy. The interlayer distance of layered silicates can be varied as a function of silicate type, anionic layer charge, type of interlayer gallery ions and water-swelling of clay. Montmorillonite has high swelling capacity within the water. Intracrystalline swelling is observed in clay minerals having a medium cation density between the silicate layers. It is caused by the hydration of these cations, which draw the

water in between the silicate sheets. If there is no cations between the silicate sheets, the mineral can not swell [35].

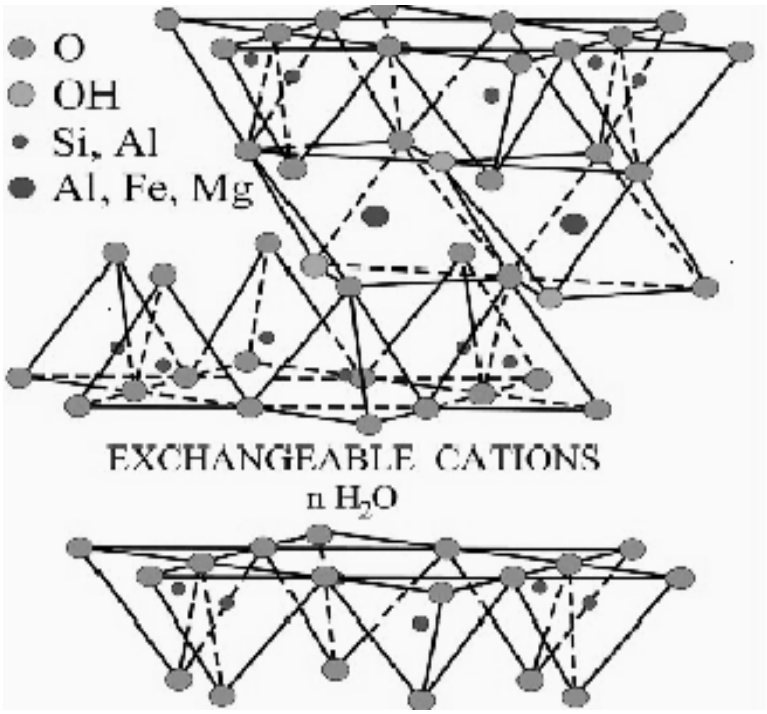

Figure 2.3. Structure of Montmorillonite

2.2.6. Pillared Clays

In the search for materials having large pores, which could accommodate and crack large molecules, pillared interlayer clays (PILCs) were considered as one of the important candidates for this specific purpose. These materials were reported to have strong acidity, large pore sizes and thermally stable up to 600ºC [36].

A simplified picture of the stages involved in pillaring is shown in Figure 2.4 [37]. It is apparent that the replacement of the exchangeable cations by large inorganic ions is responsible for creation of pore structure, which is then stabilized by thermal treatment with the removal of H_2O and OH groups. In this manner, dense nano-scale oxide pillared clays are inserted into the interlayer 'galleries' [27].

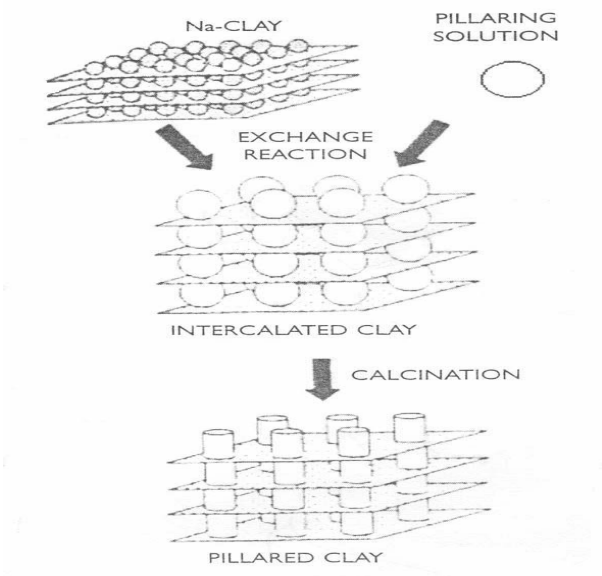

Figure 2.4. Pillaring

Polyoxocations of aluminum are the most often used cations for pillaring. Other inorganic polyoxocations often been used are made from the nitrate or chloride salts of transition metals such as zirconium, iron, chromium, or titanium. The large polycations are thought to make cross-links with basal layers through condensation of the hydroxyl groups after calcination at temperatures above 400ºC and result in a stable porous network that is similar to the structure of zeolites. Depending on the pillar species used, the resultant PILC's have their interlayer free spacings (d) expanded to 4-20 Å and surface area increased to 200-400 m^2g^{-1}. Different from zeolites, the pore size of PILC's is not unity and the pore size distribution is dependent on the calcination temperature. At temperatures higher than 700ºC, a portion of the microporous structure collapses and results in larger pores [32].

TiO_2 pillared clay has attracted much attention as a new type of photocatalyst, since the superior adsorption function accelerates photocatalytic reactions. TiO_2 pillared clay has a structure in which parallel two-dimensional silicate layers of clay are supported by nanoparticles of TiO_2 and micro to meso pores with large interlayer surface area are formed. On TiO_2 pillared clay, the organic substances in water are adsorbed and enriched in the pores, then photodegraded efficiently. Thus, TiO_2 pillared clay would be suitable for elimination of diluted organic pollutants [38].

2.3. Literature Survey

There are number of recent publications concerning the destruction of organic pollutants by photocatalytic degradation using TiO_2 incorporated clays.

In 1986, Sterte [39] studied on the synthesis and characterization of the TiO_2-cross-linked montmorillonite by cation exchange of montmorillonite with polymeric, partially hydrolyzed, Ti bearing cations. It was found that the most important difference between TiO_2-cross-linked montmorillonite (TiO_2-CLM) and other cross-linked smectites is the considerably larger interlayer spacing of this material. The interlayer spacing of TiO_2-CLM is approximately 18 Å compared with about 10 Å for smectites cross-linked with hyroxy-Al or hydroxy-Zr oligomeric cations. The larger interlayer distance is accompanied by a thermal and hydrothermal stability comparable with that of hydroxy-Al and hydroxy-Zr cross-linked smectites in various forms. Due to the large pore size of TiO_2-CLM, cracking of heavy oil fractions and biomass oils are two of the most interesting catalytic applications of this material.

In 1998, Kiteyama et al [40] carried out preparation of TiO_2-pillared saponite in a CH_3COOH aqueous solution. Titanium ion species to intercalate into the interlayer of saponite were obtained by an addition of Ti $(C_3H_7O)_4$ to an aqueous solution of CH_3COOH and by subsequent aging of the solution for prescribe time. Ti^{+4}-intercalated saponite including organic materials was obtained by ion exchange. After the sample was calcined at 500^oC in air, TiO_2 pillared saponite was obtained. The resulting Ti-pillared saponite possessed a large surface area and sharp pore size distribution. The molar ratio of Ti to CEC (cation exchange capacity) value of the clay in the reactant solution plays an important role for the intercalation of titanium ion into saponite.

Kaneko, Fuji, Kodama and Kiteyama [41] studied the preparation of TiO_2 pillared mica by using fluorine mica that is composed with magnesium silicate layer, in an aqueous solution of CH_3COOH containing titanium ion sol. Its characterization was carried out by X-ray diffraction (XRD), XPS and measurements of pore distribution. Titanium ion was intercalated in the interlayer of mica as an orgnometallic polymer. It was found that the ratio of Ti/CEC in the reactant plays an important role. The TiO_2 pillared mica having

good crystallinity, a large surface area and a sharp pore size distribution could be obtained by using the reactant at Ti/CEC=40.

In 2001, Shimizu et al [42] investigated the selective photo-oxidation of benzene and cyclohexane using TiO_2 pillared clays (mica, montmorillonite and saponite). The characterization results indicated that all the TiO_2 pillared clays contain TiO_2 with similar structure, anatase-like small particles, in the different silicate layers of clays. The solvent effect on the photo-oxidation of benzene on TiO_2 pillared clay was significant; both the activity and selectivity were increased by an addition of 10 per cent water into the acetonitrile solvent and they were further increased when the reaction was performed in the aqueous environment. In the latter condition, TiO_2 pillared clays showed higher selectivity to oxygenates than TiO_2 (Degussa P-25). The product distribution among oxygenates also depends on the type of the clay host, indicating that the photocatalytic properties of TiO_2 depend strongly on the type of clay host. For the cyclohexane photooxidation, TiO_2 pillared clay showed much higher selectivity than TiO_2, possibly because of the hydrophobic nature of pillared clay.

In another study, Ooka et al [43] used the TiO_2 pillared clay for the adsorption-photocatalytic degradation of the endocrine disruptors with various hydrophobicities (di-n-butyl phthalate and bisphenol-A) and discussed their influence on the photocatalytic degradation rate. The extent of hydrophobicity of interlayer surface of the TiO_2 pillared clay hydrothermally treated was compared with that of the untreated one. They found that, TiO_2 pillared clay both hydrothermally treated and untreated have hydrophobic interlayer surface. Hydrophobic interaction between adsorbate and interlayer surface of the TiO_2 pillared clay was one of the most predominant factors in adsorption of the endocrine disruptor in water. Adsorption of the endocrine disrupter in the TiO_2 pillared clay caused enrichment of the reactant and enhanced photocatalytic degradation. Photocatalytic degradation of endocrine disruptor on the TiO_2 pillared clay was also affected by crystallinity of TiO_2 pillar and quantum-size effect arising in TiO_2.

Four kinds of TiO_2 pillared clays were prepared from different raw clays (montmorillonite, saponite, fluorine, hectorite and fluorine mica), and their surface hydrophobicities and performances in adsorption-photocatalytic degradation of phthalate

esters (di-n-butylphtalate) were investigated in 2003 by Ooka et al [44]. It was found that surface hydrophobicity of the TiO_2 pillared clay could be controlled by the selection of host clay and it increased in order Sapo-Ti < Hecto-Ti < Mont-Ti < Mica-Ti. Adsorption performances of the TiO_2 pillared clay for the phthalate ester largely varied with the host clay and order agreed with that of surface hydrophobicity of the pillared clay. More hydrophobic-pillared clays showed a higher performance in adsorption. More hydrophilic-pillared clays showed a higher performance in photocatalytic degradation of Di-*n*-butyl phthalate (DBP) and dimethyl phthalate (DMP). Among the TiO_2 pillared clays prepared in this study, Mica-Ti showed the highest performance.

Ooka et al [38] studied the crystallization of TiO_2 pillars in the pillared montmorillonite by aqueous H_2O_2 treatment. They discovered that the treatment with aqueous H_2O_2 of sufficient concentration such as 1 wt per cent at room temperature improved anatase crystallinity and photocatalytic activity of TiO_2 pillars in the pillared montmorillonite with only a small effect on the porous structure and the hydrophobicity of the pillared clay. This method was found quite simple to be compared to hydrothermal treatment method and suggested for the improvement of crystallinity not only to the nanoparticle of TiO_2, but also to other oxide systems.

Witmann et al [45] studied the structural and photocatalytic properties of ordered mesoporous Ti-silicates, prepared by both impregnation (IMP) and coprecipitation (CP) methods. Catalyst characterization was carried out by inductively coupled plasma analysis, nitrogen adsorption-desorption, X-ray diffraction (XRD), transmission electron microscopy (TEM), and scanning electron microscopy (SEM) with energy dispersive X-ray analysis (EDX). Photocatalytic activity was evaluated for gaseous trichloroethylene (TCE) decomposition in a batch reactor under near-UV irradiation. It was found that; initial photocatalytic TCE degradation rate constants obtained with CP catalysts were systematically higher (up to a factor of 6) than those measured with IMP catalysts. To conclude, this work shows that CP Ti-silicates might be a promising new class of photocatalysts providing high adsorption capacity and photocatalytic activity towards gaseous volatile organic chemicals degradation.

3. EXPERIMENTAL

3.1. Actinometric Study

All the photochemical and photoelectrochemical methodologies require the measurement of accurate output/intensity of the illumination source. Indeed, an important step in studying any photo process involves a proper demonstration of actinometry either by physical methods employing photosensitive detectors or by chemical methods employing chemical actinometers. Due to the high sensitivity, chemical actinometer has widely been used where the intensity measurement relies on a light induced chemical process. Potassium ferrioxalate actinometry developed by Hatchard and Parker [44] has been appeared as the unique photochemical approach of liquid phase chemical actinometry.

3.1.1. Measurement Principle

Photolysis of aqueous solution of ferrioxalate in sulphuric acid proceeds according to the following stoichiometry;

$$[Fe^{3+}(C_2O_4)_3]^{3-} + h\nu \rightarrow [Fe^{2+}(C_2O_4)_2]^{2-} + C_2O_4^{-} \quad (3.1)$$

$$[Fe^{3+}(C_2O_4)_3]^{3-} + C_2O_4^{-} \rightarrow [Fe^{3+}(C_2O_4)_3]^{2-} + C_2O_4^{2-} \quad (3.2)$$

$$[Fe^{3+}(C_2O_4)_3]^{2-} \rightarrow [Fe^{2+}(C_2O_4)_2]^{2-} + 2CO_2 \quad (3.3)$$

The proceeding photo process produces one Fe^{2+} ion as a function of every Fe^{3+} ion lost and thus the conventional photochemical detection relies on the monitoring of product (Fe^{2+}) formation via the visible absorption spectroscopy of Fe^{2+}-phenanthroline complex at 254-510 nm [46,47].

3.1.2. Preparation of the Actinometer Solution

For all quantitative work, the preparation and the manipulation of the ferrioxalate solutions were carried out in a dark room using a red photographic safe light. Green crystals of $K_3Fe(C_2O_4)_3.3H_2O$ were prepared by mixing 3 volumes of 1.5 molar potassium oxalate solution with 1 volume of 1.5 molar ferric chloride solution with vigorous stirring. Green crystals were then recrystallized three times from water and then dried at 45˚C. The crystals were kept in the dark A one-actinometer depth of a 0.006 M solution absorbs 99 per cent or more of light of wavelengths up to 390 nm. In order to prepare the 0.006M solution, 2.947 g of the crystals were dissolved in 800 mL of water, 100 mL of 1N H_2SO_4 was added to the solution and this mixture was diluted to one liter.

The phenanthroline solution was 0.1 per cent by weight 1,1-phenanthroline monohydrate in water. It was prepared by dissolving 0.1 g of the solid in water and completing the volume to one liter. Solutions of phenanthroline were freshly prepared and kept in the dark, to avoid the slow photodegradation of the phenanthroline solution.

A buffer solution was prepared from 600 mL of 1N $NaC_2H_3O_2$ and 360 mL of 1N H_2SO_4 diluted to one liter [47].

3.1.3 Procedure for Actinometric Measurements

The actinometric solution of volume V_1 was irradiated for an appropriate period of time t determined experimentally , so as to produce a Fe^{2+} concentration between $1x10^{6-}$ and $3x10^{6-}$ mole/mL.. At time t, an aliquot volume V_2 pipetted in a volumetric flask V_3. A volume of buffer equal to about one half the volume of the photolyte taken is added, prior to the addition of 2 mL of phenanthroline solution, as recommended [47]. After dilution to V_3 with water and mixing the solution is allowed to stand for 30 minutes. An identical but unirradiated solution is used as the blank. All these operations are performed in the absence of actinometrically active light.

When $K_3Fe(C_2O_4)_3$ solutions in H_2SO_4 were irradiated, simultaneous reduction of ferric ion to the ferrous state and oxidation of oxalate ion occur. The complex mechanism can be simplified to the overall reaction represented by equation 3.4 [49];

$$2Fe(C_2O_4)_3^{3-} + h\nu \rightarrow 2Fe^{2+} + 5C_2O_4^{2-} + 2CO_2 \qquad (3.4)$$

The numbers of moles of Fe^{2+} formed are determined spectrophotometrically by developement with 1,10-phenanthroline resulting in the formation of a red $[Fe(phen)_3]^{2+}$ moiety (l_{max}=510nm). The absorbance of this solution is a measure of the quantity of light absorbed by the actinometer [49]. The measured optical density corresponds to the net ferrous ions value.

The equation 3.5 stated below was used for calculating the number of photons incident on the cell per second [50].

$$n_{abs}=\Sigma n_{abs}/t= \frac{6.023x1020\ V_1\ V_3\ (OD)}{V_2\ l\ (\varepsilon)\ (\varphi_\lambda)\ t} \qquad (3.5)$$

where, t=irradiation time of the actinometer (sec), V_1=volume of the actinometer solution irradiated (mL), V_2=volume of aliquot taken for analysis (mL), V_3=Final volume to which V_2 is diluted (mL), l=path lenght of the spectrophotometric cell (1.0 cm), (OD), measured "optical density difference" of the final solution at 510 nm, ε=the molar extinction coefficient of the Fe^{2+} complex (1.11x1014 L/mol.cm), φ_λ= quantum yield for the Fe^{2+} formation [47].

It has been reported that at least 10^{14} photons are necessary to initiate a photochemical reaction [51].

3.2. Reagents

All chemicals (Table 3.1) which were used in the experiments were of laboratory reagent grade and they were used without further purification. Deionized water was used for the preparation of all solutions.

3.2.1. β-Naphthol

β-Naphthol is an important chemical used extensively in the dyestuff, pigment, parfume and pesticide sectors. It also plays a significant role in the chemical industry. More than 130 dyestuffs and pigments and more than 20 dyestuff intermediates can be directly synthesized from β-Naphthol. It is a carcinogenic substance and possesses a great ecotoxicological problem. Phenol and Naphthalene like toxicity symptoms are induced by this compound [52].

Table 3.1. Reagents

Name	Formula	Supplier	Molecular weight (g/mol)	Purity %
Acetic Acid	CH_3COOH	Merck	60	100
Titanium dioxide Degussa P-25	TiO_2	Degussa	80	-
Titanium tetra propoxide	$Ti(OC_3H_7)_4$	Aldrich	284,26	98
Acetonitrile	CH_3CN	Merck	41,05	99,9
β-Naphthol	$(C_{10}H_8O)$ 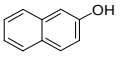	Aldrich	144,17	99
Iron(III) Nitrate	$Fe(NO_3)_3.9H_2O$	Merck	404	-
Sepiolite	$(Mg_4Si_6O_{15}(OH)_26H_2O)$	Eskişehir	658	-
Na-Montmorillonite	$(Na_{0.3}(Al,Mg)_2 Si_4O_{10}(OH)_24H_2O)$	University of Missouri Columbia	487	-

3.2.2. Sepiolite

Sepiolite is also called Meerschaum in German describing a soft mineral, which literally means ‘sea foam’. It is said in mythology for the goddess of beauty-Aphrodite. It is of an opaque white or cream color and when first extracted is soft, but it hardens on exposure to the sun or when dried in a warm room or in a furnace.

Meerschaum is one of the major reasons for the fame of Eskişehir. The purest and quality meerschaum blocks are mined in Eskisehir / Turkey. The deposits are confined to an area of only four square miles. It occurs in other masses, in various sizes and round. Because it is less dense than the water, it floats on the water. It is soft when newly extracted and looks like soap but, it hardens overtime. It is also called ‘white gold’ because of its colour. But a lesser quality meerschaum blocks also exits in the a few countries. A pure bone white meerschaum block indicates Turkish origin and top quality; a block containing flecks indicates a lesser grade from Africa's northern coasts, or Tanzania, referred to as African Coral Meerschaum.

It contains magnesium (Mg) and hydrosilicate in its structure. Magnesium doesn't make it strong and the hydrogen and oxygen don't make it cool. It is the crystalline structure; the arrangement of the magnesium, silicon, oxygen, and hydrogen atoms in a rigid crystalline structure that makes sepiolite (the clay mineral that is identified by pipe smokers as meerschaum) so good for smoking. Its high porosity acts as "natural filter" allows to absorb the nicotin that is why it takes a rich brown color as used [53].

3.2.3. Titanium Dioxide

Degussa P-25 TiO_2 was used in our preliminary experiments as a photocatalyst. It’s average particle size was 30 nm and BET surface area was 50 ± 15 m^2/g. TiO_2 has bandgap energy of 3.2 eV which corresponds to a wavelength of 380 nm. Its adsorption spectrum is given in Figure 3.1 [47].

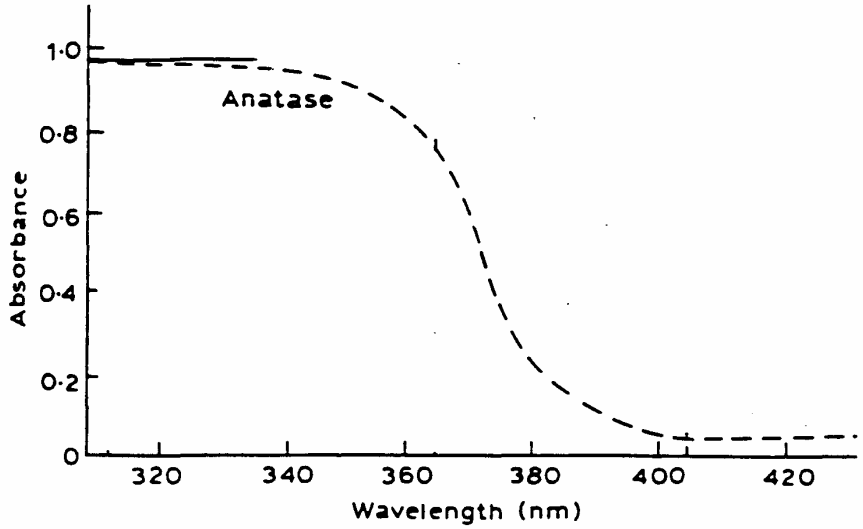

Figure 3.1. Adsorption spectrum of TiO_2 (Anatase)

3.3. Reactor

All the experiments were conducted in a Pyrex beaker of 200 mL. Pyrex glass is transparent to radiation over 300 nm. A laboratory constructed "irradiation box" (Figure 3.2) is equipped with eight black light fluorescent lamps (Philips TL 8W/08 F 8 T 5BLB) which provide light of wavelength 320-440 nm. Emission spectrum of a black light fluorescent lamp is given in Figure 3.3 [47]. The lamps are placed parallel to each other at equal distances to the reactor. The temperature of the system was controlled by a fun placed at the top of the irradiation box.

3.4. Preparation of Catalysts

3.4.1. TiO_2 Incorporated Clays

TiO_2 incorporated clays were prepared with the procedure reported by Kiteyama et al [44]. Titanium tetra propoxide [Ti $(OC_3H_7)_4$] (20 mL) was added to acetic acid solution of 80 wt per cent and produced dimeric species according to equation 3.1. The molar ratio of

Figure 3.2. Irradiation box

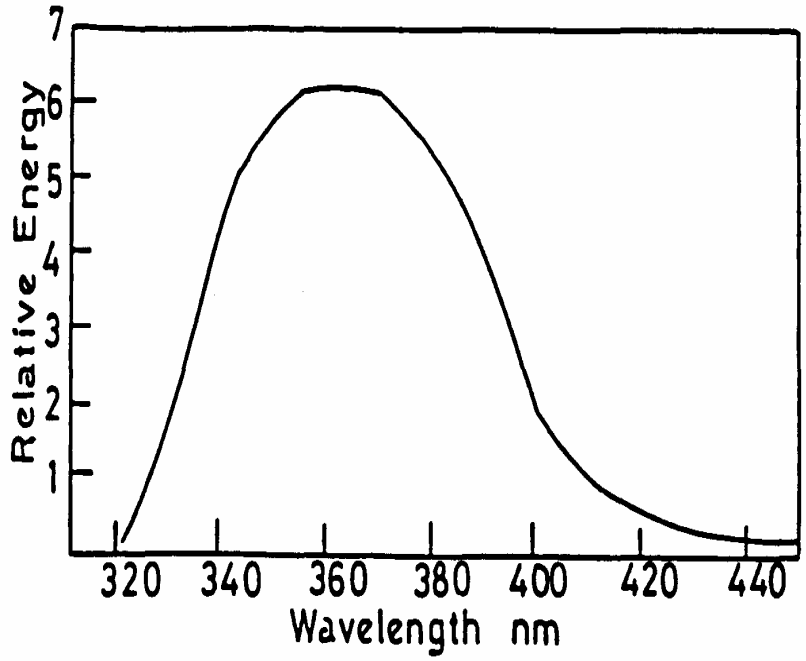

Figure 3.3. Emission spectrum of a black light fluorescent lamp

acetic acid to the alkoxide was 24. The resulting white slurry was stirred at 50°C for 3 hours in the dark.

$$2Ti\,(OC_3H_7)_4 + 2AcOH \rightarrow Ti_2(OC_3H_7)_6(OAc)_2 + 2C_3H_7OH \qquad (3.1)$$

Two octahedral Ti $(OC_3H_7)_3$ (OAc) units linked together by both (OC_3H_7) and (OAc) bridges. Therefore, it is suggested that the reaction of titanium tetrapropoxide with AcOH takes place during the aging process of the titanium-sol solution.

Two types of clays were used in this study, namely, Sepiolite with the cation exchange capacity (CEC) 0.15 meq g^{-1} and Na-Montmorillonite with cation exchange capacity (CEC) of 1.2 meq g^{-1} [31,42].

Additionaly, each of the clay samples were suspended in water (0.5 wt per cent) for 12 hours. Sonicator was used to ensure the uniform mixing of the suspension for 6 hours at 50˚C before the addition of the TiO_2 sol solution. The titania-sol was mixed with 0.5 wt per cent aqueous suspensions of the clays for 12 hours. In these mixed suspensions , the molar ratio of TiO_2 / raw clay was 17.7, and TiO_2 / (CEC of raw clay) was 40. Different amounts of TiO_2 sol (50 mL, 100mL and 200 mL) was added to the 0.5 wt per cent aqueous suspension of the raw clay and mixed over night at room temperature. This mixture was kept in the dark in order to prevent any interference from surrounding light before irradiation. The resulting material was separated by a centrifuge at 4000 rpm. The product was washed several times with water to remove excess sol solution and dried at 100°C for 12 hours. The resulting white product was TiO_2 incorporated clay.

3.4.2. Heat and H_2O_2 Treatments

According to the literature heat and H_2O_2 treatments improve the crystallinity of TiO_2 particles by decreasing the bulk defects and activating the lattice oxygen, respectively, resulting in enhanced photocatalytic activity of the catalysts for the degradation of organic pollutants.

In order to understand whether the photocatalytic activity is enhanced or not, catalysts prepared was exposed to the heat and H_2O_2 treatments.

In heat treated samples, TiO_2 incorporated clays were calcined at 500^oC about 6 hours. The colour of these samples was bright-yellow. In H_2O_2 treated samples, TiO_2 incorporated clays were dispersed in aqueous H_2O_2 solutions of 2 wt per cent about 2 hours at room temperature. The treated product was separated by centrifugation, washed several times with water and dried at 100^oC. The colour of these samples was bright-yellow. Calcination at 500^oC was applied to H_2O_2 treated samples about 6 hours and the colour was changed to yellow.

3.4.3. Preparation of Na-Sepiolite-TiO_2 Catalysts

1 L of 0.25 M, 1 M and 3 M of sodium chloride solution were prepared by solving the required amount of NaCl in water. 12.5 g of Sepiolite was then added to each of these solutions to obtain Na-Sepiolite. These solutions were mixed for 24 hours at room temperature. The products were separated by centrifugation at 4000 rpm, washed with deionized water several times and dried at 60^oC, at room temperature for 5 days. Then, TiO_2 was intercalated into the layers of these samples according to the procedure mentioned above.

3.4.4. Fe^{3+}-Exchanged TiO_2 Incorporated Sepiolite and Na-Montmorillonite

The iron exchanged TiO_2 incorporated catalysts were prepared by using the conventional ion-exchange procedure. 1 g of Sepiolite-TiO_2 (100^oC) and Na-Montmorillonite-TiO_2 (100^oC) were added to 100 mL of 0.05 M $Fe(NO_3)_3.9H_2O$ solution with constant stirring. The mixture was kept at 50˚C for 6 hours and then filtered and washed with deionized water. The exchange process repeated three times. The obtained Fe-Sepiolite-TiO_2 and Fe-Na-Montmorillonite-TiO_2 (100^oC) catalysts were first dried at 120˚C in air over night then calcined at 500^oC for 6 hours.

3.5. Analysis

3.5.1. Characterization of the Catalysts

The thermal property of the samples was studied by Universal V 3.9 A TGA operating in N_2 atmosphere. The runs were carried out in dynamic conditions at $10^oC\ min^{-1}$ in between 30-750^{o}C. X–ray diffraction patterns of the samples were recorded on a Rigaku-D/MAX-Ultima diffractometer using Cu Kα radiation (λ = 1.54 Å) operating at 40 kV and 40 mA and scanning rate of $2^o\ min^{-1}$. The surface morphology of the sample was obtained by using Scanning Electron Microscopy in combination with Energy Dispersive X-ray analysis on an ESEM-FEG/EDAX Philips XL-30 instrument operating at 20 kV. Samples for STEM were prepared by placing a drop of 1 wt per cent suspension solution on a carbon grid and dried at 70^{o}C.

3.5.2. Photocatalytic Degradation of β-Naphthol

Prior to illumination, suspensions containing 0.2 g of catalyst in 200 mL of β-Naphthol were magnetically stirred at constant speed for the 30 minutes needed to achieve adsorption-desorption equilibration at room temperature. After commencing UV illumination, small aliquots of the stirred suspension were withdrawn by a syringe from the UV-illuminated suspension and filtered by using Millipore films (0.45 μm).

Following photodegradation, the concentration of remaining β-Naphthol was analyzed by High Performance Liquid Chromatography (HPLC, CECIL 1100 series), using a CE 1100 liquid chromatography pump with CE 1220 variable wavelength monitor and a UV detector. The stationary phase was a Hypersil ODS column (particle size 10 μm). The mobile phase was an acetonitrile:water (70:30) mixture for β-Naphthol. Periodic sampling (once in a hour) and duplicate HPLC analysis was continued for 5 hours.

4. RESULTS and DISCUSSION

4.1. Results for the Actinometric Measurement

The results of the actinometric study is given in Table 4.1.

Table 4.1. Actinometric results for black-light flourescent lamps

V_1=100 mL
V_2=10 mL
V_3=2 mL
t=120 s
OD=0.78
φ_λ=1.21
n_{abs}=4.7x10^{15} photon/sec or 7.8x10^{-9} einstein/sec

4.2. Characterization

4.2.1. Thermal Gravimetric Analysis (TGA)

4.2.1.1. Na-Montmorillonite and Na-Montmorillonite–TiO_2 Catalysts: Figure 4.1 represents the TGA curves of the pure Na-Montmorillonite and Na-Montmorillonite-TiO_2 in the temperature range from 30 to 750ºC. After losing the physically adsorbed water at a temperature of less than about 100ºC, the weight of the Na-Montmorillonite remained nearly constant to about 500ºC, where weight loss due to dehydroxylation of the structure began. The Na-Montmorillonite-TiO_2 sample, however, showed a more continous loss of weight in temperature range of 110-370ºC. The weight loss in this process is attributed to the combustion of organic compound adsorbed on the surface of the sample. Between 390 and 750ºC, due to the combustion of the organic compound which exist in the interlayer of Na-Montmorillonite. The results indicate that there are two types of organic compounds: one is intercalated into the interlayer of Na-Montmorillonite as Ti-organic compound and the other is organic compound such as acetic acit and propanol adsorbed on the surface of Na-Montmorillonite-TiO_2.

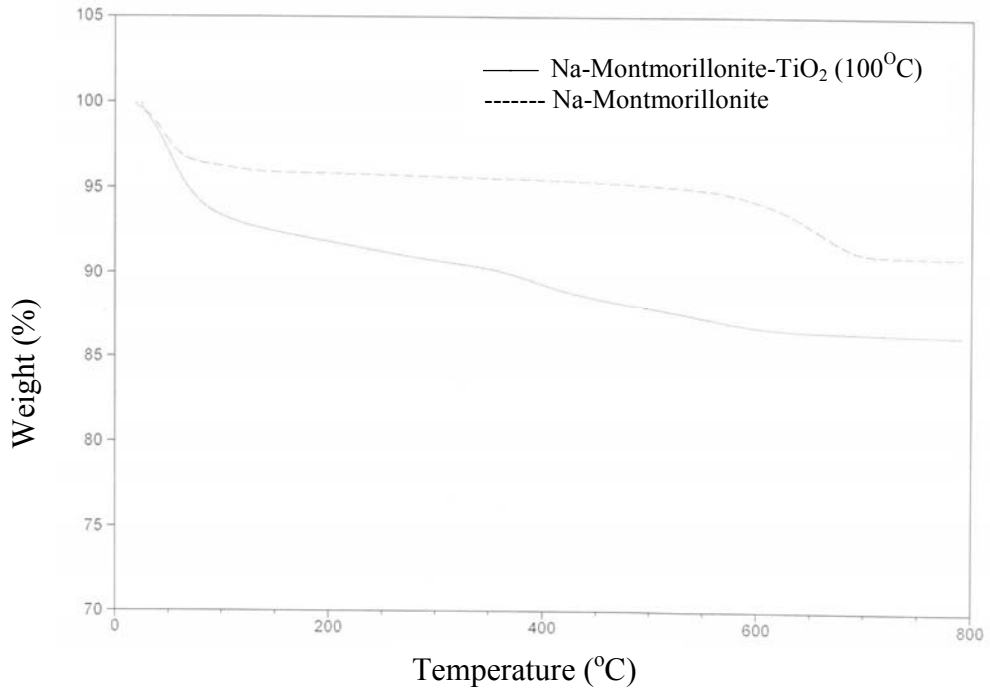

Figure 4.1. TGA curves of the pure Na-Montmorillonite and Na-Montmorillonite-TiO_2

4.2.1.2. Sepiolite and Sepiolite–TiO_2 Catalysts: TGA curves of the pure Sepiolite and Sepiolite-TiO_2 were examined in the temperature range from 30 to 750ºC (Figure 4.2). Pure Sepiolite showed a higher loss of weight (7.8 wt per cent) compared to the Sepiolite-TiO_2 (7 wt per cent) below 100ºC. This is attributed to dehydration of the physically adsorbed water. After that point, Sepiolite gradually lost its weight (14 per cent) between 120 and 750ºC due to dehydroxylation of the structural water. However, Sepiolite-TiO_2 showed a little bit larger amount of weight loss (15 per cent) than the pure Sepiolite in the same temperature range. This may be attributed to the decomposition of organic compound present on the surface of the catalyst. Since there is no more loose observable, it is accepted that an interlayer organic compound does not form in the presence of Sepiolite-TiO_2 catalyst.

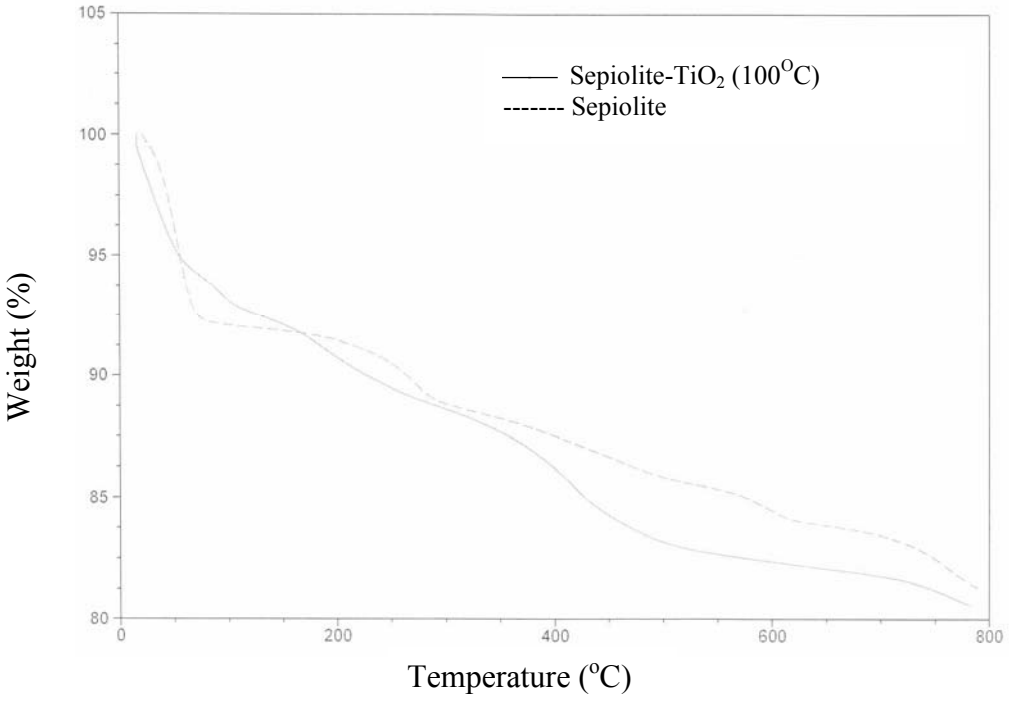

Figure 4.2. TGA curves of the pure Sepiolite and Sepiolite-TiO_2

4.2.2. X-ray Diffraction Analysis (XRD)

W.L Bragg treated the diffraction of X-rays by crystals [54]. When X-ray beam strikes a crystal surface at some angle θ, a portion is scaterred by the layer of atoms at the surface. The unscattered portion of the beam penetrates to the second layer of atoms where again a fraction is scattered, and the remainder passes on to the third layer (Figure 4.3) [54]. The cumulative effect of this scattering from the regularly spaced centers of the crystal is diffraction of the beam.

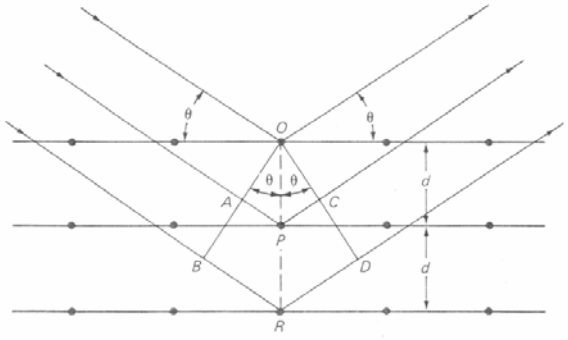

Figure 4.3. Diffraction of X-rays by a crystal

The requirements for X-ray diffraction are that (1) the spacing between layers of atoms must be roughly the same as the wavelength of the radiation and (2) the scattering centers must be spatially distributed in a highly regular way. Here, a narrow beam of radiation strikes the crystal surface at incident angle θ; scattering occurs as a consequence of interaction the radiation with atoms located at O, P, and R. If the distance

$$AP\text{-}PC = n\lambda \tag{4.1}$$

where n is an integer, the scattered radiation will be in the phase at OCD, and the crystal will appear to reflect the X-radiation. But it is readily seen that

$$AP = PC = d \sin \theta \tag{4.2}$$

where d is the interplaner distance of the crystal. Thus, it can be written that the conditions for constructive interference of the beam at angle θ are

$$n\lambda = 2d \sin \theta \tag{4.3}$$

Equation 4.3 is called the Bragg equation and is of fundamental importance [50]. Note that X-rays appear to be reflected from the crystal only if the angle of incidence satisfies the condition that

$$\sin \theta = n\lambda / 2d \tag{4.4}$$

Thus, there is an inverse relation between θ and d, i.e, a decrease in the value of θ can be interpreted as an increase in the d-spacings of the clay minerals or vice versa.

4.2.2.1. Anatase: In order to obtain information about the structural characterization of TiO_2, titania-sol was examined, before the addition of clay minerals. Briefly, TiO_2 material was prepared by the sol-gel method. Titanium tetrapropoxide was used as a precursor for the preparation and suspended in 80 wt per cent acetic acid, to which an appropriate amount of water was added while the suspension was ultrasonically dispersed

to ensure good homogeneity during hydrolysis. Precipitation of hydrated TiO_2 occurred in a few minutes at room temperature. The powder was then washed, and the precipitate was dried at 100°C over night. After these processes, the solid powders obtained had been calcined at different temperatures. Samples heated at 100°C and 200°C showed clear anatase diffractions of (101), (004), (200), (105), (211) at 2θ=25.3, 37.8, 48, 54, 55°, respectively (Figure 4.4). For the sample heated at 500°C, additional anatase diffractions of (103) and (112) were observed at 2θ =37 and 38.6°. This is due to the heat-induced growth of titania particles. This growth contributes to the increase of crystallinity since higher ordering in the structure of titania particles makes X-ray peaks sharper and narrower. Although anatase-rutile transtion is known to occur at calcination temperatures above 400°C, no rutile formation was observed in the samples calcined up to 500°C, as examplified by the absence of the main rutile (110) diffraction peak at 2θ=27.4°. The heights, full width half-maximum (FWHM) values and the crystallite sizes of the prepared anatase samples were summarized in Table 4.2. The crystallite size of TiO_2 particles has been estimated from the Scherrer's equation using the XRD line broadening for (101) plane diffraction of main anatase peak at 2θ=25.4°. Highest values of height and crystallite sizes were obtained for the samples prepared at 500°C.

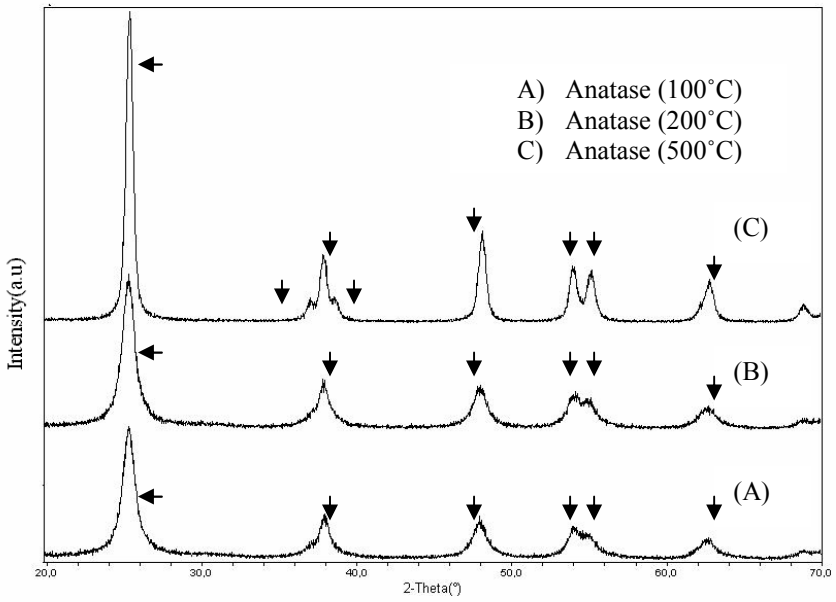

Figure 4.4. XRD patterns of A) Anatase (100˚C), B) Anatase (200˚C), C) Anatase (500˚C)

Table 4.2. Heights, FWHM values and crystallite sizes of the anatase samples $2\theta=25.4^{o}$

	Height	FWHM	Crystallite Size (nm)
Anatase 100°C	449	0.718	1.9
Anatase 200°C	544	0.696	2.0
Anatase 500°C	1283	0.495	3.0

4.2.2.2. Sepiolite-TiO_2 Catalysts: Effect of TiO_2 Content X-ray diffraction patterns of Sepiolite-TiO_2 complexes were prepared as containing mixtures of Sepiolite and different titania-sol amounts, 50 mL, 100 mL and 200 mL, referred as Sepiolite-TiO_2-50 mL, Sepiolite-TiO_2-100 mL and Sepiolite-TiO_2-200 mL, respectively.

For pure Sepiolite, the XRD pattern on a small angle range (Figure 4.5) showed (110) difraction at $2\theta=7.4^{o}$ with a basal spacing (d) of 11.93 Å. For the catalysts, Sepiolite-TiO_2 (50 mL), Sepiolite-TiO_2 (100 mL), Sepiolite-TiO_2 (200 mL), (110) peak intensity of the original clay was found to decrease. In addition to this, there was a small decline in 2θ values which corresponded to small increments in the d-spacing of the Sepiolite (Table 4.3). These observations deduce that with the addition of the titania-sol, the ordered silicate structure of the clay was lost.

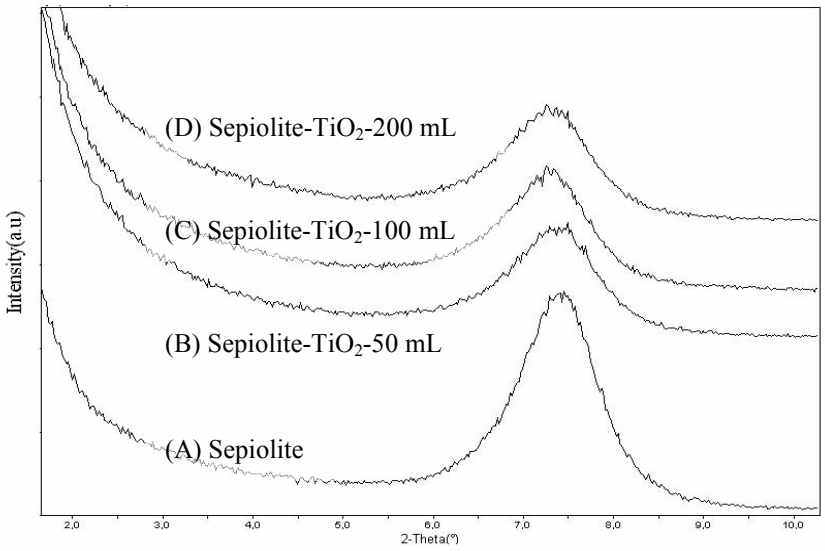

Figure 4.5. Small angle XRD patterns of A) Sepiolite, B) Sepiolite-TiO_2 (50 mL), C) Sepiolite-TiO_2 (100 mL), D) Sepiolite-TiO_2 (200 mL)

Table 4.3. 2θ (^{o})and d_{110} (Å) values of pure Sepiolite and Sepiolite-TiO_2 catalysts

Clay	2θ	d_{110}
Sepiolite	7.40	11.93
Catalysts		
Sepiolite-TiO_2 (50 mL)	7.33	12.06
Sepiolite-TiO_2 (100 mL)	7.26	12.16
Sepiolite-TiO_2 (200 mL)	7.36	12.00

On wide angle range (2θ=15-70º), XRD patterns showed clear anatase diffractions of (101), (103), (004), (112), (200), (105) overlapped with (211) at 2θ=25.3, 37.8, 38.68, 48, 54, 55^{o}, respectively and were indicated by arrows (Figure 4.6). No anatase peak was observed in the pure Sepiolite.

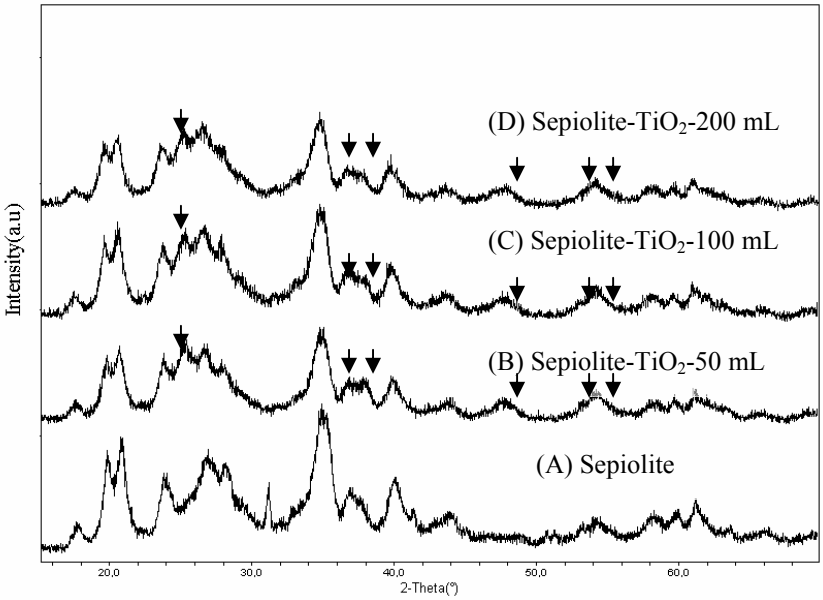

Figure 4.6. Wide angle XRD patterns of A) Sepiolite, B) Sepiolite-TiO_2 (50 mL), C) Sepiolite-TiO_2 (100 mL), D) Sepiolite-TiO_2 (200 mL)

Table 4.4. gives the height, FWHM values and the crytallite size values of anatase main peak at 2θ=25.4^{o} in the corresponding samples. For 50 mL and 100 mL titania incorparated catalysts, heights and crystallite sizes of the anatase main peak were increased. Also, a relatively narrower FWHM value was obtained for the catalyst including 100 mL of titania as it was expected. However, a further increase in titania

loading (200 mL), decreased the anatase main peak height and the crystalline size, increased the FWHM value. This may be attributed to the enhanced silica-titania interaction and thereby suppresed growth of anatase crystallite size. Besides, pores of the clay were thought to be more occupied with the increasing titania loading and limiting the number of available active sites for the adsorption of the probe molecule. Therefore, 50 mL of titania incorporation was used as an optimal amount throught the experiments.

Table 4.4. Heights, FWHM values and crystallite sizes of the anatase main peak at $2\theta=25.4^{o}$

	Height	FWHM	Crystallite Size (nm)
Sepiolite-TiO_2 (50mL)	43	0.330	4.2
Sepiolite-TiO_2 (100mL)	115	0.317	4.4
Sepiolite-TiO_2 (200mL)	90	0.457	3.0

4.2.2.3. Sepiolite-TiO_2 Catalysts: Effect of Heat and H_2O_2 Treatment The XRD patterns of pure Sepiolite, Sepiolite-TiO_2 (100^{o}C) and Sepiolite-TiO_2-H_2O_2 (100^{o}C) catalysts (Figure 4.7) were first examined on small angle range (2θ=0-10º).

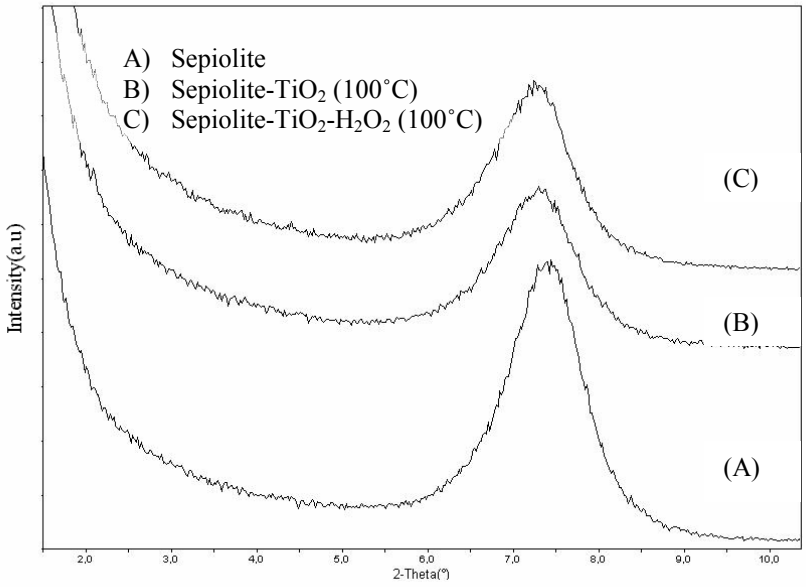

Figure 4.7. Small angle XRD patterns of A) Sepiolite, B) Sepiolite-TiO_2 (100˚C), C) Sepiolite-TiO_2-H_2O_2 (100˚C)

Pure sepiolite showed (110) diffraction at 2θ=7.40º with a basal spacing of 11.93 Å. An obvious decrease in the peak intensity of the pure clay was observed after addition of the titania-sol. Also, in accordance with Bragg's Law, toward smaller angles, the d-spacings of Sepiolite-TiO_2 (100°C) and Sepiolite-TiO_2-H_2O_2 (100°C) catalysts were found to be 11.96 and 12.17 Å, respectively (Table 4.5). Since these increments were not significant, separation of silicate layers throught the clay was not enough for the formation of TiO_2 pillars.

Table 4.5. 2θ (°)and d_{110} (Å) values of pure Sepiolite and Sepiolite-TiO_2catalysts

Clay	2θ	d_{110} of clay
Sepiolite	7.40	11.93
Catalysts		
Sepiolite-TiO_2 (100°C)	7.38	11.96
Sepiolite-TiO_2-H_2O_2 (100°C)	7.26	12.17
Sepiolite-TiO_2 (500°C)	7.50	11.77
Sepiolite-TiO_2-H_2O_2 (500°C)	7.50	11.77

At higher angles (2θ=15-70º), information was gained about TiO_2 crystallinity. No anatase peak was observed in the pure clay sample. On the other hand, Sepiolite-TiO_2 (100°C) and Sepiolite-TiO_2-H_2O_2 (100°C) catalysts showed clear anatase diffractions of (101), (103), (004), (112), (200), (105) overlapped with (211) at 2θ=25.3, 37.8, 38.68, 48, 54, 55°, respectively and were indicated by arrows (Figure 4.8). Thus, considering both small and wide angle patterns of the catalysts prepared at 100°C, though TiO_2 particles did not form pillars, they are believed to be incorporated into the structural channels and edges of the Sepiolite.

For heat treated titania loaded catalysts, small angle peak intensities were observed to be extremely smaller than those prepared at 100°C (Figure 4.9). The insignificant intensities compensate with a shift in 2θ toward higher values and smaller d-spacings (Table 4.5). These indicated a higher fractional loss of ordered silica structure of the Sepiolite.

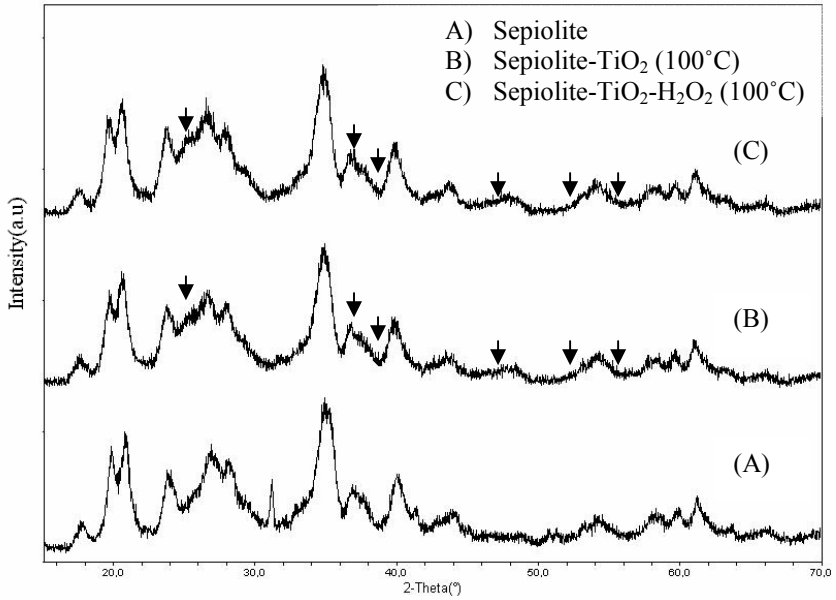

Figure 4.8. Wide angle XRD patterns of A) Sepiolite, B) Sepiolite-TiO_2(100˚C), C) Sepiolite-TiO_2-H_2O_2 (100˚C)

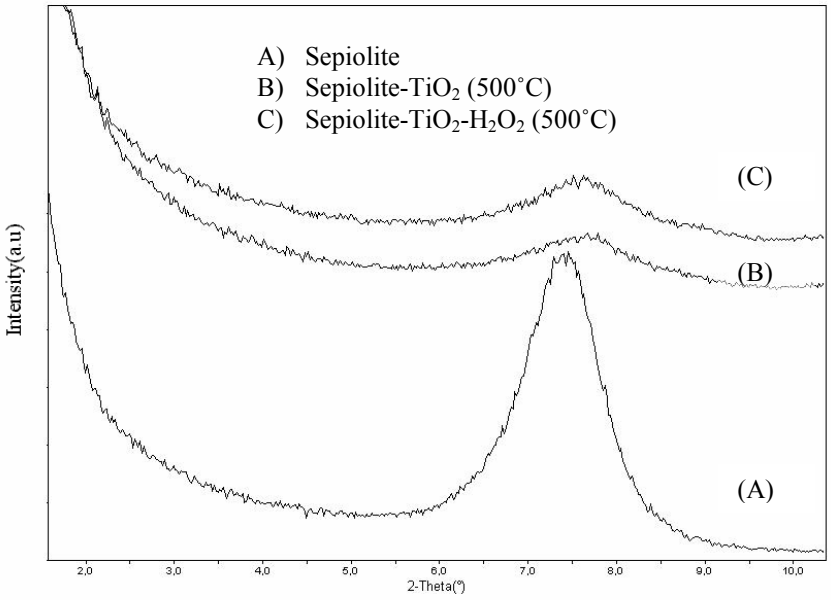

Figure 4.9. Small angle XRD patterns of A) Sepiolite, B) Sepiolite-TiO_2 (500˚C), C) Sepiolite-TiO_2-H_2O_2 (500˚C)

The wide angle XRD patterns of Sepiolite-TiO_2 (500^oC) and Sepiolite-TiO_2-H_2O_2 (500^oC) were characteristics of anatase TiO_2 with diffractions of (101), (103), (004), (112), (200), (105) overlapped with (211) at 2θ=25.3 37, 37.8, 38.68, 48, 54, 55^o, respectively and were indicated by arrows (Figure 4.10).

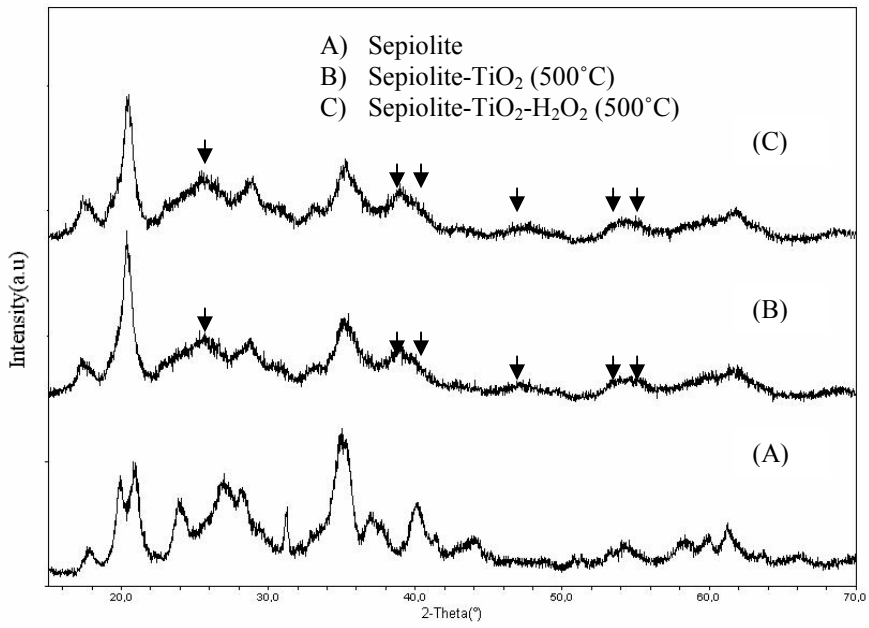

Figure 4.10. Wide angle XRD patterns of A) Sepiolite, B) Sepiolite-TiO_2 (500˚C), C) Sepiolite-TiO_2-H_2O_2 (500˚C)

Heights of the main anatase peaks were found to increase in both H_2O_2 and heat treated samples (Table 4.6). However, the XRD peaks did not become sharper as the calcination temperature was increased. Instead, for H_2O_2 treated samples (prepared at different temperatures) and for heat treated samples (prepared without H_2O_2), a broadening was observed in the peaks which has resulted with higher FWHM values. Due to this broadenig, at higher calcination temperature, the crystallites formed were smaller in size. H_2O_2 treatment did not change this crystalline growth either. Therefore, it can be concluded that neither H_2O_2 nor heat treatment promoted the crystalline growth in the Sepiolite-TiO_2 based catalysts. The highest crystalline size was obtained for Sepiolite-TiO_2 (100^oC) catalysts as 6.9 nm.

Table 4.6. Heights, FWHM values and crystallite sizes of the anatase main peak at 2θ = 25.4°

	Height	FWHM	Crystallite Size (nm)
Sepiolite-TiO_2 (100°C)	29	0.203	6.9
Sepiolite-TiO_2-H_2O_2 (100°C)	30	0.302	4.6
Sepiolite-TiO_2 (500°C)	33	0.633	2.2
Sepiolite-TiO_2-H_2O_2 (500°C)	45	0.634	2.2

4.2.2.4. Montmorillonite-TiO_2 Catalysts: Effect of Heat and H_2O_2 Treatment Small angle XRD patterns (2θ=0-10º) of pure Na-Montmorillonite, Na-Montmorillonite-TiO_2 (100°C) and Na-Montmorillonite-TiO_2-H_2O_2 (100°C) catalysts were exhibited in Figure 4.11.

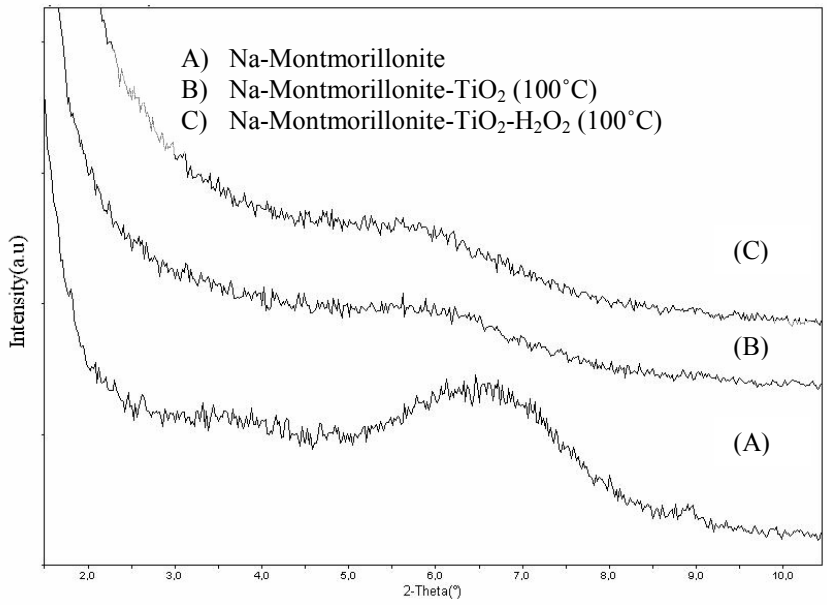

Figure 4.11. Small angle XRD patterns of A) Na-Montmorillonite, B) Na-Montmorillonite-TiO_2 (100˚C), C) Na-Montmorillonite-TiO_2-H_2O_2 (100˚C)

Pure Na-Montmorillonite showed clear (001) diffraction at 2θ=6.70° with the corresponding basal spacing (d) value of 13.18 Å. (001) peak intensity of the pure clay showed a clear decrease by the addition of the titania-sol. Na-Montmorillonite-TiO_2 (100°C) and Na-Montmorillonite-TiO_2-H_2O_2 (100°C) presented a shift with respect to the pure Na-Montmorillonite in their 2θ values towards smaller angles (Table 4.7). Additionally, the d-spacings of the Na-Montmorillonite-TiO_2 (100°C) and Na-

Montmorillonite-TiO_2-H_2O_2 (100^oC) catalysts were found as 15.33 and 17.04 Å, respectively (Table 4.7). Therefore, in contrast to the Sepiolite-TiO_2 catalysts, formation of TiO_2 pillars is possible in between the separated silicate layers of Na-Montmorillonite.

Table 4.7. 2θ (^{o}) and d_{001} (Å) values of pure Na-Montmorillonite and Na-Montmorillonite-TiO_2 catalysts

Clay	2θ	d_{001} of clay
Na-Montmorillonite	6.70	13.18
Catalysts		
Na-Montmorillonite-TiO_2 (100^oC)	5.75	15.33
Na-Montmorillonite-TiO_2-H_2O_2 (100^oC)	5.18	17.04
Na-Montmorillonite-TiO_2 (500^oC)	5.06	17.41
Na-Montmorillonite-TiO_2-H_2O_2 (500^oC)	5.03	17.51

Wide angle XRD analysis of pure Na-Montmorillonite indicated the presence of quartz mainly at 2θ=20.86 and 26.66^o (Figure 4.12). No anatase peak was observed in the pure clay. Na-Montmorillonite-TiO_2 (100^oC) and Na-Montmorillonite-H_2O_2-TiO_2 (100^oC) catalysts, however, showed very clear and broad anatase diffractions of (101), (004), 112), (200) and (105) overlapped with (211) at 2θ=25, 37.6, 38.6, 48, 54 and 55^o, respectively. Anatase peaks did not coincide with the peaks of quartz especially in between 2θ=20-30^o. Peak intensities of the quartz and pure Na-Montmorillonite decreased with the intercalation of TiO_2 in the silicate layers.

Heat treated catalysts displayed shifts in (001) diffraction peak of the clay toward smaller angles with an increase in d-spacings (Table 4.7, Figure 4.13). Although H_2O_2 treatment at 500^oC did not significantly change the d-spacing of the corresponding catalyst, it can be still accepted that heat treated samples lost the ordered structure of Na-Montmorillonite more compared to the ones prepared at 100^oC.

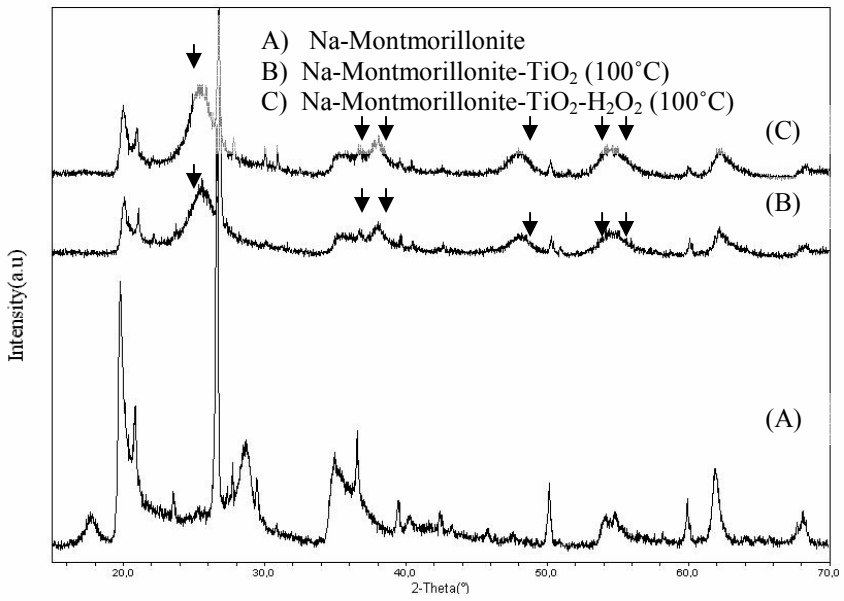

Figure 4.12. Wide angle XRD patterns of A) Na-Montmorillonite, B) Na-Montmorillonite-TiO_2 (100˚C), C) Na-Montmorillonite-TiO_2-H_2O_2 (100˚C)

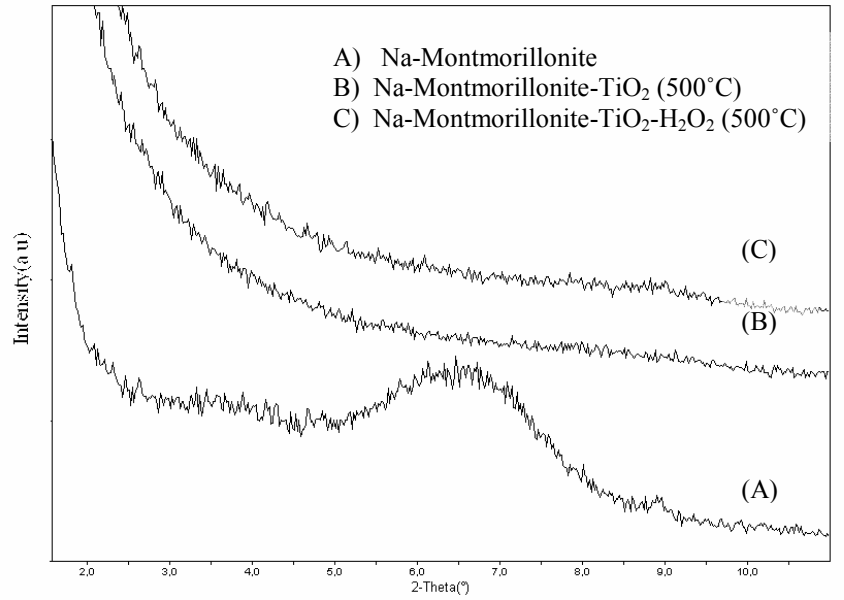

Figure 4.13. Small angle XRD patterns of A) Na-Montmorillonite, B) Na-Montmorillonite-TiO_2 (500˚C), C) Na-Montmorillonite-TiO_2-H_2O_2 (500˚C)

Wide angle XRD patterns of the Na-Montmorillonite-TiO_2 (500^oC) and Na-Montmorillonite-TiO_2-H_2O_2 (500^oC) presented the anatase phase of the TiO_2 with diffractions of (101), (004), 112), (200) and (105) overlapped with (211) at 2θ=25, 37.6, 38.6, 48, 54 and 55^o, respectively (Figure 4.14).

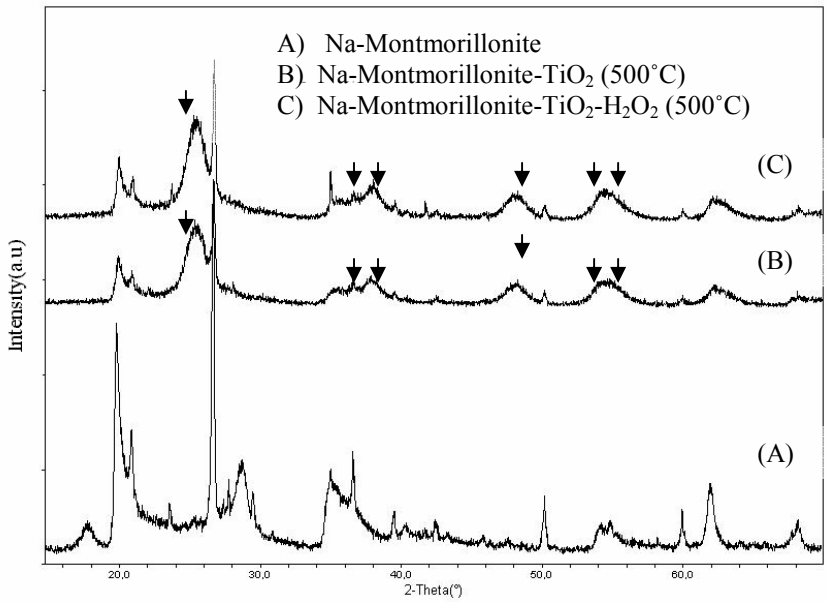

Figure 4.14. Wide angle XRD patterns of A) Na-Montmorillonite, B) Na-Montmorillonite-TiO_2 (500˚C), C) Na-Montmorillonite-TiO_2-H_2O_2 (500˚C)

For the Na-Montmorillonite based catalysts, as it can be seen from the Table 4.8, Na-Montmorillonite-TiO_2 (100^oC) showed a relatively higher crystallite size value compared to the Na-Montmorillonite-TiO_2-H_2O_2 (100^oC). Similar to the samples prepared at 100^oC, Na-Montmorillonite-TiO_2 (500^oC) also showed a relatively higher crystallite size compared to the Na-Montmorillonite-TiO_2-H_2O_2 (500^oC). Thus, H_2O_2 treatment did not affect the crystallite growth of the titania. Besides, an improvement in the peak intensities and a slight increase in the crystallite sizes were observed after the application of heat treatment. However, neither heat treated nor H_2O_2 treated catalysts showed a significant difference in the heights, full-width half maximum values and crystallite sizes of the main anatase peak.

Table 4.8. Heights, FWHM values and crystallite sizes of the anatase main peak at $2\theta = 25.4^{o}$

	Height	FWHM	Crystallite Size (nm)
Na-Montmorillonite-TiO_2 ($100^{o}C$)	85	0.868	1.6
Na-Montmorillonite-TiO_2-H_2O_2 ($100^{o}C$)	103	0.908	1.5
Na-Montmorillonite-TiO_2 ($500^{o}C$)	140	0.806	1.7
Na-Montmorillonite-TiO_2-H_2O_2 ($500^{o}C$)	175	0.868	1.6

4.2.2.5. Sepiolite-TiO_2 Catalysts: Effect of Na^+ Ion Concentration and H_2O_2 Treatment In natural Sepiolite, Mg^{2+} ions located at the borders of the Sepiolite's channels. However, by submitting Sepiolites to NaCl treatment it is possible to replace part of Mg^{2+} ions by Na^+ ions. Once, the Na^+ form of Sepiolite is obtained, the ion exchange of Na^+ by any other alkali or transition metal ion can be easily achieved [32].

Considering this, Sepiolite-TiO_2 catalysts were submitted to NaCl treatment to enhance the formation of TiO_2 nano particles at the edges of the clay's channels (Figure 4.15) [32].

Small angle range ($2\theta = 0–10^{o}$) XRD patterns of Sepiolite, Sepiolite-TiO_2 and Na-Sepiolite-TiO_2 catalysts containing Na^+ ions in the range of 0.25 M to 3.0 M were presented in Figure 4.16. Every sample showed (110) diffraction near 2θ=7.10-7.38º originating from pure Sepolite (2θ=7.40°). Those values of basal spacing were in the range from 11.93 to 12.40 Å. According to these results, there was a small shift on the (110) diffraction toward smaller angles and no significant increase between the silicate layers of the clay (Table 4.9).

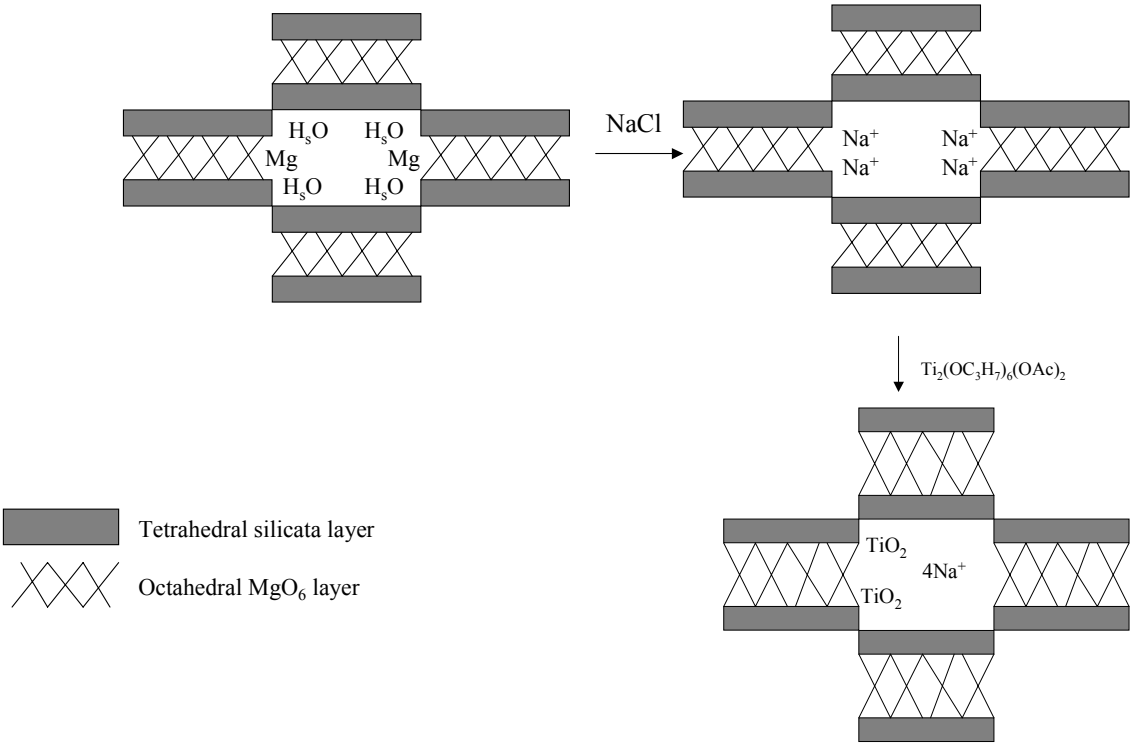

Figure 4.15. NaCl treatment: Replacement of Mg^{2+} ions by Na^+ ions around the channels of the Sepiolite structure

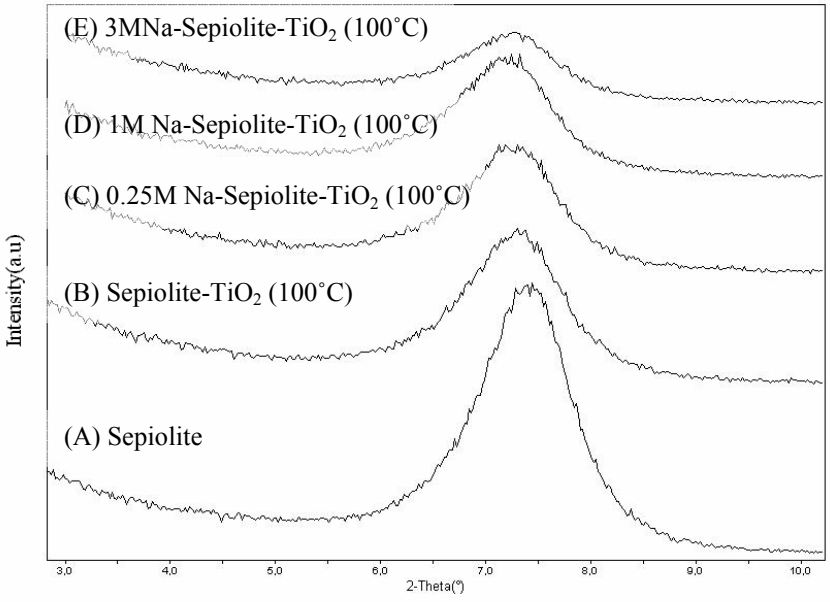

Figure 4.16. Small angle XRD patterns of A) Sepiolite, B) Sepiolite-TiO_2 (100˚C), C) 0.25M Na-Sepiolite-TiO_2 (100˚C), D) 1M Na-Sepiolite-TiO_2 (100˚C) E) 3M Na-Sepiolite-TiO_2 (100˚C)

Table 4.9. 2θ (^{o}) and d_{110} (Å) values of pure Sepiolite and Na-Sepiolite-TiO_2 catalysts

Clay	2θ	d_{110}
Sepiolite	7.40	11.93
Catalysts		
Sepiolite-TiO_2	7.38	11.96
0.25M Na-Sepiolite-TiO_2	7.10	12.40
1M Na-Sepiolite-TiO_2	7.32	12.00
3M Na-Sepiolite-TiO_2	7.38	11.96
Sepiolite-TiO_2-H_2O_2	7.26	12.17
0.25M Na-Sepiolite-TiO_2-H_2O_2	7.27	12.10
1M Na-Sepiolite-TiO_2-H_2O_2	7.33	12.00
3M Na-Sepiolite-TiO_2-H_2O_2	7.18	12.30

However, a considerable decrease was observed in the (110) peak intensities of the samples. In wide angle XRD patterns of the corresponding catalysts, no anatase peak was observed in the pure Sepiolite. Other samples showed clear anatase diffractions of (101), (103), (004), (112), (200), (105) overlapped with (211) at 2θ=25.3, 37.8, 38.68, 48, 54, 55^{o}respectively (Figure 4.17).

For the H_2O_2 treated catalysts, basal spacing (d) remained almost constant with the small shift in 2θ values toward smaller angles (Figure 4.18). Wide angle XRD patterns of the H_2O_2 treated catalysts showed clear anatase diffractions of (101), (103), (004), (112), (200), (105) overlapped with (211) at 2θ=25, 37.6, 38.6, 48, 54 and 55^o, respectively (Figure 4.19).

Anatase main peak intensities were significantly raised in Na^+ ion placed Sepiolite-TiO_2 catalysts (Table 4.10). In addition, change in concentration of Na^+ ion made a remarkable effect in 2θ = 25.4^o peak intensities, specifically for the 3M Na-Sepiolite-TiO_2 (100^{o}C) sample. For the same catalysts, on the other hand, H_2O_2 treatment decreased the intensity of the main anatase peak. The lowest peak heights and FWHM values were obtained with 1M Na-Sepiolite-TiO_2 (100^{o}C) and 1M Na-Sepiolite-TiO_2-H_2O_2 (100^{o}C) catalysts.

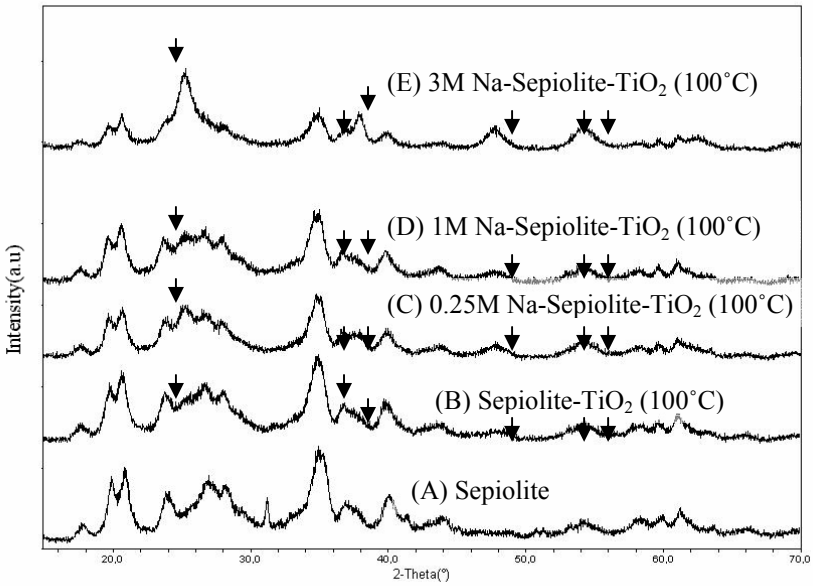

Figure 4.17. Wide angle XRD patterns of A) Sepiolite, B) Sepiolite-TiO_2 (100˚C), C) 0.25M Na-Sepiolite-TiO_2 (100˚C), D) 1M Na-Sepiolite-TiO_2 (100˚C), E) 3M Na-Sepiolite-TiO_2 (100˚C)

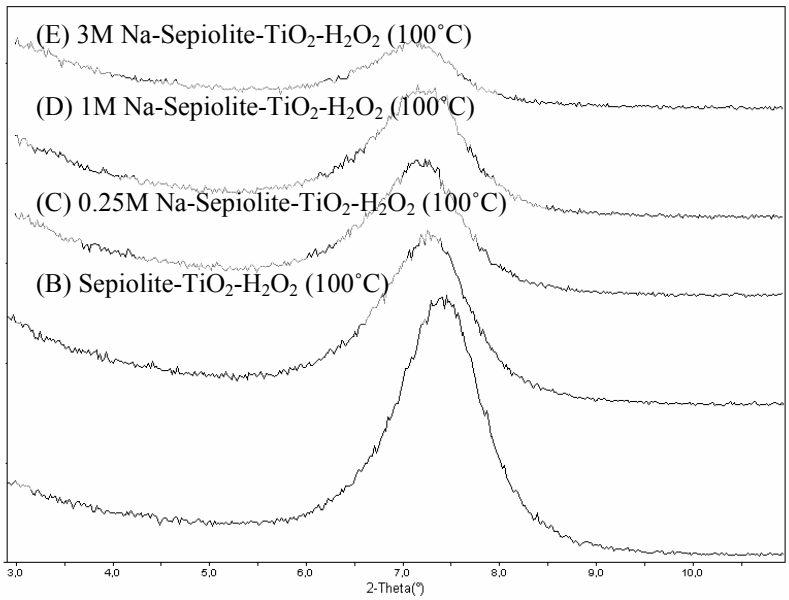

Figure 4.18. Small angle XRD patterns of A) Sepiolite, B) Sepiolite-TiO_2-H_2O_2 (100˚C), C) 0.25M Na-Sepiolite-TiO_2-H_2O_2 (100˚C), D) 1M Na-Sepiolite-TiO_2-H_2O_2 (100˚C), E) 3M Na-Sepiolite-TiO_2-H_2O_2 (100˚C)

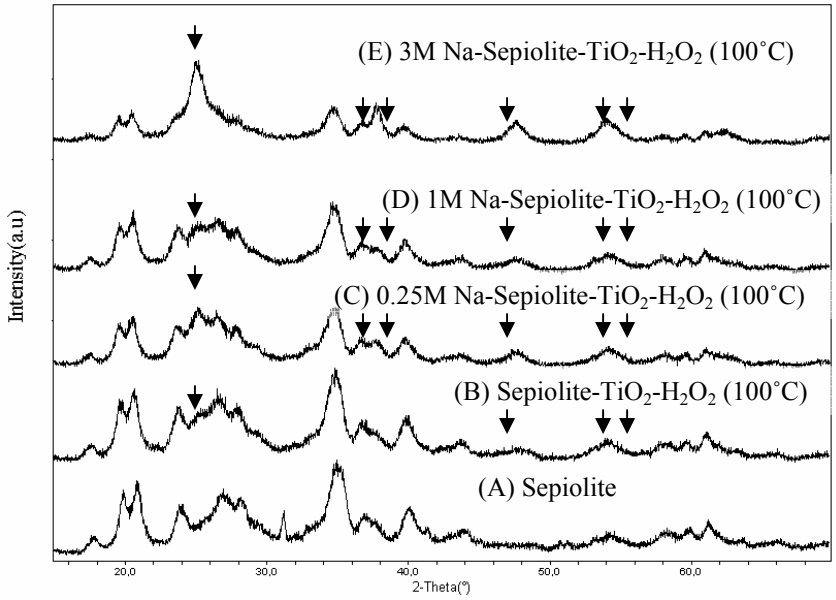

Figure 4.19. Wide angle XRD patterns of A) Sepiolite, B) Sepiolite-TiO_2-H_2O_2 (100˚C), C) 0.25M Na-Sepiolite-TiO_2-H_2O_2 (100˚C), D) 1M Na-Sepiolite-TiO_2-H_2O_2 (100˚C), E) 3M Na-Sepiolite-TiO_2-H_2O_2 (100˚C)

Relatively, crystallite sizes of these samples were much higher than that for 0.25M Na-Sepiolite-TiO_2 (100^{o}C), 0.25M Na-Sepiolite-TiO_2-H_2O_2 (100^{o}C), 3M Na-Sepiolite-TiO_2 (100^{o}C), 3M Na-Sepiolite-TiO_2-H_2O_2 (100^{o}C).

4.2.2.6. Fe^{3+} Exchanged Sepiolite-TiO_2 and Na-Montmorillonite-TiO_2 Catalysts In selective catalytic reduction reactions of NO_x, catalysts those containing Fe, Cr, Cu, or Ni have shown high activities. Iron-based catalysts are particularly attractive because of their high activity, low cost and lack of toxicity as compared to TiO_2 coupled catalysts. Recently, Fe^{3+} exchanged TiO_2-pillared clay catalysts have been found to exhibit high selective catalytic reduction activities [55]. Based on these studies, we aim to understand whether the catalytic oxidiation reaction of β-Naphthol is enhanced or suppressed in the presence of Fe^{3+} exchanged TiO_2 incorporated and pillared clays. Introduction of iron ions influence the photoreactivitiy of TiO_2 by acting as mediators and affecting charge separation, charge carrier recombination and interfacial charge-transfer rates.

Table 4.10. Heights, FWHM values and crystallite sizes of the anatase main peak at $2\theta=25.4^{o}$

	Height	FWHM	Crystallite Size (nm)
Sepiolite-TiO_2 ($100^{o}C$)	29	0.203	6.90
Sepiolite-TiO_2-H_2O_2 ($100^{o}C$)	30	0.302	4.60
0.25M Na-Sepiolite-TiO_2 ($100^{o}C$)	89	0.469	3.00
0.25M Na-Sepiolite-TiO_2-H_2O_2 ($100^{o}C$)	86	0.394	3.60
1M Na-Sepiolite-TiO_2 ($100^{o}C$)	36	0.137	10.0
1M Na-Sepiolite-TiO_2-H_2O_2 ($100^{o}C$)	60	0.080	18.0
3M Na-Sepiolite-TiO_2 ($100^{o}C$)	217	0.588	2.00
3M Na-Sepiolite-TiO_2-H_2O_2 ($100^{o}C$)	132	0.454	3.00

Accordingly, iron ions can lead to the following additional steps in the proposed mechanism (given in section 2.1).

Charge Trapping:

$$Fe^{3+} + e_{cb}^{-} \rightarrow Fe^{2+} \quad (4.5)$$

$$Fe^{3+} + h_{vb}^{+} \rightarrow Fe^{4+} \quad (4.6)$$

Charge release and migration:

$$Fe^{2+} + Ti^{4+} \rightarrow Fe^{3+} + Ti^{3+} \quad (4.7)$$

$$Fe^{4+} + OH^{-} \rightarrow Fe^{3+} + OH^{\cdot} \quad (4.8)$$

Recombination:

$$Fe^{2+} + h_{vb}^{+} \rightarrow Fe^{3+} \quad (4.9)$$

$$Fe^{2+} + OH^{\cdot} \rightarrow Fe^{3+} + OH^{-} \quad (4.10)$$

$$Fe^{4+} + e_{cb}^{-} \rightarrow Fe^{3+} \quad (4.11)$$

$$Fe^{4+} + Ti^{3+} \rightarrow Fe^{3+} + Ti^{4+} \quad (4.12)$$

Interfacial charge transfer:

$$e_{cb}^{-}(Fe^{2+}) + Ox \rightarrow Ox^{-} \quad (4.13)$$

$$h_{vb}^{+}(Fe^{4+}) + Red \rightarrow Red^{+} \quad (4.14)$$

where Ox is an electron acceptor (oxidant) and Red is an electron donor (reductant).

Thus, Fe^{3+} exchanged clays can improve the photocatalytic efficiency by acting as both electron and hole traps. Also, detrapping of charges, their transfer to catalyst's interface and to adsorbed substrates reduce the probability of electron-hole recombination reactions [56,57].

Figure 4.20 represents the XRD pattern on a small angle range (2θ=0-10) of the pure Sepiolite, Sepiolite-TiO_2 (500^{o}C) and Fe-Sepiolite-TiO_2 (500^{o}C). (110) basal reflection peak intensity of pure Sepiolite considerably decreased whereas 2θ and d_{110} values almost did not change (Table 4.11). On the wide angle range, intensities of pure clay peaks coming at 2θ>22^o almost disappeared (Figure 4.21). The broad peak at 2θ=25.4^o was assigned to (101) diffraction of anatase TiO_2 in the Sepiolite-TiO_2 (500^o) catalyst. The XRD pattern of Fe-Sepiolite-TiO_2 (500^o) catalyst was similar to that of TiO_2 incorporated clay. However, height and FWHM value of 2θ=25.4^o anatase peak decreased and the crystalline size increased with the insertion of Fe^{3+} ions (Table 4.12). No peak for Fe_2O_3 was observed in the XRD pattern of the corresponding catalyst.

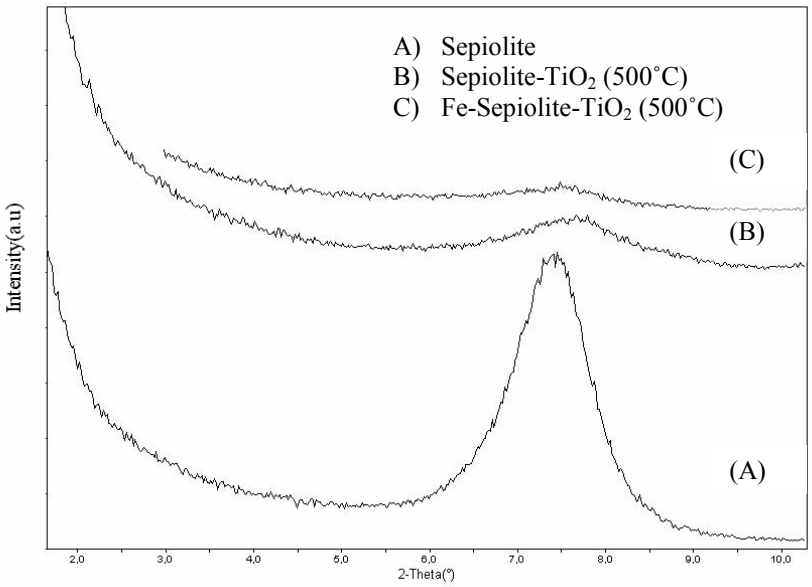

Figure 4.20. Small angle XRD patterns of A) Sepiolite, B) Sepiolite-TiO_2 (500˚C), C) Fe-Sepiolite -TiO_2 (500˚C)

Table 4.11. 2θ (^{o}) and d_{101} (Å) values of pure Sepiolite and Fe-Sepiolite-TiO_2 (500^{o}C)

Clay	2θ	d_{110}
Sepiolite	7.40	11.93
Catalysts		
Sepiolite-TiO_2 (500^{o}C)	7.50	11.77
Fe-Sepiolite-TiO_2 (500^{o}C)	7.40	11.81

Small angle XRD patterns (2θ=0-10º) of the pure Na-Montmorillonite, Na-Montmorillonite-TiO_2 (500^{o}C) and Fe-Na-Montmorillonite-TiO_2 (500^{o}C) catalysts were shown in Figure 4.22. (001) basal reflection peak of the Na-Montmorillonite detected at 2θ=6.7° was shifted toward smaller angle and spacing (d) between the silicate layers was increased from 13.10 Å to 17.41 Å after the addition of titania-sol. Furthermore, by the addition of Fe^{+3} ion, (001) basal reflection of the clay mineral disappeared completely (Table 4.13).

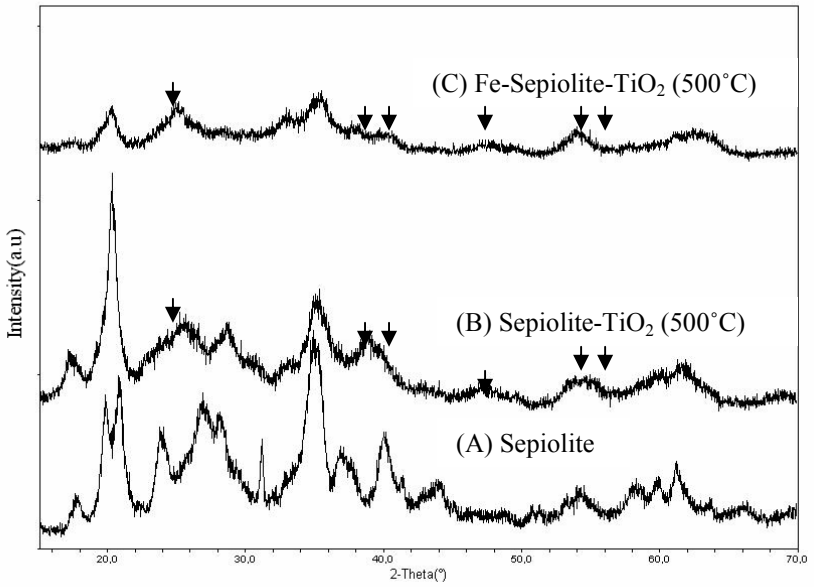

Figure 4.21. Wide angle XRD patterns of A) Sepiolite, B) Sepiolite-TiO_2 (500˚C), C) Fe-Sepiolite -TiO_2 (500˚C)

Table 4.12. Heights, FWHM values and crystallite sizes of the anatase main peak at$2\theta=25.4^o$

	Height	FWHM	Crystallite Size(nm)
Sepiolite-TiO_2 (500^{o}C)	33	0.633	2.2
Fe-Sepiolite-TiO_2 (500^{o}C)	28	0.185	7.5

Wide angle (2θ=15-70º) XRD patterns of the samples indicated the absence of anatase peak in the pure Na-Montmorillonite. However, Na-Montmorillonite-TiO_2 (500^{o}C) and Fe-Na-Montmorillonite-TiO_2 (500^{o}C) showed clear anatase diffractions of (101), (103), (004), (112), (200), (105) overlapped with (211) at 2θ=25.3, 37.8, 38.68, 48, 54, 55^o, respectively (Figure 4.23). Similar to the Fe-Sepiolite-TiO_2 (500^{o}C), no Fe_2O_3 peak was detected in Fe-Na-Montmorillonite-TiO_2 (500^{o}C). Fe-Na-Montmorillonite-TiO_2 (500^{o}C) showed lower anatase peak height and FWHM values compared to that of Na-Montmorillonite-TiO_2 (500^{o}C) (Table 4.14). Accordingly, crystallite size of the main anatase peak increased.

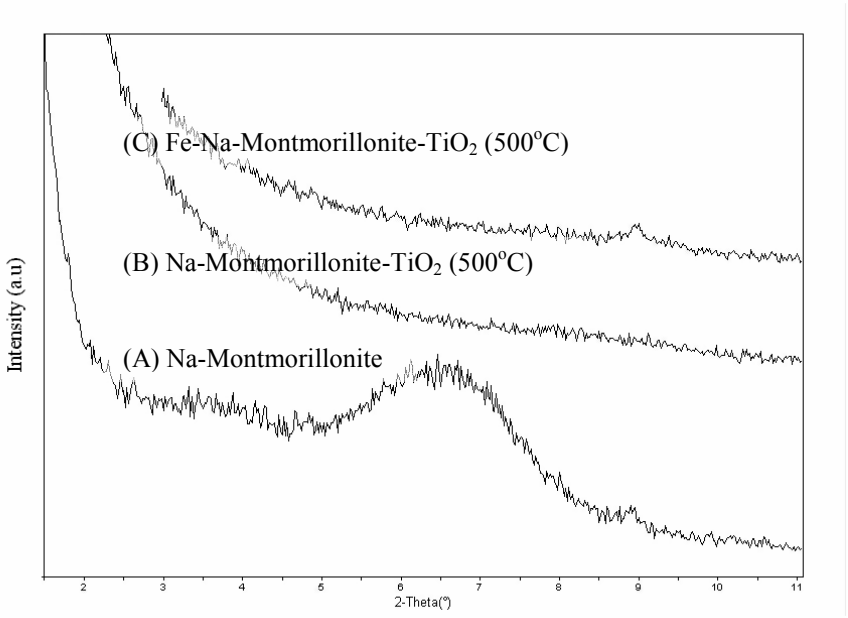

Figure 4.22. Small angle XRD patterns of A) Na-Montmorillonite, B) Na-Montmorillonite-TiO_2 (500˚C), C) Fe-Na-Montmorillonite-TiO_2 (500˚C)

Table 4.13. 2θ (^{o}) and d_{001} (Å) values of Na-Montmorillonite, Na-Montmorillonite-TiO_2 and Fe-Na-Montmorillonite-TiO_2 H_2O_2 (500^{o}C)

Clay	2θ	d_{001}
Na-Montmorillonite	6.70	13.10
Catalysts		
Na-Montmorillonite-TiO_2 (500^{o}C)	5.06	17.41
Fe-Na-Montmorillonite-TiO_2 (500^{o}C)	-	-

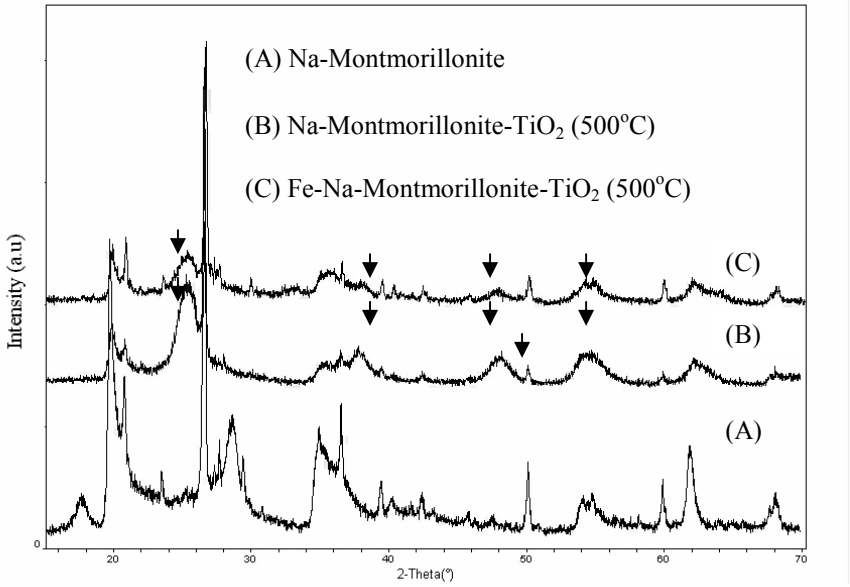

Figure 4.23. Wide angle XRD patterns of A) Na-Montmorillonite, B) Na-Montmorillonite-TiO_2 (500˚C), C) Fe-Na-Montmorillonite-TiO_2 (500˚C)

Table 4.14. Heights, FWHM values and crystallite sizes of the anatase main peak at $2\theta=25.4^o$

	Height	FWHM	Crystallite Size (nm)
Na-Montmorillonite-TiO_2 (500°C)	140	0.806	1.7
Fe-Na-Montmorillonite-TiO_2 (500°C)	67	0.561	2.4

4.2.3. Scanning Electron Microscopy (SEM)

Detailed knowledge of the physical nature and chemical composition of the surfaces of solids on a sub-micrometer scale is becoming of greater importance. Currently such knowledge is obtained by scanning electron microscopy (SEM). In obtaining an electron microscopic image and in performing an lectron microprobe analysis, the surface of a solid sample is swept in a raster pattern with a finely focused beam of electrons. A raster is a scanning pattern similar to that used in a cathode-ray tube, in which an electron beam is (i) swept across a surface in a straight line, (ii) returned to its starting position and (iii) shifted downward by a standard increment. This process is repeated until a desired area of the

surface has been scanned. Several types of signals are produced from a surface when it is scanned with an energetic beam of electrons. All of these signals have been used for surface studies [54].

4.2.3.1. Sepiolite and Sepiolite–TiO_2 Catalysts: SEM image of pure Sepiolite shows large, wavy-like structure with relatively uniform morphology (Figure 4.24). This morphology is typical for ordered mesoporous silica structures. TiO_2 distribution of the samples were studied by EDX analysis performed on the SEM images. Pure Sepiolite was found to contain approximately 0.09-0.15 wt per cent of TiO_2 (Figure 4.24 insert).

The catalyst Sepiolite-TiO_2 (100˚C) presents heterogeneously dispersed particles with non uniform diameters (Figure 4.25). When the surface of a particle was scanned, TiO_2 concentration promoted to 13.10 wt per cent (Figure 4.25 insert). According to the XRD results of the catalyst Sepiolite-TiO_2 (100˚C), after the TiO_2 addition, small angle diffraction peak of the clay was observed to diminish. This is also in good aggrement with the SEM image of the corresponding catalyst, i.e, large wavy-like structures turned to rather small particles indicating the distortion of the ordered silica structure. In the heat treated catalyst (Sepiolite-TiO_2 (500˚C)), small aggregates together with few large aggregates were observable (Figure 4.26). When one of these poorly distributed larger aggregates analyzed, TiO_2 concentration was found to decrease (10.72 wt per cent) (Figure 4.26 insert). Thus, one can see the damagement of ordered structure of the clay with increasing temperature.

When both H_2O_2 and heat treatments were applied (Sepiolite-TiO_2-H_2O_2 (500˚C)), the surface morphology did not differ much from the other catalysts (only heat treated or only H_2O_2 treated) (Figure 4.27). However, an obvious increase was obtained in the TiO_2 concentration (26.42 wt per cent) for the same catalyst (Figure 4.27 insert).

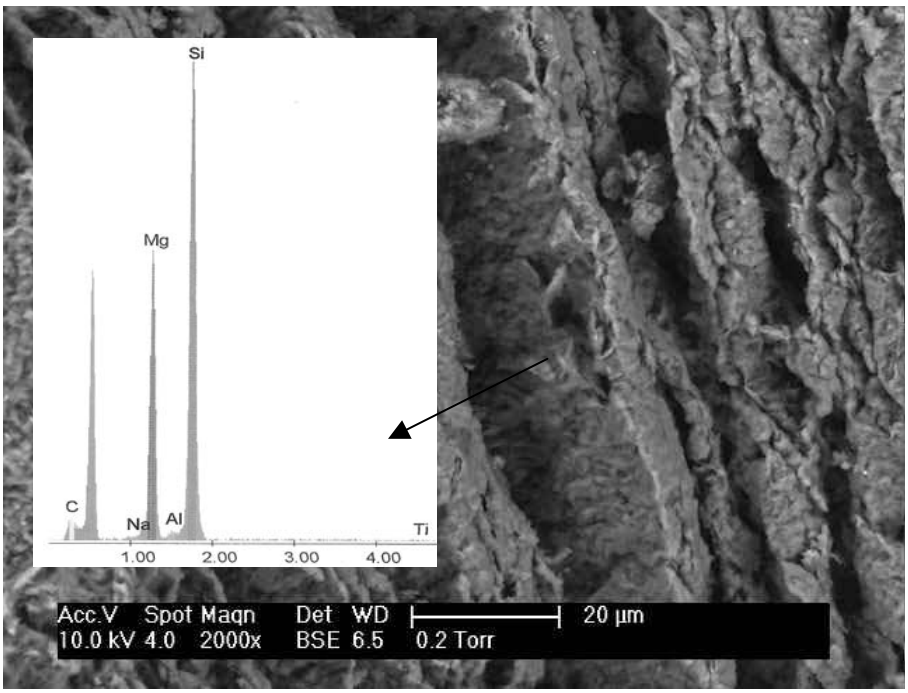

Figure 4.24. SEM image of pure Sepiolite. Insert: EDX spectra of a selected surface region

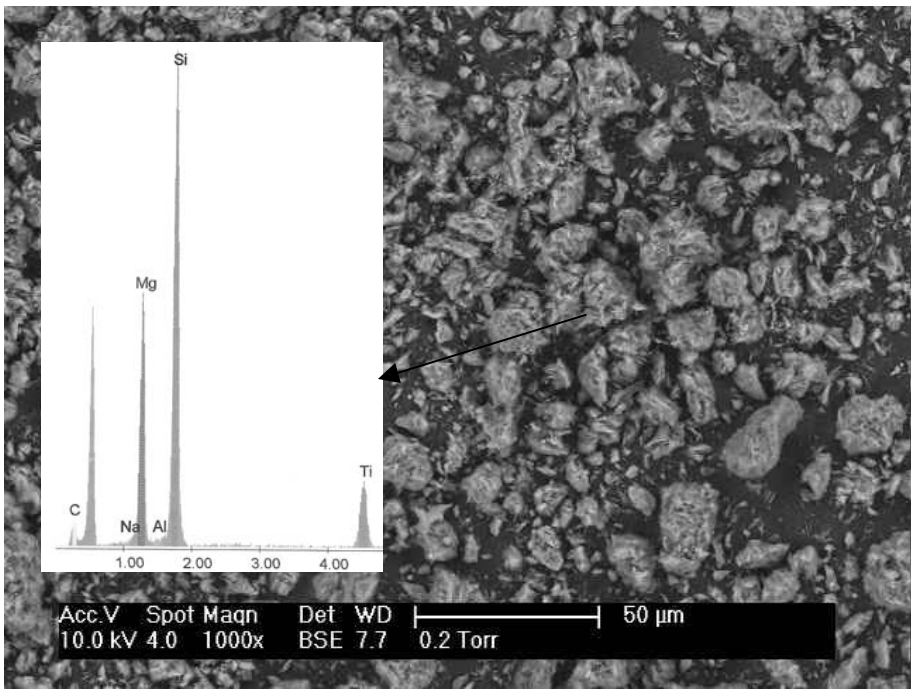

Figure 4.25. SEM image of Sepiolite-TiO_2 (100^{o}C). Insert: EDX spectra of a selected particle

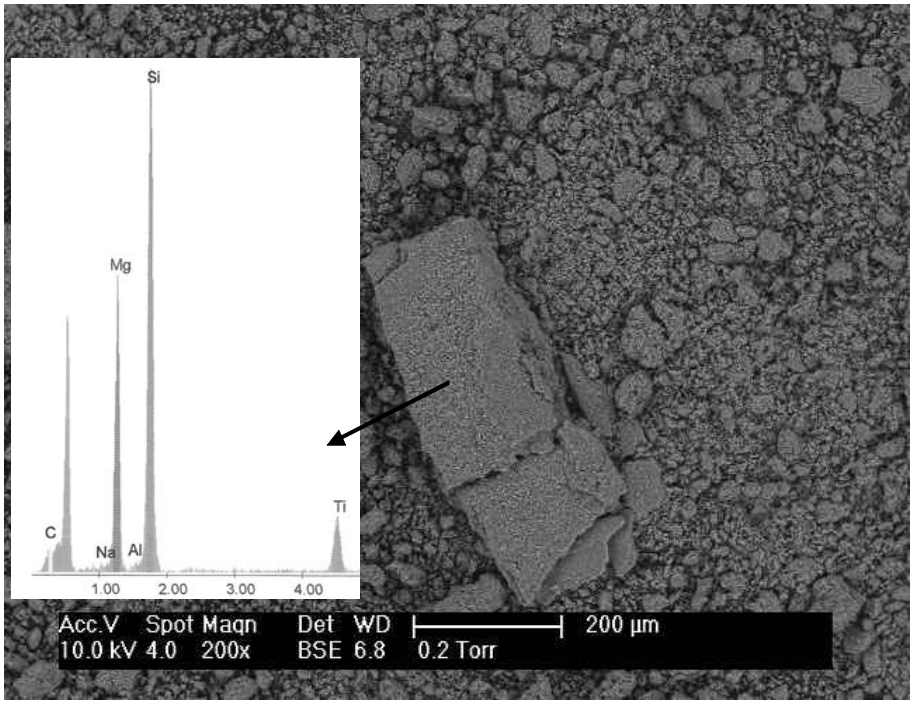

Figure 4.26. SEM image of Sepiolite-TiO_2 (500˚C). Insert EDX spectra of a large aggregate

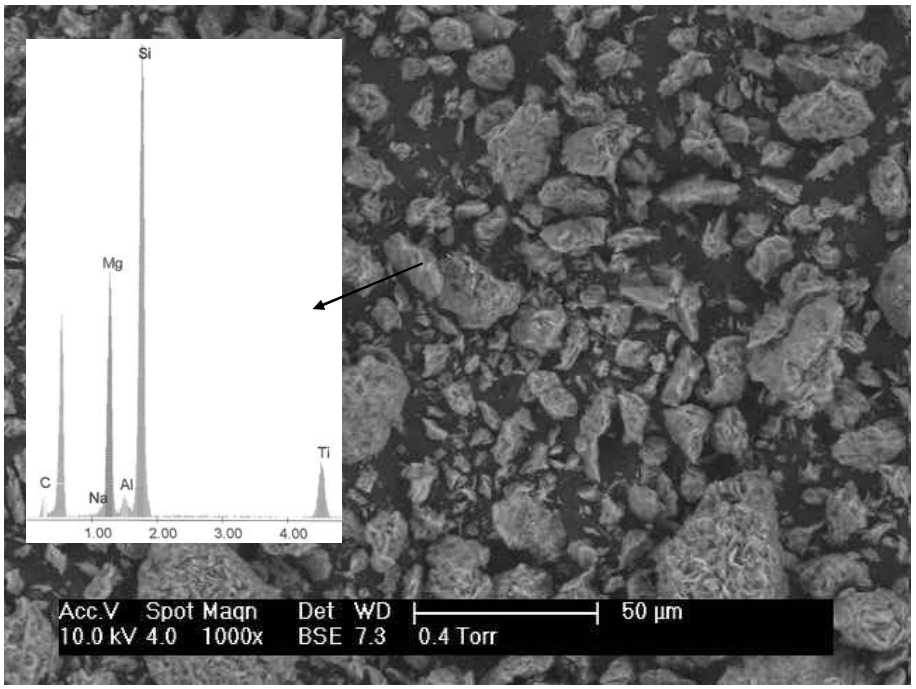

Figure 4.27. SEM image of Sepiolite-TiO_2-H_2O_2 (500˚C). Insert: EDX spectra of a selected particle

The last analysis was related with the SEM image of 50 mL titania-sol inserted clay. This catalyst consists of smooth surfaces which was not obtained with the previous samples (Figure 4.28). The EDX analysis of such smooth surface gave a higher percentage of TiO_2 (69.88 wt per cent) (Figure 4.28 insert). Hence, formation of titania particles on the Sepiolite surface was improved by the use of higher amount of titania-sol during the preparation step of the catalyst. However, there should be an upper limit in the amount of titania-sol addition, so that a number of active sites will be available for the adsorption of the probe molecule.

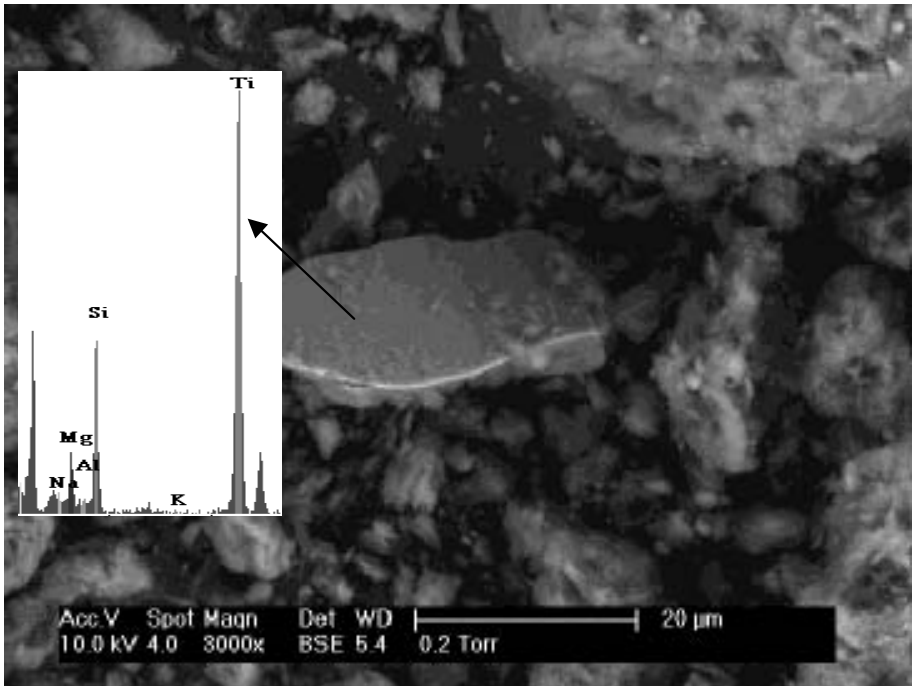

Figure 4.28. SEM image of Sepiolite-TiO_2 (50 mL) (100˚C). Insert: EDX spectra of the smooth surface

4.2.3.2. Na-Montmorillonite and Na-Montmorillonite–TiO_2 Catalysts: Figure 4.29 represents the SEM image of pure Na-Montmorillonite. Pebble-like structures and irregularly dispersed white and small particles were observable in the figure. Small particles were attributed to the quartz mineral naturally occuring in the clay. EDX analysis of stone-like structures showed that pure Na-Montmorillonite does not contain TiO_2 (Figure 4.29 insert).

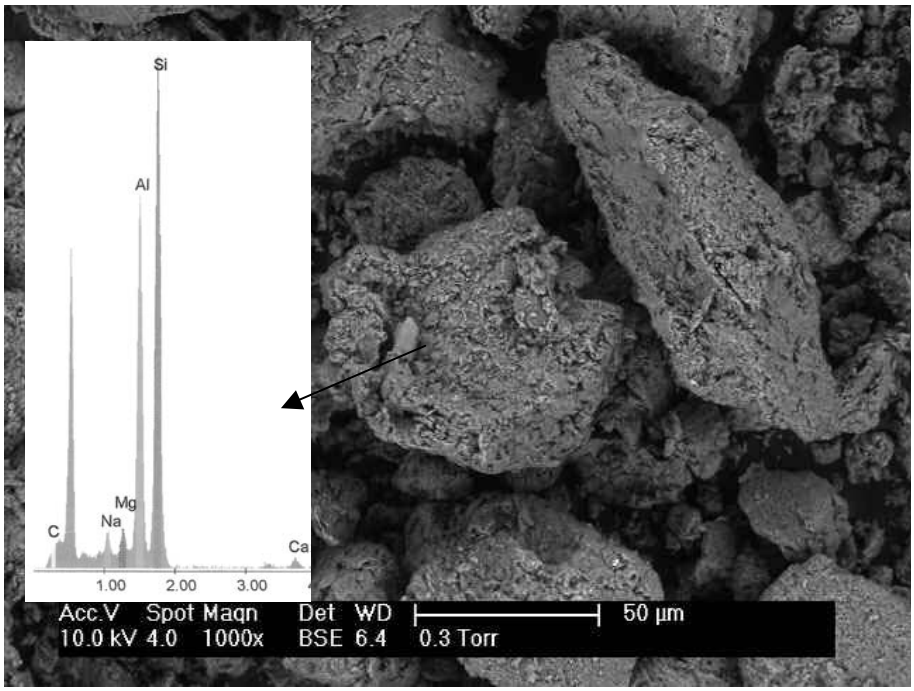

Figure 4.29. SEM image of Na-Montmorillonite. Insert: EDX spectra of a stone-like structure

For the catalyst Na-Montmorillonite-TiO_2 (100˚C) rough and smooth particles were identified among the stone-like structure of the clay (Figure 4.30). These were not obtained in the SEM image of the pure Na-Montmorillonite and were therefore expected to be titania. This was supported by EDX analysis as represented in the insert of Figure 4.30. TiO_2 percentage was found as 56.14 wt per cent. A similar percentage (54.75 wt per cent TiO_2) was obtained when a large particle scanned in the Na-Montmorillonite-TiO_2–H_2O_2 (100˚C) catalyst (Figure 4.31 and insert).

When 50 mL titania-sol was added to the clay, again apart from small particles and stone-like structures, a flat was surface was noticed (Figure 4.32). According to the EDX analysis, this particle was found to contain 75.88 wt per cent of TiO_2 (Figure 4.32 insert).

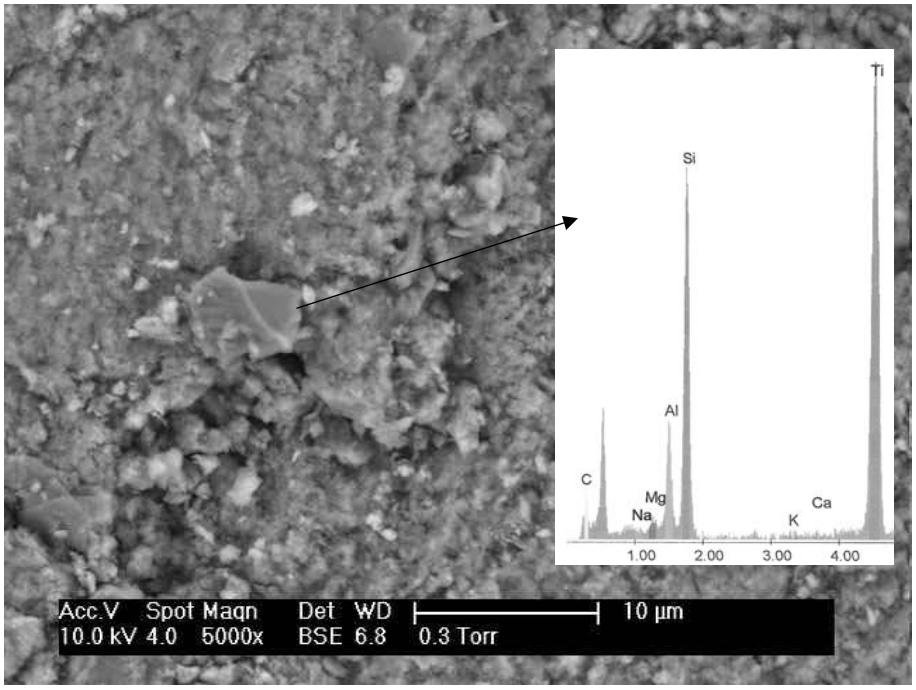

Figure 4.30. SEM image of Na-Montmorillonite-TiO_2 (100˚C). Insert: EDX spectra of a smooth particle

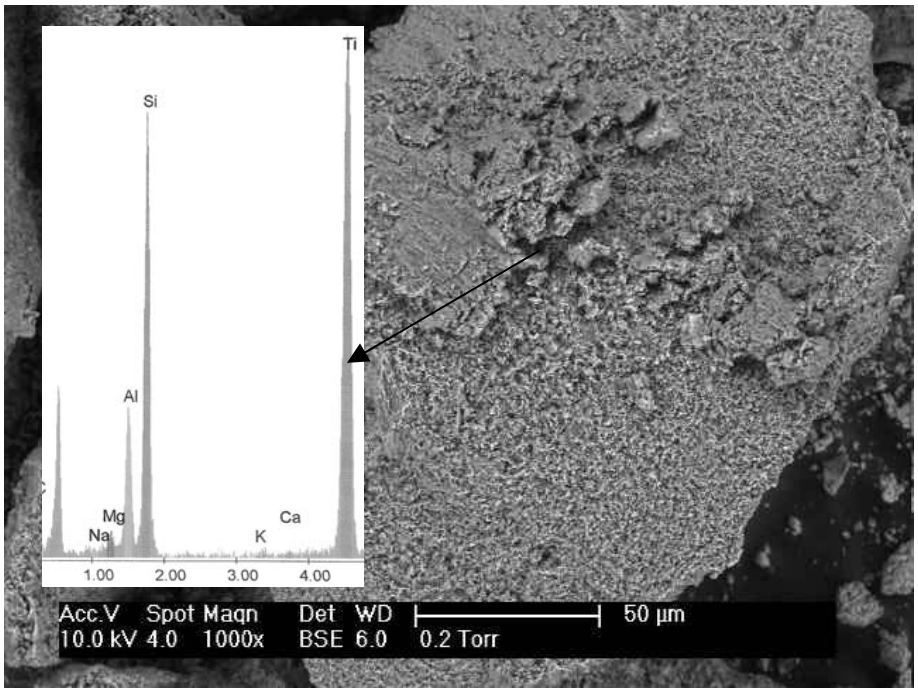

Figure 4.31. SEM image of Na-Montmorillonite-TiO_2-H_2O_2 (100˚C). Insert: EDX spectra of a smooth surface

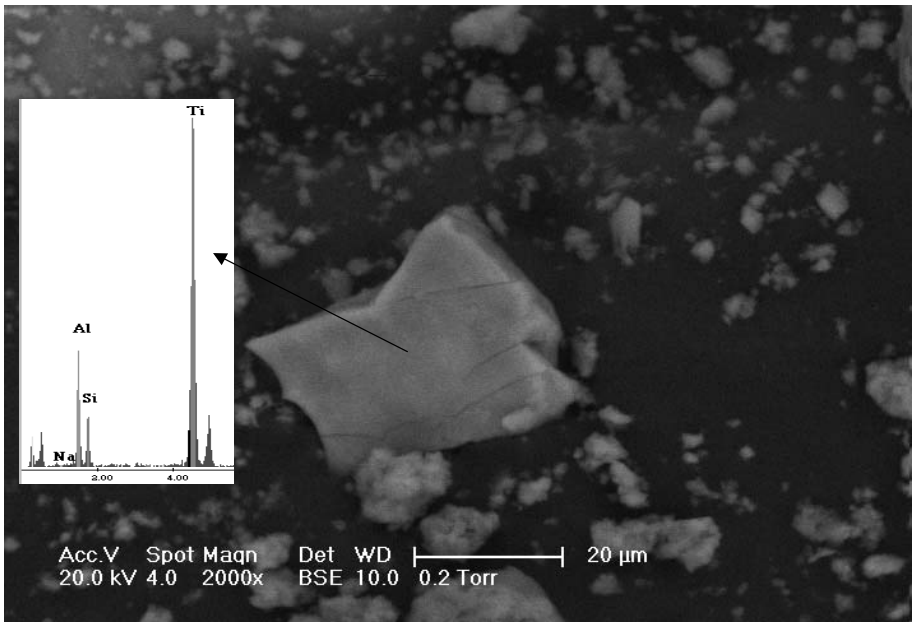

Figure 4.32. SEM image of Na-Montmorillonite-TiO_2 (50 mL) (100^oC).
Insert: EDX spectra of a flat surface

4.2.3.3. Na-Sepiolite–TiO_2 Catalysts: Na-Sepiolite-TiO_2 catalysts were prepared at different concentrations of Na^+ precursor, i.e, 0.25 M, 1 M and 3 M NaCl solution was mixed with the same amount of Sepiolite in each run. The amount of titania-sol for each mixture was 50 mL (assuming that this volume is the maximum limit of titania insertion into the clay system) and all of the catalysts were calcined at 100^oC.

Sharp-edged flat surfaces and also large-wavy like structures were considered in the SEM images of the catalysts. The first sample, 0.25M Na-Sepiolite-TiO_2 consists of 21.29 wt per cent TiO_2 when a big surface was scanned (Figure 4.33 and insert). However, a bright and relatively flat structure was detected among the large particles with a higher TiO_2 percentage (60.04 wt per cent) (Figure 4.34 and insert). Differing from the previous catalysts, for 1 M Na-Sephiolite-TiO_2 the number of sharp-edged bright and flat structures was higher. Figure 4.35, 4.36, 4.37 and their inserts show SEM images and EDX analysis

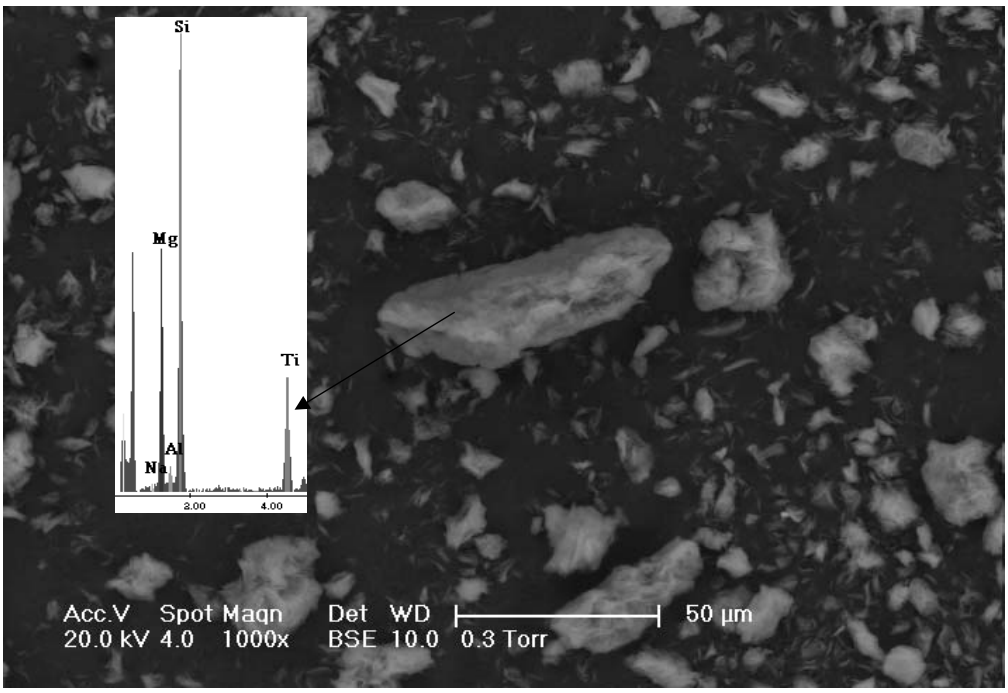

Figure 4.33. SEM image of 0.25M Na-Sepiolite-TiO_2. Insert: EDX spectra of a big surface

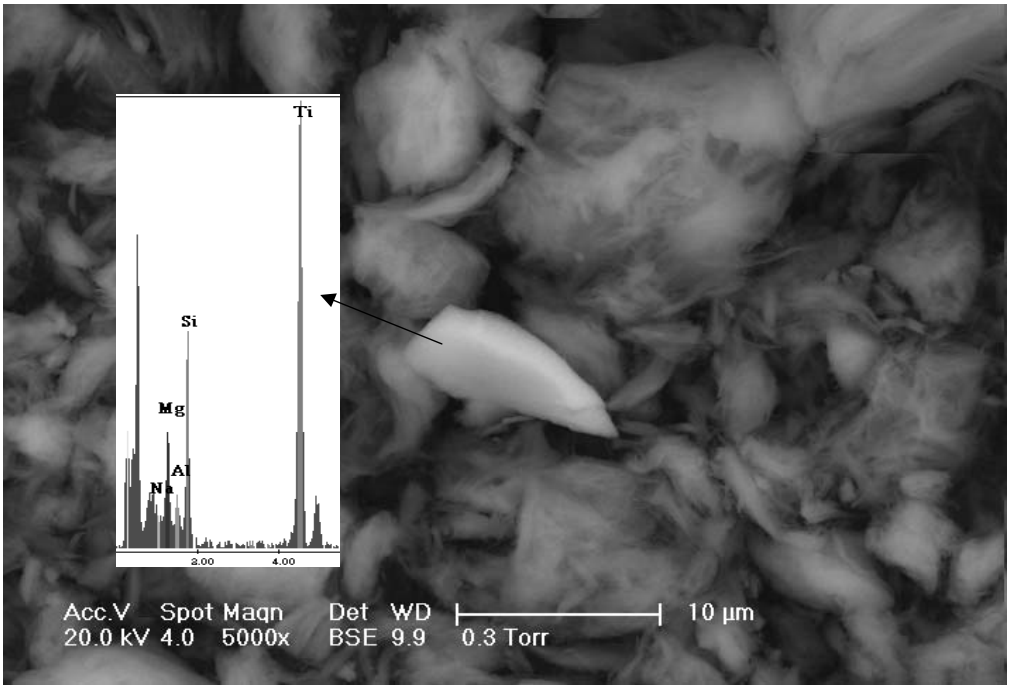

Figure 4.34. SEM image of 0.25M Na-Sepiolite-TiO_2. Insert: EDX spectra of a bright-flat particle

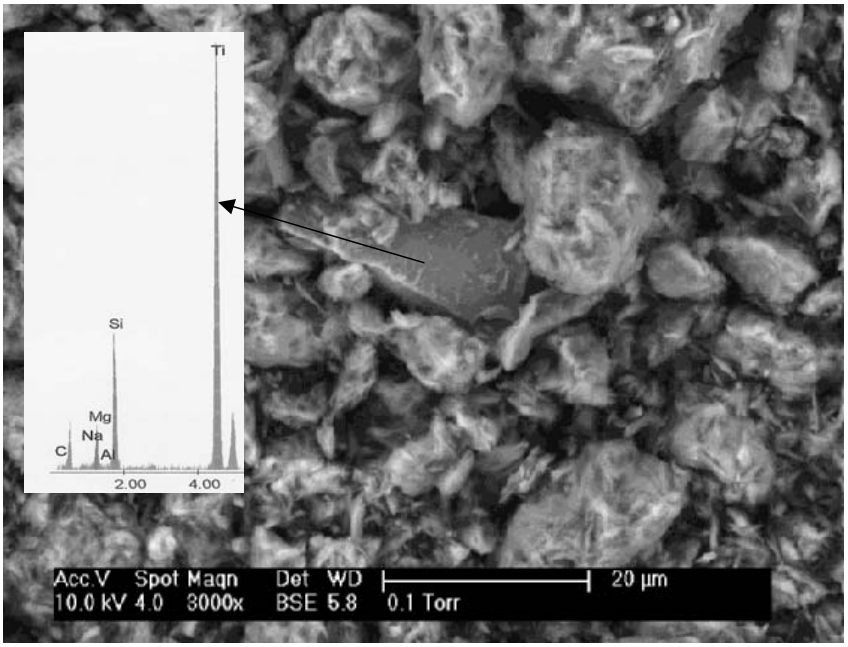

Figure 4.35. SEM image of 1M Na-Sepiolite-TiO_2. Insert: EDX spectra of a bright particle

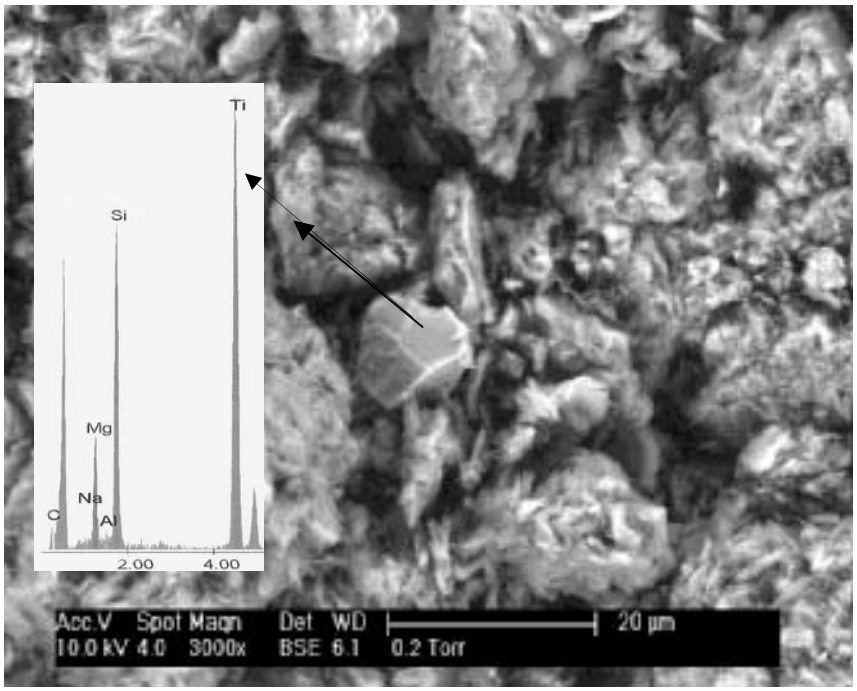

Figure 4.36. SEM image of 1M Na-Sepiolite-TiO_2. Insert: EDX spectra of a sharp-edged particle

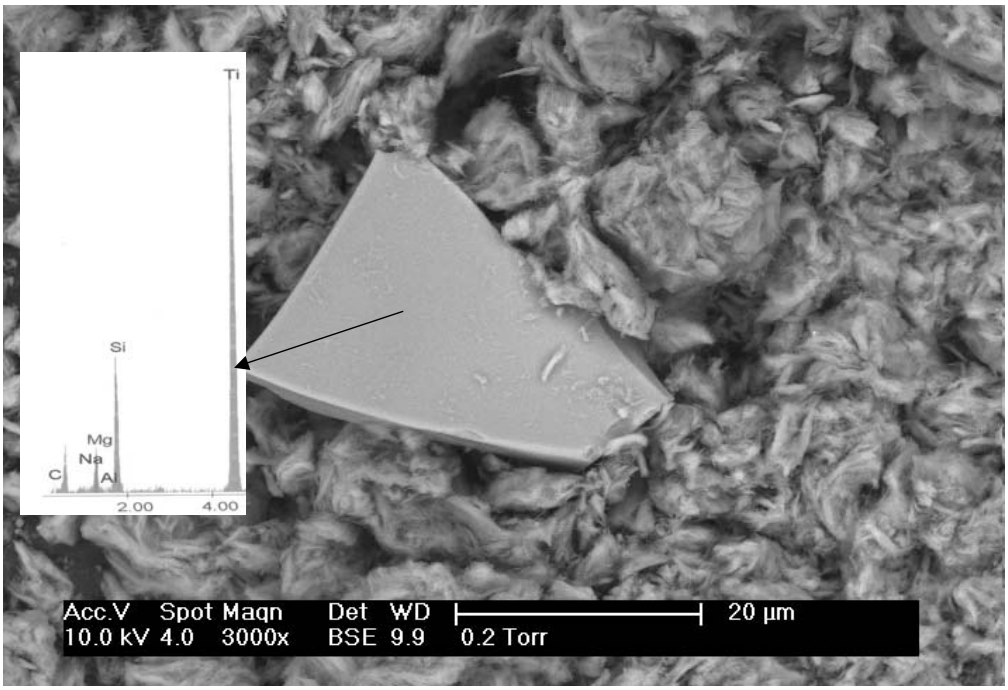

Figure 4.37. SEM image of 1M Na-Sepiolite-TiO_2. Insert: EDX spectra of a sharp-edged, bright, flat particle.

of different surface morphologies of the same catalyst. 67.64 wt per cent, 45.49 wt per cent and 41.78 wt per cent TiO_2 were obtained in corresponding morphologies, respectively.

3M Na-Sepiolite-TiO_2 showed the highest TiO_2 percentage considering both bright-flat structures (78.37 wt per cent TiO_2 and 72.09 wt per cent TiO_2, Figure 4.38 and insert) and a big surface (34.52 wt per cent TiO_2, Figure 4.39 and insert). Since maximum percentages were obtained with this catalyst compared to the others, H_2O_2 treatment was applied to this catalyst only. When larger surfaces were analyzed, it was found that TiO_2 percentages was about twice the value of similar surfaces prepared in the absence of H_2O_2 (61.50 wt per cent TiO_2 and 63.85 wt per cent TiO_2, Figure 4.40 and inserts). However, bright-edged structures gave similar TiO_2 percentages in H_2O_2 treated samples (75.66 wt per cent TiO_2 and 57.68 wt per cent TiO_2, Figure 4.41 and inserts).

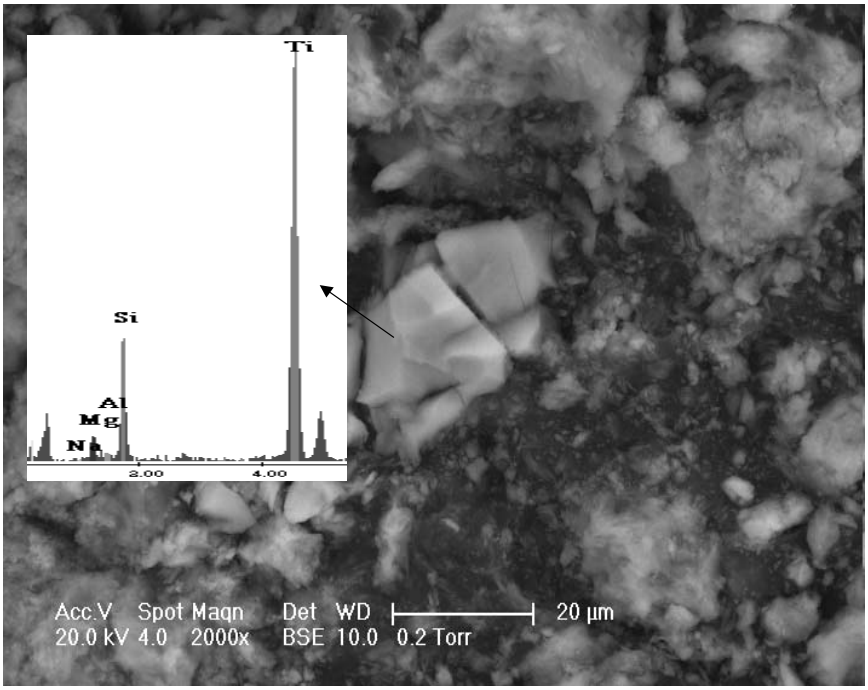

Figure 4.38. SEM image of 3M Na-Sepiolite-TiO_2. Insert: EDX spectra of a bright-flat structure

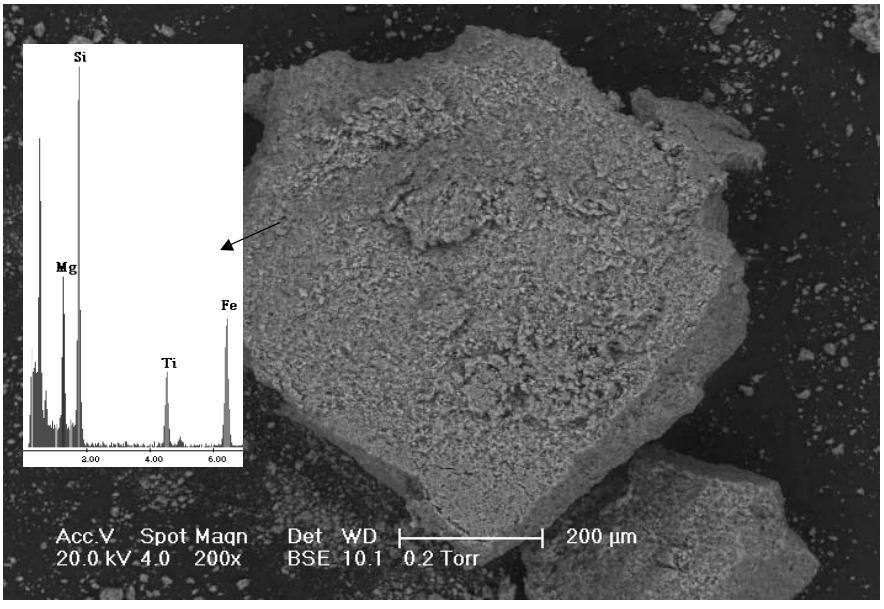

Figure 4.39. SEM image of 3M Na-Sepiolite-TiO_2. Insert: EDX spectra of a big surface

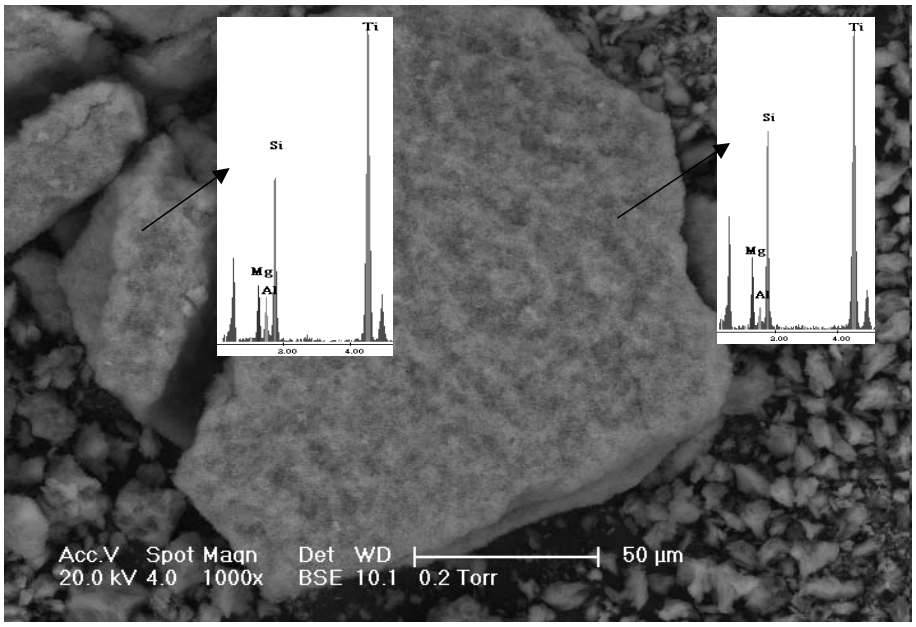

Figure 4.40. SEM image of 3M Na-Sepiolite-TiO_2-H_2O_2. Inserts: EDX spectras of large surfaces

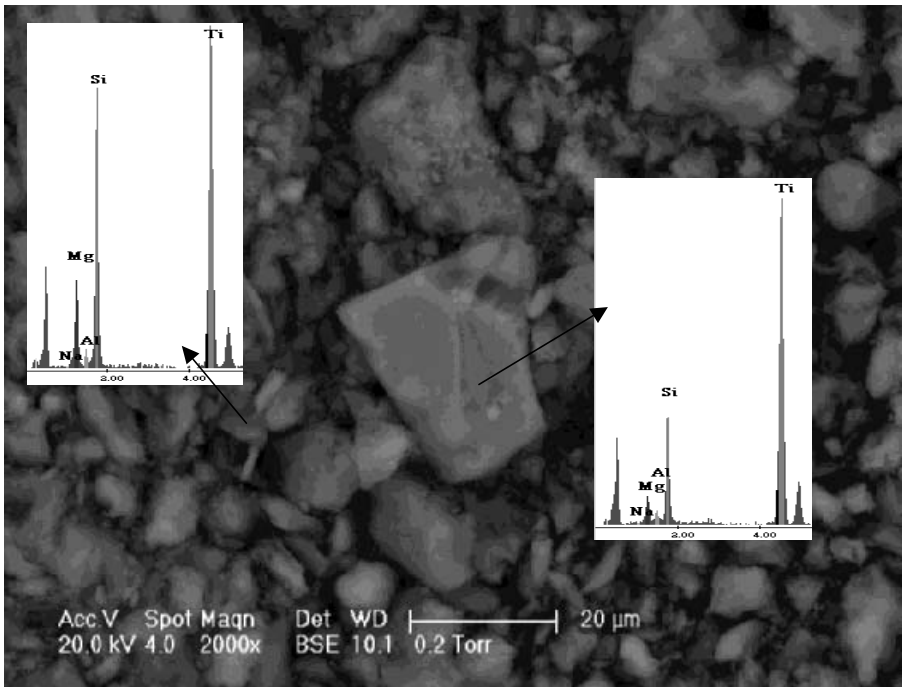

Figure 4.41. SEM image of 3M Na-Sepiolite-TiO_2-H_2O_2. Inserts: EDX spectra of bright-edged particles.

4.2.3.4. Fe-Sepiolite–TiO_2 Catalysts: In the SEM image of Fe-Sepiolite-TiO_2 (500˚C) (Figure 4.42), long range order of Sepiolite was lost by the addition of Fe^{3+} ions and the titania-sol. Although, formation of Fe_2O_3 was not detected in the XRD analysis, energy dispersive X-ray spot analysis as represented in the inserts of the Figure 4.42 exhibited ironoxide peaks. The sharp-edged particle gave 59.43 wt per cent TiO_2 and 15.49 wt per cent Fe_2O_3. The one at the right-hand corner of this particle presented a relatively lower TiO_2 and a relatively higher Fe_2O_3 percentages; 12.20 wt per cent and 26.39 wt per cent respectively. As a result, it was inferred that TiO_2 displayed a decrease in its concentration with the increasing Fe_2O_3 percentage.

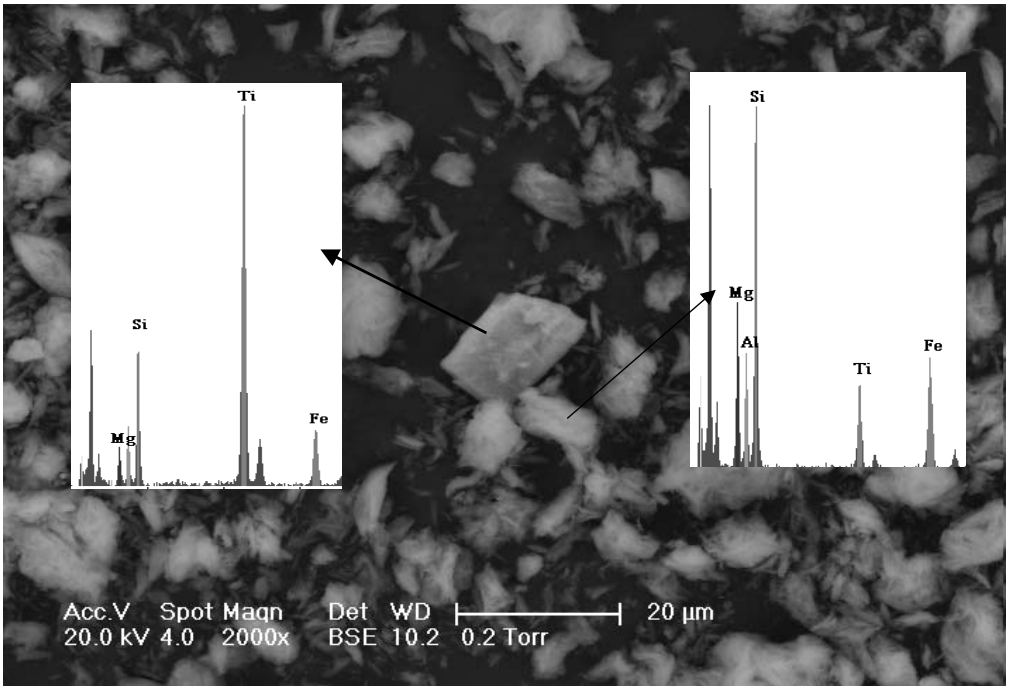

Figure 4.42. SEM image of Fe-Sepiolite-TiO_2 (500˚C). Inserts: EDX spectras of sharp-edged particles.

4.2.4 .Scanning-Transmission Electron Microscopy (STEM) Analysis

4.2.4.1. Sepiolite–TiO_2 (50mL):. Fibrous structure of Sepiolite described in literature was well recognized in the STEM image of the Sepiolite–TiO_2 (50mL) (Figure 4.43). This image displayed some small dark spots on the silica framework and they were probably due to the formation of TiO_2. Also, a narrow particle size distribution and less aggregation were observable among TiO_2 particles.

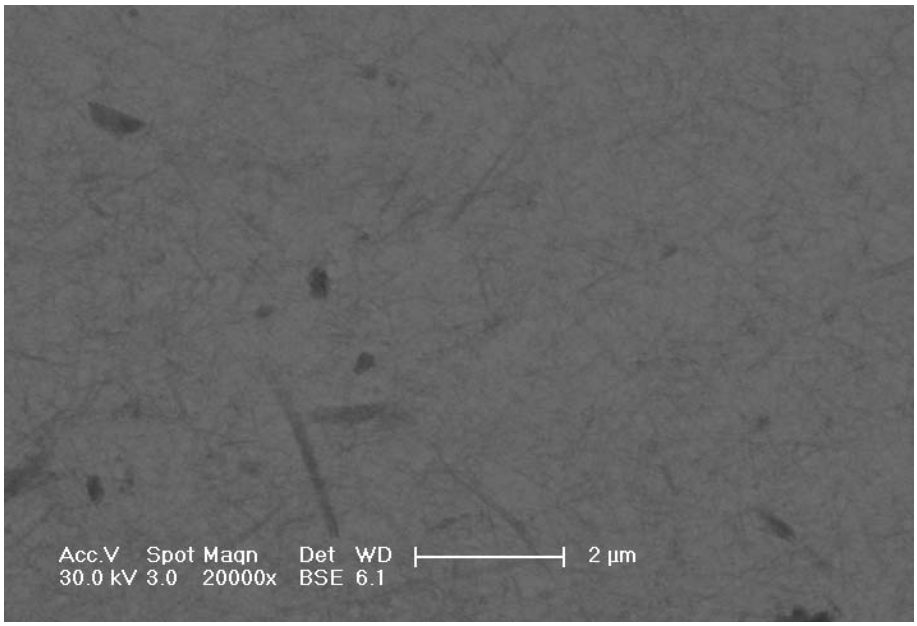

Figure 4.43. STEM image of Sepiolite-TiO_2 (50 mL)

4.2.4.2. Na-Montmorillonite–TiO_2 (50mL): In contrast to the Sepiolite–TiO_2 (50mL), STEM image of the Na-Montmorillonite–TiO_2 (Figure 4.44) exhibited large and dark spots on the silica framework and they were thought to be titania. In corporation of titania on the surface and formation of TiO_2 pillars among the layers of the clay may be distinguished as agglomerated dark regions in the Figure 4.44.

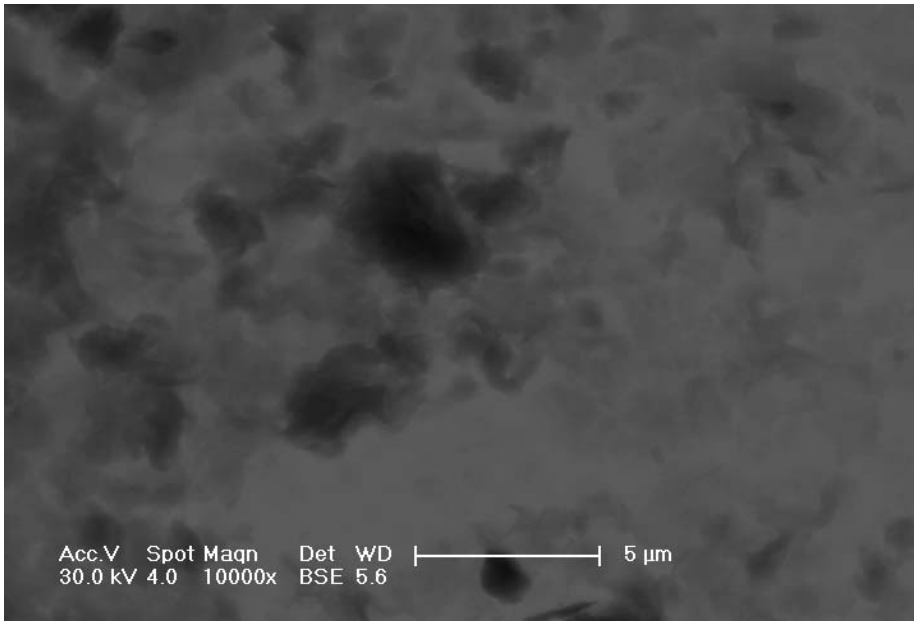

Figure 4.44. STEM image of Na-Montmorillonite-TiO_2 (50 mL)

4.3. Photocatalytic Degradation of β-Naphthol

In this section, photocatalytic degradation of β-Naphthol is investigated in the presence of Anatase (prepared in this study), Sepiolite-TiO_2, Na-Montmorillonite-TiO_2, Na-Sepiolite-TiO_2, Fe-Sepiolite-TiO_2 and Fe-Na-Montmorillonite-TiO_2 catalysts. Photoinduced degradation of this model compound is followed by monitoring the decrease in its initial concentration. Some control experiments (examination of the effect of β-Naphthol concentration, effect of titania-sol amount, effect of dilution in clay solutions) precede the photodegradation studies to optimize the conditions necessary for the catalytic efficiencies.

Figure 4.45 shows results of four preliminary experiments. First, the substrate's stability was checked under UV illumination. 100 μM β-Naphthol solution was photolyzed about 3 hours without photocatalyst. Although β-Naphthol does not absorb the UV light in 320-440 nm range, a 5 per cent decrement is emerged in its initial concentration. This may be attributed to the existence of some impurities, but not accepted as a drawback in our experiments. In the second, third and fourth preliminary experiments adsorption capacities of the catalysts (TiO_2 Degussa P-25, Na-Montmorillonite-TiO_2 and Sepiolite-TiO_2) in the dark measured and these followed by the degradation studies under irradiation. For every dark experiment, adsorption equilibrium was achieved in about 30 minutes after adding the catalyst into the substrate's solution. The variation in the dark-adsorption capacities among the catalysts was small and approximately 60 μM of β-Naphthol concentration was subjected to degradation experiments before irradiation. Under about 3 hours illumination, a remarkable decrease in the β-Naphthol concentration observed. Meanwhile, photocatalytic performances of Sepiolite-TiO_2 and Na-Montmorillonite-TiO_2 were found to be higher than that of TiO_2 Degussa P-25. Porous structures of the clays, incorporation of TiO_2 into the silicate layers, channels and/or edges of the clay structures are believed to play an important role in the enhancement of these catalytic efficiencies.

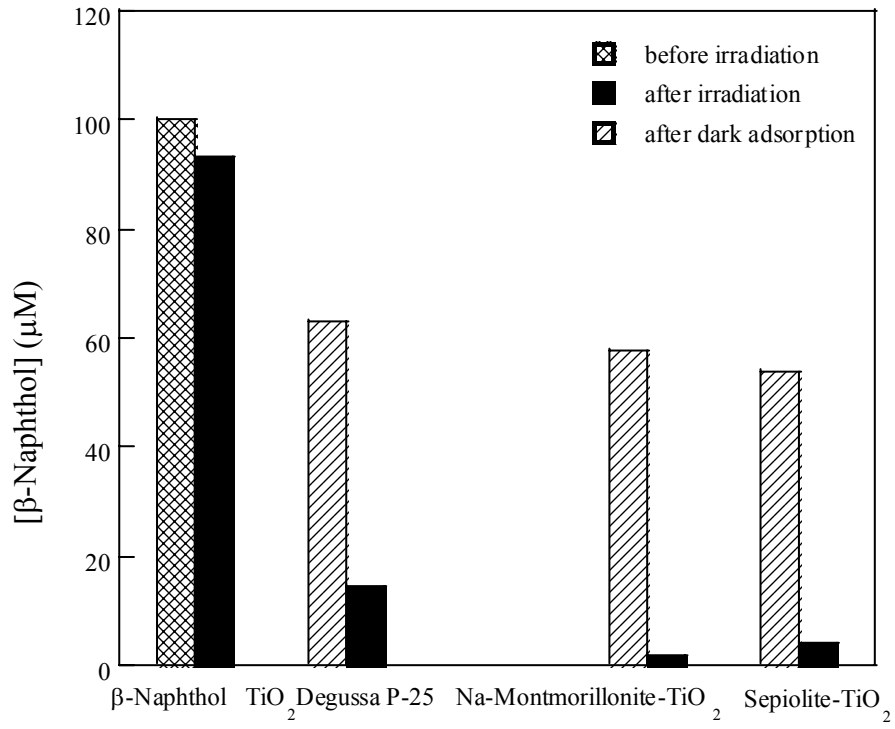

Figure 4.45. Results of preliminary experiments

The effect of β-Naphthol concentration on the degradation process is examined in 100 μM, 250 μM and 500 μM β-Naphthol solutions in the presence of Sepiolite-TiO_2 (100^oC) catalysts (Figure 4.46). For each concentration, steady state of dark adsorption is reached in 30 minutes. Concentrated solution was yielded the lowest degradation after 5 hours illumination. This may be explained by the formation of some intermediates and their competition with non-adsorbed β-Naphthol molecules present in the reaction media. However, it is expected that, for less concentrated solutions, the amount of intermediate concentration and their competition with the probe molecule will much lower. Thus, initial 100 μM β-Naphthol concentrations are selected for all photoinduced experiments before irradiation.

Figure 4.47 exhibits the results of photocatalytic degradation experiments as a function of the added concentration of titania-sol referred asTi-50 mL, Ti-100 mL and Ti-200 mL. Due to the decrease in number of available surface active sites by the formation

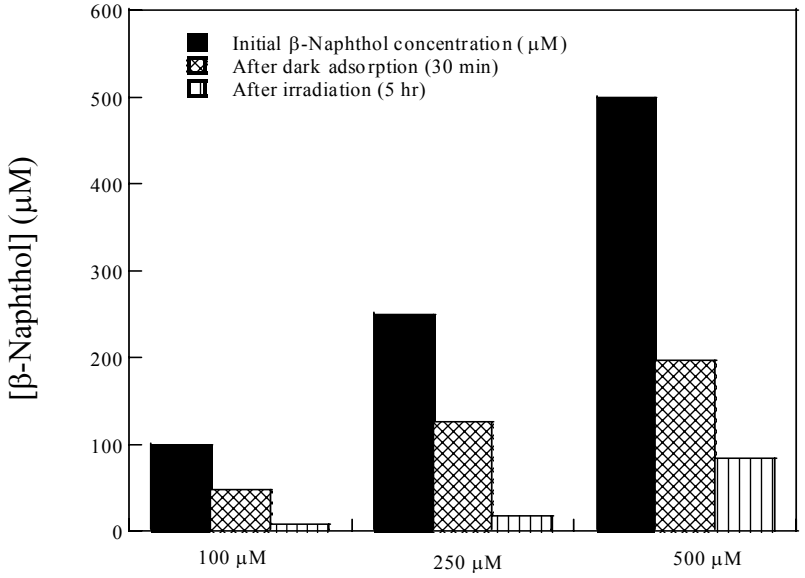

Figure 4.46. Photocatalytic degradtion of β-Naphthol in the presence of Sepiolite-TiO_2: Effect of β-Naphthol concentration

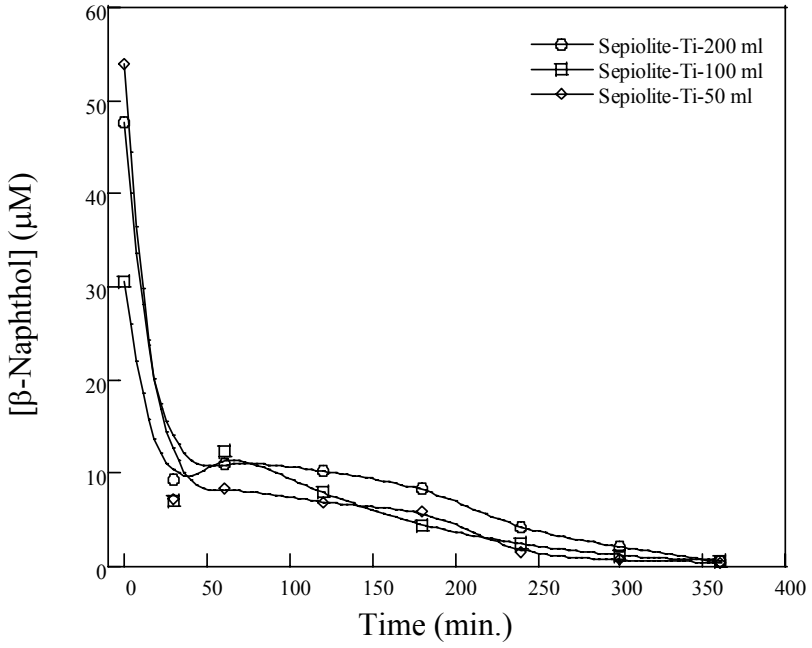

Figure 4.47. Photocatalytic degradation of β-Naphthol in the presence of Sepiolite-TiO_2: Effect of amount of titania-sol addition

of aggregated TiO_2 particles, 200 mL titania-sol addition yields lowest degradation.For 50 mL and 100 mL titania-sol added experiments, results were quite similar but the lowest amount of sol addition was preferred for all degradation processes.

Effect of dilution on the photocatalytic degradation experiments was investigated by means of 400 and 600 mL aqueous suspended clay solutions containing 50 mL of titania-sol (Figure 4.48). It was observed that the former catalyst (400 mL Sepiolite+50 mL titania-sol) exhibited better degradation result than the latter after 6 hours irradiation. It was believed that in the diluted catalyst (600 mL Sepiolite+50 mL titania-sol), TiO_2 particles were dispersed in the aqueous solution and not an efficient incorporation possesed on the clay surface. Hence, 400 mL aqueous suspensions of the clay solutions were used in all experiments.

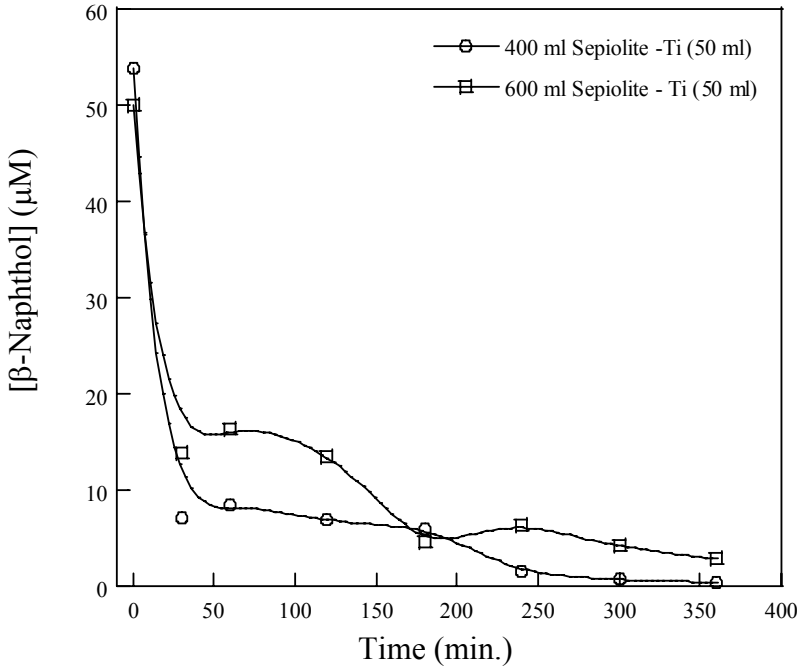

Figure 4.48. Photocatalytic degradation of β-Naphthol in the Sepiolite-TiO_2: Effect of dilution

4.3.1. Photocatalytic Degradation of β-Naphthol in the Presence of Anatase

Photoactivities of Anatase catalysts were determined by following 5 hours irradiation experiments (Figure 4.49). After the dark adsorption, 100 μM initial β-Naphthol concentrations decreased to 45 μM. Further decrements in the β-Naphthol concentration obtained after illumination. The catalysts prepared at 100°C showed the maximum efficiency, i.e., β-Naphthol concentration remaining in the solution has the lowest value in the presence of this catalyst. It was evidenced by the XRD results that in the heat treated catalysts (200°C and 500°C) crystallite size of the anatase phase was higher. This causes formation of agglemorates and may reduce the probability of β-Naphthol adsorption.

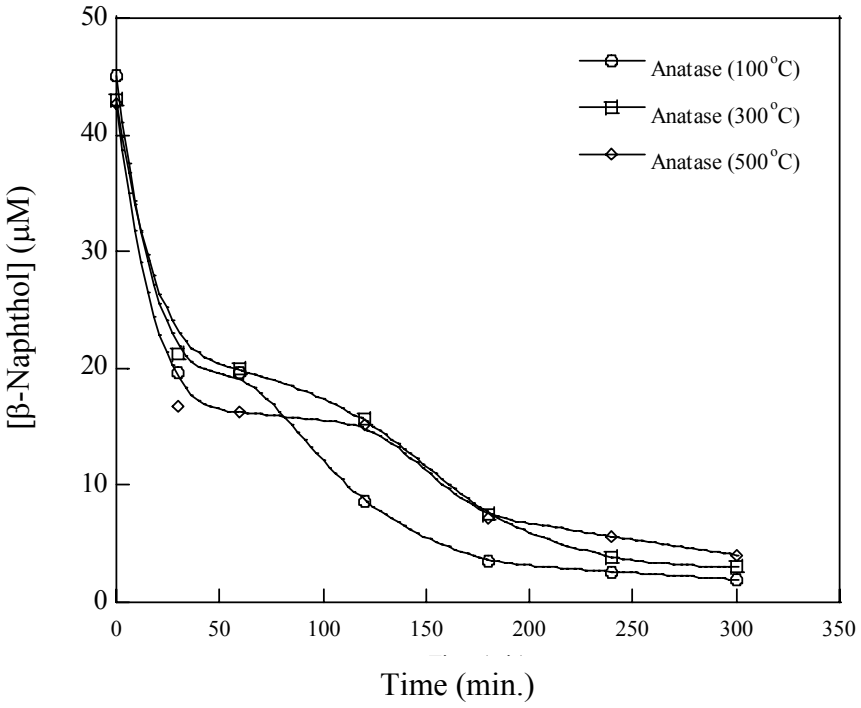

Figure 4.49. Photocatalytic degradation experiments of β-Naphthol in the presence of Anatase

4.3.2. Photocatalytic Degradation of β-Naphthol in the Presence of Sepiolite-TiO_2 Catalysts

In this set of experiments, degradation studies were carried out in the presence of Sepiolite-TiO_2 (100°C), Sepiolite-TiO_2-H_2O_2 (100°C), Sepiolite-TiO_2 (500°C), Sepiolite-TiO_2-H_2O_2 (500°C) (Figure 4.50). For each of the catalysts, after the dark adsorption experiments, β-Naphthol concentration showed a dramatic decrease during first 30 minutes of irradiation. In between 30-180 minutes, remaining β-Naphthol concentration in the solution increased and remained constant. In this period of time, some portion of the β-Naphthol was forced to desorp from the catalyst surface by the species that are acting as intermediates. These species are believed to make different charge-transfer complexation with the surface. After 180 minutes, degradation of β-Naphthol started again. Thus, the competition between β-Naphthol and intermediate species for the active surface sites lasted within 180 minutes. The highest degradation yields were obtained in the presence of Sepiolite-TiO2 (100^oC) catalyst. H_2O_2 treatment at (100^oC), heat treatment (500^oC), and both H_2O_2 and heat treatments did not enhanced the β-Naphthol degradation. However, for each of the catalyst with the progress of the experiments, a decrease in the β-Naphthol concentration was successfully obtained. Figure 4.50 insert indicates the decrement in the β-Naphthol concentration after 120 minutes irradiation as a bar plot.

4.3.3. Photocatalytic Degradation of β-Naphthol in the Presence of Na-Montmorillonite-TiO_2 Catalysts

Figure 4.51 presents the results of degradation experiments in the presence of Na-Montmorillonite-TiO_2 (100^oC), Na-Montmorillonite-TiO_2-H_2O_2 (100^oC), Na-Montmorillonite-TiO_2 (500^oC) and Na-Montmorillonite-TiO_2-H_2O_2 (500^oC) photocatalysts. Similar to the Sepiolite based catalysts, a sudden decrease was observed in the β-Naphthol concentration after 30 minutes irradiation. An increase in β-Naphthol concentration at 60 minutes irradiation time was immediately followed by the degradation process since the competition between the probe molecule and intermediate species did not have a pronounced effect in the presence of Na-Montmorillonite-TiO_2 catalysts. Maximum degradation was achieved in the presence of Na-Montmorillonite-TiO_2 (100^oC). H_2O_2 and heat treated catalysts did not exhibit enhanced yields, however, for all catalysts

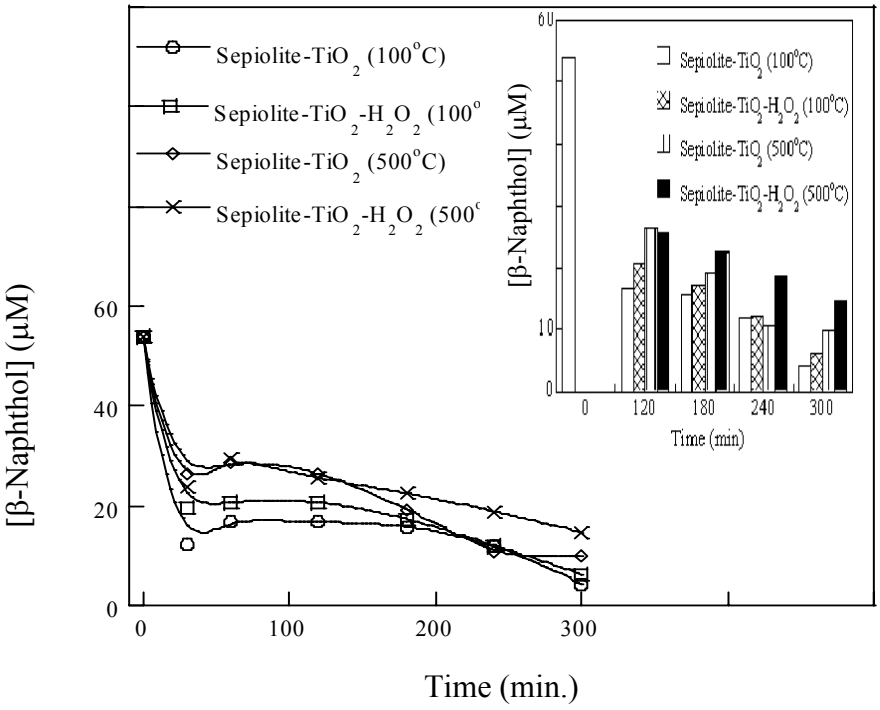

Figure 4.50. Photocatalytic degradation experiments of β-Naphthol in the presence of Sepiolite-TiO_2 catalysts

following the dark adsorption experiments, a gradual decrease in the β-Naphthol concentration was observable after 120 minutes irradiation (Figure 4.51 insert).

4.3.4. Photocatalytic Degradation of β-Naphthol in the Presence of Na-Sepiolite-TiO_2 Catalysts

Na-Sepiolite-TiO_2 catalysts were investigated in the degradation process of β-Naphthol (Figure 4.52). At the end of dark adsorption experiments, β-Naphthol concentrations in solution were 25.2 μM, 41.6 μM and 49.3 μM for 0.25M Na-Sepiolite-TiO_2; 1M Na-Sepiolite-TiO_2 and 3M Na-Sepiolite-TiO_2, respectively. These initial concentrations (before photodegradation studies) were in good agreement with the Na^+ ion concentrations inserted into the clay structure. Accordingly, for 3M Na-Sepiolite-TiO_2, adsorption of β-Naphthol on the catalyst surface was less compared to those in the present

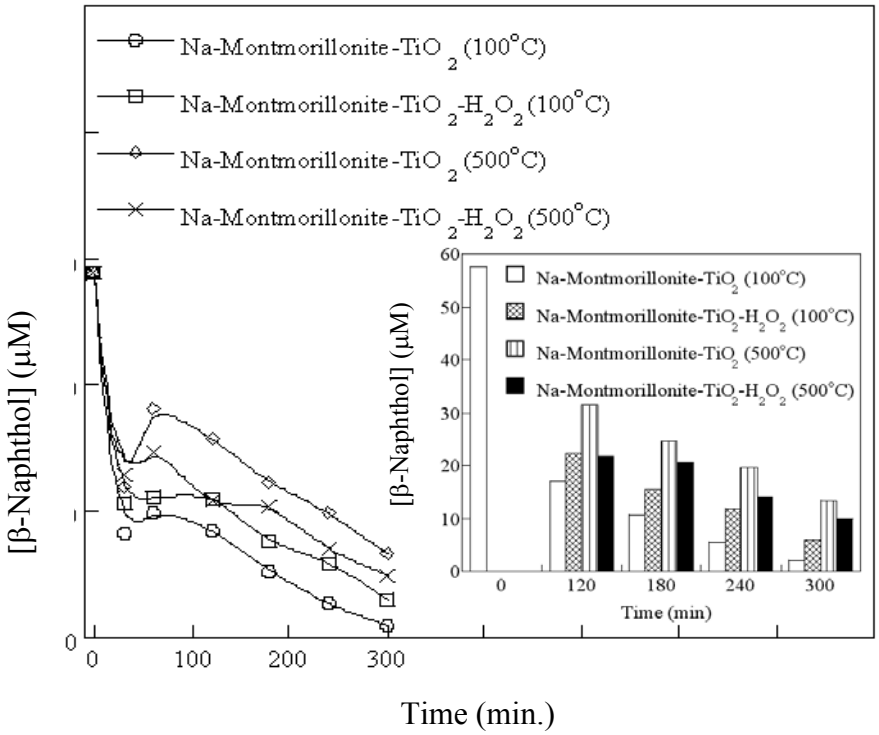

Figure 4.51. Photocatalytic degradation experiments of β-Naphthol in the presence of Na-Montmorillonite-TiO_2 catalysts

of 0.25M Na-Sepiolite-TiO_2 and 1M Na-Sepiolite-TiO_2. Improved degradation yields were obtained in the presence of catalysts prepared at 100°C. Na^+ ion concentration was effective in the process, thus the catalytic activity of 3M Na-Sepiolite-TiO_2 was the best after 5 hours irradiation time. Similar to Sepiolite-TiO_2 and Na-Montmorillonite-TiO_2 photocatalysts, H_2O_2 and heat treatments did not enhance the degradation process.

4.3.5. Photocatalytic Degradation of β-Naphthol in the Presence of Fe-Sepiolite-TiO_2 (500°C) and Fe-Na-Montmorillonite-TiO_2 (500°C)

$Fe(NO_3)_3.9H_2O$ salt was used as the precursor of Fe^{3+} ions in our experiments. According to literature, the $Fe(NO_3)_3$ solution contains about 75 per cent Fe^{3+} and 25 per cent $Fe_2(OH)_2^{4+}$ ions at room temperature [58]. They exchange with cations in Sepiolite-TiO_2 and Na-Montmorillonite-TiO_2, i.e., Na^+, K^+, Mg^{2+}. After the exchange process, samples were calcined at 500°C, some $Fe_2(OH)_2^{4+}$ was decomposed to Fe_2O_3 and Fe^{3+} via

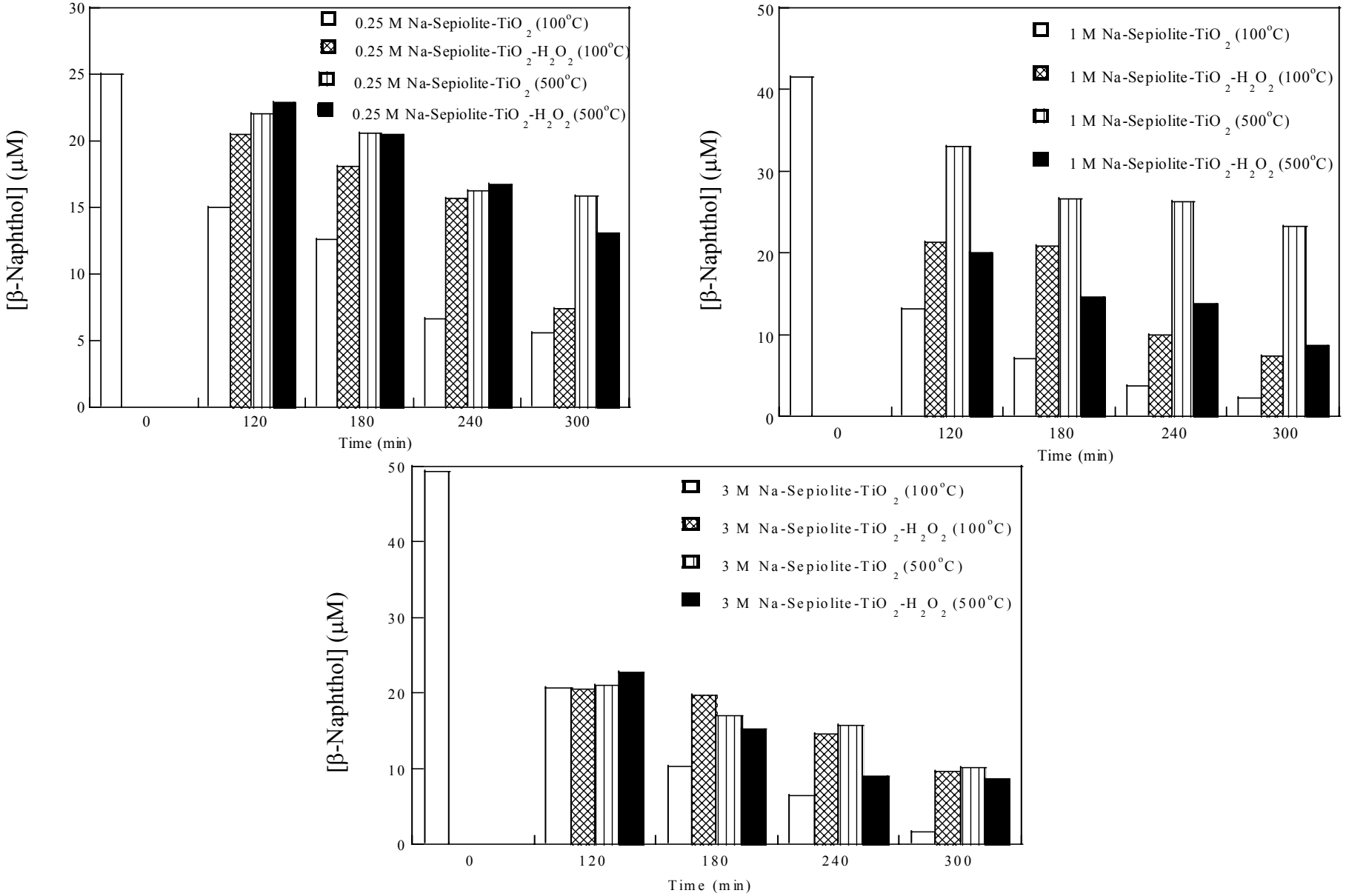

Figure 4.52. β-Napthol degradation in the presence of Na-Sepiolite catalysts

$$2\ Fe_2(OH)_2^{4+} \rightarrow Fe_2O_3 + 2Fe^{3+} + H_2O + 2H^+ \quad (4.15)$$

Hence, the iron in Sepiolite-TiO_2 and Na-Montmorillonite-TiO_2 may exist in the form of isolated Fe^{3+} ions and/or they may bind to titania species (or pillars) in the catalysts. Another possibility, some iron ions may hydrolyze to iron hydroxide and precipitate on the surface of the catalysts. This led to higher iron contents on the catalyst surfaces which block some of the pores by the formation of aggregates.

In the presence of Fe^{3+} ions, the probability of electron-hole pair recombination reactions reduces due to the additional steps in the proposed mechanism of TiO_2 photocatalysis given in section 4.2.2.6. Thus, it is reasonable to expect an increase in the degradation process of β-Naphthol in iron exchanged catalysts. However, in the presence of Fe-Sepiolite-TiO_2, a lower degradation was obtained in contrast to the higher destruction observed in the case of Fe-Na-Montmorillonite-TiO_2 catalysts (Figure 4.53).

The reason behind the lower catalytic activity of Fe-Sepiolite-TiO_2 catalyst may be due to the precipitation of iron hydroxide and formation of Fe_2O_3 blocks on top of the TiO_2 species. These drawbacks will either cause a lower absorption of UV light and a subsequent decrease in the formation rate of electron-hole pairs or in the case of absorption of light, the system behaves as a coupled oxide (Fe_2O_3-TiO_2) and serves as a recombination center rather than as a trap site.

Higher degradation rate in the presence of Fe-Na-Montmorillonite-TiO_2 catalyst may be due to the presence of additional TiO_2 pillars in the structure. Since titania hydroxyl cations already replaced the charge-compensating cations between the clay layers, exchange of Fe^{3+} ions with these cations, formation of iron hydroxide and Fe_2O_3 aggregates will be much lower.

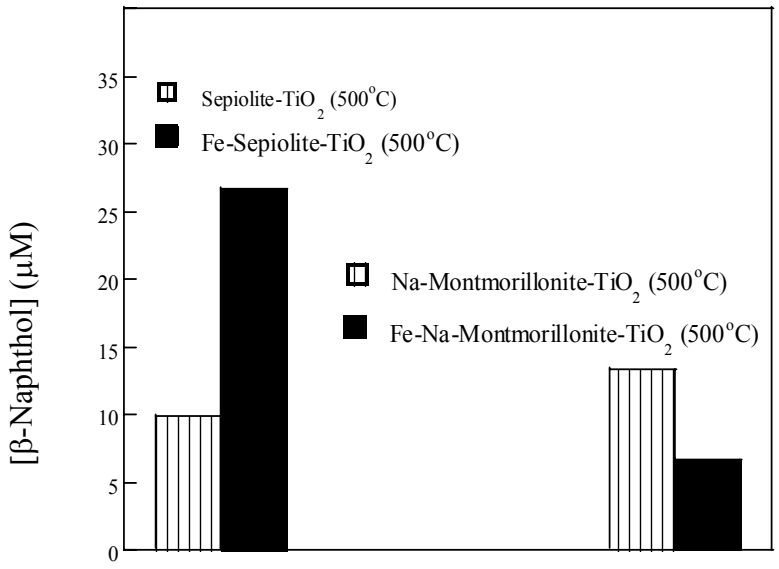

Figure 4.53. Photocatalytic degradation of β-Naphthol in the presence of Fe-Sepiolite-TiO_2 (500°C) and Fe-Na-Montmorillonite-TiO_2 (500°C)

4.3.6. Proposed .Mechanism for the Photocatalytic Degradation of β-Naphthol

Advanced oxidation processes are based on the production of hydroxyl radicals. These highly reactive species attack on to organic molecules and oxidize them in the presence of oxygen in serious of subsequent steps up to CO_2, H_2O and mineral acids. The heterogeneous system of TiO_2-clay solution produces hydroxyl radicals following light absorption. Formed electron-hole pairs are seperated; holes can be trapped by surface bound hydroxyl and hydroperoxyl radicals.

In this study, the photocatalytic degradation of β-Naphthol is proposed by the following reaction mechanism (Figure 4.54). According to the mechanism, formation of 2-formylcinnamaldehyde (V) as the main intermediate throught the degradation process, is accepted. Unstable tetraoxide (III) that initially results from the termination reaction undergoes further intramolecular rearrangements. Splitting of two O-O bonds and one C-C bond candirectly lead to stable open-ring structure. According to the proposed reaction pathway, various oxidized compounds can result from the initial OH attack onto theβ-Naphthol structure [59].

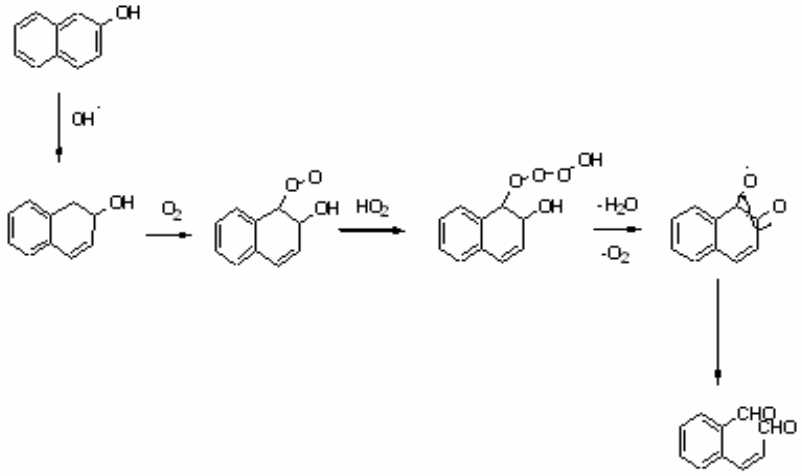

Figure 4.54. Photocatalytic degradation experiments of β-Naphthol

5. CONCLUSIONS

TGA results indicated that titania-sol incorporated Sepiolite showed only decomposition of the organic compound present on the surface of the catalyst. However, for Na-Montmorillonite-TiO_2, two types of organic compounds detected; one was surface adsorbed and the other was intercalated (pillared).

According to the XRD analysis, titania-sol was examined before the addition of clay minerals. Clear anatase diffractions were obtained for all samples.

For the Sepiolite-TiO_2 catalysts, when the effect of TiO_2 content was investigated, in small angle XRD patterns, (110) peak intensity of the original clay was found to decrease with the addition of the titania-sol. Wide angle XRD patterns gave information about the anatase peaks. 50 mL of titania addition was used as an optimal amount throughout the experiments. Neither H_2O_2 nor heat treatment promoted the crystalline growth. Anatase main peak intensities were significantly raised in Na^+ ion placed Sepiolite-TiO_2 catalysts. In addition, change in concentration of Na^+ ion made a remarkable effect in 25.4^o peak intensities, specifically for the 3M Na-Sepiolite-TiO_2 (100^{o}C) sample. The XRD pattern of Fe-Sepiolite-TiO_2 (500^o) catalyst was similar to that of TiO_2 incorporated clay. However, height and FWHM value of the anatase peak decreased and the crystalline size increased with the insertion of Fe^{3+} ions. No peak for Fe_2O_3 was observed in the XRD pattern of the corresponding catalyst.

However, after the titani-sol addition, formation of TiO_2 pillars is possible for the Na-Montmorillonite-TiO_2 catalysts due to the increments in the d-spacing values of the Na-Montmorillonite. Not a considerable change obtained in the main anatase peak after heat and H_2O_2 treatments. Fe-Na-Montmorillonite-TiO_2 (500^{o}C) showed lower anatase peak height and FWHM values compared to that of Na-Montmorillonite-TiO_2 (500^{o}C). Similar to the Fe-Sepiolite-TiO_2 (500^{o}C), no Fe_2O_3 peak was detected in Fe-Na-Montmorillonite-TiO_2 (500^{o}C).

According to the SEM results, large wavy-like structures of pure Sepiolite turned to be rather small particles with the addition of titani-sol. Each catalyst was having a higher percentage of TiO_2 compared to that exist in the pure clay. With the Na^+ ion insertion, sharp-edged bright and flat structures were obtained. 3M Na-Sepiolite-TiO_2 showed the highest TiO_2 percentage considering both bright-flat structures and big surfaces. Although, formation of Fe_2O_3 was not detected in the XRD analysis of the iron exchanged catalyst, energy dispersive X-ray spot analysis of edged particles exhibited iron-oxide peaks. In addition, TiO_2 percentages decreased with an increase in Fe_2O_3 percentages.

For the Na-Montmorillonite-TiO_2 catalysts, irregularly dispersed white, small particles were observable and attributed to the quartz mineral naturally occuring in the clay. EDX analysis of stone-like structures showed that pure Na-Montmorillonite does not contain TiO_2. However, rough and smooth particles with higher TiO_2 percentyages were identified among the stone-like structures in the SEM image of the titania-pillared catalyst Na-Montmorillonite-TiO_2 (100˚C). TiO_2 percentage of such a particle was found as 56.14 wt per cent.

As a result of STEM analysis, small dark spots and less aggregated particles were observed on the silica framework of Sepiolite-TiO_2 catalyst. However, in Na-Montmorillonite-TiO_2, large agglomerates were noticed and attributed to TiO_2 pillars among the layers of the clay.

Preliminary experiments examined substrate's stability under UV illumination, and followed investigation of adsorption capacities of the catalysts; TiO_2 Degussa P-25, Na-Montmorillonite-TiO_2 and Sepiolite-TiO_2 both in the dark and under irradiation. Control experiments; examination of the effect of β-Naphthol concentration, effect of titania-sol amount, effect of dilution in clay solutions precede the photodegradation studies to optimize the catalytic processes. Photoactivity of Anatase catalyst prepared at 100^{o}C showed the maximum degradation of β-Naphthol after 5 hours irradiation time. In Sepiolite-TiO_2 catalysts with the progress of the experiments, a decrease in the β-Naphthol concentration was successfully obtained. The best efficiency was obtained in the presence of Sepiolite-TiO_2 (100^{o}C) catalyst. In the case of Na-Montmorillonite-TiO_2 catalysts, β-Naphthol concentration has its lowest value with the one prepared at 100^{o}C. For Na-

Sepiolite-TiO_2 catalysts, Na^+ ion concentration was effective in the degradation process and also improved degradation yields were obtained in the presence of catalysts prepared at 100^oC. In the presence of Fe-Sepiolite-TiO_2, a lower degradation was obtained due to the precipitation of iron hydroxide and formation of Fe_2O_3 blocks on top of the TiO_2 species. In contrast, probability of Fe_2O_3 aggregates' formation was much lower due to the presence of additional TiO_2 pillars in the structure of the Na-Montmorillonite-TiO_2 catalyst.

REFERENCES

1. Yu, P. and M. Cardona, *Fundamentals of Semiconductors*: Physics and Materials Properties, 2nd ed., Springer, Newyork, 1999.

2. Herrmann, J. and M. Herrmann, "Heterogeneous Photocatalysis: Fundamentals and Applications to the Removal of Various Types of Aqueous Pollutants", *Catalysis Today*, Vol. 53, pp. 115-129, 1999.

3. Carp, O., C. L. Huisman and A. Reller, "Photoinduced Reactivity of Titanium Dioxide", *Progress in Solid State Chemistry*, Vol. 32, pp. 33-177, 2004.

4. Fujishima, A., T. N. Rao and D. A. Tryk, "Titanium Dioxide Photocatalysis", *Journal of Photochemistry and Photobiology C: Photochemistry Reviews*, Vol. 1, No. 1, pp. 1-21, 2000.

5. Ikeda, K., H. Sakai, R. Baba, K. Hashimoto and A. Fujishima, "Photocatalytic Reactions Involving Radical Chain Reactions Using Microelectrodes", *Journal of Photochemistry B*, Vol. 101, No. 14, pp. 2617-2620, 1998.

6. Muzyka, J. L. and M. A. Fox, "Oxidative Photocatalysis in the Absence of Oxygen: Methyl Viologen as an Electron Trap in the TiO_2-mediated Photocatalysis of the Diels-Alder Dimerization of 2,4-dimethyl-1,3-pentadiene", *Journal of Photochemistry and Photobiology A: Chemistry*, Vol. 57, No. 1-3, pp. 27-39, 1991.

7. Herrmann, J. M., C. Guillard, M. Arguello, A. Agüera, A. Tejedor, L. Piedra and A. Fernández-Alba, "Photocatalytic Degradation of Pesticide Pirimiphos-methyl: Determination of the Reaction Pathway and Identification of Intermediate Products by Various Analytical Methods", *Catalysis Today*, Vol. 54, No. 2-3, pp. 353-367, 1999.

8. Fox, M. A., D. D. Sackett and J. N. Younathan, "Competitive Reactions of Diene Cation Radicals Formed on Irradiated Metal Oxide Surfaces", *Tetrahedron*, Vol. 43, No. 7, pp. 1643-1660, 1987.

9. Turchi, C. S. and D. F. Ollis, "Photocatalytic Degradation of Organic Water Contaminants: Mechanisms Involving Hydroxyl Radical Attack", *Journal of Catalysis*, Vol. 122, No. 1, pp. 178-192, 1990.

10. Parra, S., J. Olivero and C. Pulgarin, "Relationships Between Physicochemical Properties and Photoreactivity of Four Biorecalcitrant Phenylurea Herbicides in Aqueous TiO_2 Suspension", *Applied Catalysis B: Environmental*, Vol. 36, No. 1, pp. 75-85, 2002.

11. Rakhshandeh, P. D., *Heterogeneous Photocatalytic Activity of Transition-Metal Cation Impregnated TiO_2*, M.S. Thesis, Boğaziçi University, 1993.

12. Daßler, A., A. Feltz, J. Jung, W. Ludwig and E. Kaiserberger, "Characterization of Rutile and Anatase Powders by Thermal Analysis", *Journal of Thermal Analysis and Calorimetry*, Vol. 33, .No. 3, pp. 803-809, 1988.

13. So, W. W., S. B. Park, K. J. Kim, C. H. Shin and S. J. Moon, "The Crystalline Phase Stability of Titania Particles Prepared at Room Temperature by the Sol-gel Method", *Journal of Materials Science*, Vol. 36, .No. 17, pp. 4299-4305, 2001.

14. Thevenet, F., O. Guaitella, J. M. Herrmann, A. Rousseau and C. Guillard, "Photocatalytic Degradation of Acetylene Over Various Titanium Dioxide-Based Photocatalysts", *Applied Catalysis B: Environmental*, Vol. 61, pp. 62-72, 2005.

15. Matijevi, E., M. Budnik and L. Meites, "Preparation and Mechanism of Formation of Titanium Dioxide Hydrosols of Narrow Size Distribution", *Journal of Colloid and Interface Science*, Vol. 61, No. 2, pp. 302-311, 1977.

16. Stir, M., T. Traykova, R. Nicula, E. Burkel, C. Baehtz, M. Knapp and C. Lathe, "In Situ High-Pressure and High-Temperature Diffraction Experiments on Pure and Ag-

Dopped TiO_2 Nanopowders", *Nuclear Instruments and Methods in Physics Research Section B: Beam interactions with Materials and Atoms*, Vol. 199, pp. 59-63, 2003.

17. Yang, P., C. Lu, N. Hua and Y. Du, "Titanium Dioxide Nanoparticles Co-doped with Fe^{3+} and Eu^{3+} Ions for Photocatalysis", *Materials Letters*, Vol. 57, No. 4, pp. 794-801, 2002.

18. Livage, J., M. Henry and C. Sanchez, "Sol-gel Chemistry of Transition Metal Oxides", *Progress in Solid State Chemistry*, Vol. 18, No. 4, pp. 259-341, 1998.

19. Li, Y., T. J. White and S. H. Lim, "Low-Temperature Synthesis and Microstructural Control of Titania Nano-particles", *Journal of Solid State Chemistry*, Vol. 177, No. 4-5, pp. 1372-1381, 2004.

20. Jung, Y. K., S. B. Park, "Anatase-phase Titania: Preparation by Embedding Silica and Photocatalytic Activity for the Decomposition of Trichloroethylene", *Journal of Photochemistry amd Photobiology A: Chemistry*, Vol. 127, pp. 117-122, 1999.

21. Zhang, Z., C. Wang, R. Zakaria and J. Y. Ying, "Role of Particle Size in Nanocrystalline TiO_2-based Photocatalysts", *Journal of Physical Chemistry B*, Vol. 102, No. 52, pp. 10871-10878, 1998.

22. Ilisz, I., A. Dombi, K. Mogyorósi, A. Farkas and I. Dékány, "Removal of 2-chlorophenol from Water by Adsorption Combined with TiO_2 Photocatalysis", *Applied Catalysis B: Environmental*, Vol. 39, No. 3, pp. 247-256, 2002.

23. Dijkstra, M. F. J., A. Michorius, H. Buwalda, H. J. Panneman, J. G. M. Winkelman and A. A. C. M. Beenackers, "Comparison of the Efficiency of Immobilized and Suspended Systems in Photocatalytic Degradation", *Catalysis Today*, Vol. 66, No. 2-4, pp. 487-494, 2001.

24. Yoneyama, H. and T. Torimoto, "Titanium Dioxide/Adsorbent Hybrid Photocatalysts for Photodestruction of Organic Substances of Dilute Concentrations", *Catalysis Today*, Vol. 58, No. 2-3, pp. 133-140, 2000.

25. Chen, H., A. Matsumoto, N. Nishimiya and K. Tsutsumi, "Preparation and Characterization of TiO_2 Incorporated Y-zeolite", *Colloids and Surfaces A: Physicochemical and Engineering Aspects*, Vol. 157, No. 1-3, pp. 295-305, 1999.

26. Ao, C. H. and S. C. Lee, "Enhancement Effect of TiO_2 Immobilized on Activated Carbon Filter for the Photodegradation of Pollutants at Typical Indoor Air Level", *Applied Catalysis B: Environmental*, Vol. 44, No. 3, pp. 191-205, 2003.

27. Rouquerol, F., J. Rouquerol and K. S. W. Sing, *Adsorption by Powders and Porous Solids: Principles, Methodology and Applications*, Academic press,San Diego, 1999.

28. Varma, R. S., "Clay and Clay-supported Reagents in Organic Synthesis", *Tetrahedron*, Vol. 58, pp. 1235-1255, 2002.

29. Pelizetti, E. and N. Serpone (editors), *Homogeneous and Heterogeneous Photocatalysis*,Raidel Publishing Co., France, 1986.

30. Murray, H. H., "Traditional and New Applications for Kaolin, Smectite, and Polygorskite: A General Overview", *Applied Clay Science*, Vol. 17, pp. 207-221, 2000.

31. Casal, B., J. Merino, J. M. Serratosa and E. R. Hitzky, "Sepiolite Based Materials for the Photo- and Thermal Stabilization of Pesticides", *Applied Clay Science*, Vol. 18, pp245-254, 2001.

32. Corma, A., "Alkali-Exchanged Sepiolites Containing Palladium as Bifunctional (Basic Sites and Noble Metal) Catalysts for the Heck and Suzuki Reactions", *Applied Catalysis A: General*, Vol. 257, pp. 77-83, 2004.

33. Molina-Sabio, M., "Porous Structure of a Sepiolite as Deduced From the Adsorption of N_2, CO_2, NH_3, and H_2O", *Microporous and Mesoporous Materials*, Vol. 47, pp. 389-396, 2001.

34. Akyüz, S. and T. Akyüz, "FT-IR Spectroscopic Investigations of Surface and Intercalated 2-aminopyrimidine Adsorbed on Sepiolite and Montmorillonite From Anatolia", *Journal of Molecular Structure*, Vol. 651-653, pp. 205-210, 2003.

35. Şen, S., *A Study on Polymer-Clay Nanocomposites*, M. S. Thesis, Boğaziçi University, 2005.

36. Cheng, S., " From Layer Compounds to Catalytic Materials", *Catalysis Today*, Vol. 49, pp. 303-312, 24 February 1999.

37. Wilson, M., K. Kannangara, G. Smith, M. Simmons and B. Raguse, *Nanotechnology: Basic Science and Emerging Technologies*, Chapman & Hall/CRC, Washington, 2002.

38. Ooka, C., H. Yoshida, S. Takeuchi, M. Maekawa, Z. Yamada and T. Hattori, "Hydrogen peroxide Improving Crystallinity of TiO_2 Nanoparticle in Layer Compound", *Catalysis Communications*, Vol. 5, pp. 49-54, 2004.

39. Sterte, J., "Synthesis and Properties of Titanium Oxide Cross-Linked Montmorillonite", *Clays and Clays Minerals*, Vol. 34, No. 6, pp. 658-664, 1986.

40. Kiteyama, Y., T. Kodama, M. Abe, and H. Shimotsuma, "Synthesis of Titania Pillared Saponite in Aqueous Solution of Acetic Acid", *Journal of Porous Materials*, Vol. 5, pp. 121-126, 1998.

41. Kaneko, T., and M. Fujii, "Synthesis of Titania Pillared Mica in Agueous Solution of Acetic Acit", *Journal of Porous Materials*, Vol. 8, pp. 99-109, 2001.

42. Shimizu, K., T. Kaneako, T. Fujishima, T. Kodama, H. Yoshida and Y. Kiteyama, "Selective Oxidation of Liquid Hydrocarbons Over Photoirradiated TiO_2 Pillared Clays", *Applied Catalysis A: General*, Vol. 225, pp. 185-191, 2002.

43. Ooka, C., H. Yoshida, M. Horio, K. Suzuki and T. Hattori, "Adsorptive and Photocatalytic Performance of TiO_2 Pillared Montmorillonite in Degradation of Endocrine Disruptors Having Different Hydrophobicity", *Applied Catalysis B: Environmental*, Vol 41, pp. 313-321, 2003.

44. Ooka, C., H. Yoshida, K. Suzuki and T. Hattori, "Highly Hydrophobic TiO_2 Pillared Clay for Photocatalytic degradation of Organic Compounds in Water", *Microporous and Mesoporous Materials*, Vol. 67, pp. 143-150, 2004.

45. Witmann, G., K. Demeestere, A. Dombi, J. Dewulf, and H. L. Langenhove, "Preparation, Structural Characterization and Photocatalytic Activity of Mesoporous Ti-silicates", *Applied Catalysis B: Environmental*, Vol. 61, pp. 55-61, 2005.

46. Samina, A., "Photo Electrochemical Study of Ferrioxalate Actinometry at a Glassy Carbon Electrode", *Journal of Photochemistry and Photobiology A: Chemistry*, Vol. 161, pp. 151-154, 2004.

47. Ökte, A. N., *Photocatalytic Degradation of Phthalic Anhydride and Carboxylic Acids*, M.S. Thesis, Boğaziçi University, 1994.

48. Haciu, D., "*Heterogeneous Photocatalytic Elimination of Metal Ions*", Ph.D. Dissertation, Boğaziçi University, 1992.

49. Edward, W.,and E. Boschmann, "The Ferrioxalate Actinometer: A Lecture Demonstration", *Journal of Chemical Education*, Vol. 58, pp. 655, 1981.

50. Kuhn, H. J., S. E. Braslavsky and R., Schmidt, "Chemical Actinometry", *Pure and Applied Chemistry*, Vol. 61, pp. 187-210, 1989.

51. Shizuka, H. and P., De Mayo, *Photochemistry*, De Reidel, Newyork, 1972.

52. Wang, K. H., Y. H., Hsieh, M. Y. Chou and C. Y., Chang, "Photocatalytic degradation of 2-chloro and 2-nitrophenol by Titanium Dioxide Suspensions in Agueous Solutions", *Applied Catalysis B: Environmental*, Vol. 21, pp. 1-8, 1999.

53. http://www.meerschaumstore.com/lopedia.

54. Skoog, D. A. and J. J. Leary, *Principles of Instrumental Analysis*, 4th ed., Saunders College Pub, Philadelphia, 1992.

55. Long, R. Q. and R. T. Yang, "Selective Catalytic Reduction of Nitrogen Oxides by Ammonia over Fe3+-Exchanged TiO_2-Pillared Clay Catalysts", *Journal of Catalysis*, Vol 186, pp. 254-268, 1999.

56. Mrowetz, M. and E. Selli, "Effect of Iron Species in the Photocatalytic Degradation of an Azo Dye in TiO_2 Aqueous Suspensions", *Journal of Photochemistry andPhotobiology A: Chemistry*, Vol. 162, No. 1, pp. 89-95, 2004.

57. Zhu, J., W. Zhang, B. He, J. Zhang and M. Anpo, "Characterization of Fe-TiO_2 Catalysts Synthesized by Hydrothermal Method and Their Photocatalytic Reactivity for Photodegradation of XRG Dye Diluted in Water" *Journal of Moleculer Catalysis A: Chemistry*, Vol. 216, No. 1, pp. 35-43, 2004.

58. Baes, C. F. and R. E. Mesmer, *The Hydrolysis of Cations*, Wiley, Newyork, 1976.

59. Hykrdova, L., J. Jirkovsky, G. Mailhot and M. Bolte, “Fe(III) Photoinduced and Q-TiO2 Photocatalysed Degradation of Naphthalene: Comparison of Kinetics and Proposal of Mechanism”, *Journal of Photochemistry and Photobiology A: Chemistry*, Vol. 151, pp. 181-193, 2002.